

# **The role of linear energy transfer in modulating radiation-induced NF- $\kappa$ B activation and its down-stream target genes**

## **Dissertation**

zur  
Erlangung des Doktorgrades (Dr. rer. nat.)  
der  
Mathematisch-Naturwissenschaftlichen Fakultät  
der  
Rheinischen Friedrich-Wilhelms-Universität Bonn

vorgelegt von

Arif Ali Chishti  
aus  
Karachi, Pakistan

Bonn 2014

Angefertigt mit Genehmigung der Mathematisch-Naturwissenschaftlichen Fakultät  
der Rheinischen Friedrich-Wilhelms-Universität Bonn

1. Gutachter: PD Dr. Ruth Hemmersbach

2. Gutachter: Prof. Dr. Waldemar Kolanus

Tag der Promotion: 09.07.2014

Erscheinungsjahr: 2014

## Table of Contents

1	Introduction.....	7
1.1	Radiation exposure during tumor therapy.....	7
1.1.1	Radiation research and tumor radiotherapy centers .....	10
1.2	Radiation exposure and risk estimation during space missions .....	10
1.3	Biological consequences of exposure to ionization radiation.....	12
1.3.1	Ionizing radiation-induced DNA damages .....	13
1.3.2	Ionizing radiation-induced DNA damage repair response.....	16
1.3.3	Regulation of cell cycle as part of DNA damage response .....	17
1.3.4	Ionizing radiation-induced cell death.....	19
1.3.5	Ionizing radiation-induced non-targeted effects .....	19
1.3.6	Ionizing radiation-induced transcription factors and signaling pathways.....	20
1.3.7	Activation of NF- $\kappa$ B as part of DNA damage response .....	21
1.3.8	Down-stream events after NF- $\kappa$ B activation.....	23
1.3.9	Role of NF- $\kappa$ B and cytokines in the bystander effect .....	24
1.4	Aim of the study.....	25
2	Materials and methods .....	26
2.1	Materials.....	26
2.1.1	Equipment.....	26
2.1.2	Consumables .....	27
2.1.3	Kits and assays.....	27
2.1.4	Chemicals .....	28
2.1.5	Cell lines and plasmids .....	29
2.1.6	Media, buffers and solutions .....	31
2.1.7	Software.....	33
2.2	Methods.....	34
2.2.1	Routine tissue culture methods.....	34
2.2.2	Radiation exposure .....	35

2.2.3	Analysis of cellular radiation response.....	38
2.2.4	Gene expression analysis by reverse transcriptase RT-qPCR .....	44
2.2.5	Gene expression analysis by target gene array .....	52
3	Results .....	56
3.1	Effect of ionizing radiation on NF- $\kappa$ B activation in HEK reporter cell lines... ..	57
3.1.1	Activation of NF- $\kappa$ B by the canonical pathway is quicker than by the genotoxic stress induced pathway.....	57
3.1.2	Activation of NF- $\kappa$ B in response to space-relevant radiation qualities ..	58
3.2	Cellular responses to exposure with ionizing radiation .....	60
3.2.1	Effect of ionizing radiation on cellular survival .....	60
3.2.2	Relative biological effectiveness of the tested radiation qualities.....	65
3.2.3	Effect of ionizing radiation on cell cycle progression.....	65
3.3	Contribution of NF- $\kappa$ B activation in different cellular responses .....	72
3.3.1	NF- $\kappa$ B down-regulation decreases cell survival after X-irradiation.....	72
3.3.2	Pre-activation of NF- $\kappa$ B decreases cell survival after high dose X-ray exposure.....	72
3.3.3	NF- $\kappa$ B deactivation results in impairment of DNA damage recovery ....	74
3.3.4	NF- $\kappa$ B down-regulation delays cell cycle progression.....	78
3.4	The regulation of NF- $\kappa$ B down-stream target genes after ionizing radiation exposure .....	79
3.4.1	NF- $\kappa$ B-dependent gene expression analysis after X-irradiation .....	79
3.4.2	NF- $\kappa$ B-dependent gene expression after heavy ion exposure .....	80
3.5	The effect of LET on the up-regulated NF- $\kappa$ B target genes.....	82
3.5.1	Heavy ions induce expression of chemokine and cytokine genes most efficiently at LET values relevant for NF- $\kappa$ B activation .....	82
4	Discussion .....	85
4.1	Effect of ionizing radiation on the NF- $\kappa$ B pathway in HEK cells.....	86
4.1.1	Activation of NF- $\kappa$ B in HEK cells.....	86

4.1.2	Activation of NF- $\kappa$ B by the canonical and the genotoxic stress induced pathway .....	87
4.1.3	NF- $\kappa$ B activation is both ionizing radiation dose and LET-dependent ...	88
4.2	Relative Biological Effectiveness of the tested radiation qualities .....	90
4.3	Effect of ionizing radiation in different cellular responses .....	90
4.3.2	Effect of LET on cellular survival .....	91
4.3.3	Effect of LET on cell cycle progression .....	92
4.4	Contribution of NF- $\kappa$ B activation in different cellular responses .....	94
4.4.1	NF- $\kappa$ B down-regulation decreases cell survival after X-irradiation .....	94
4.4.2	NF- $\kappa$ B deactivation results in impairment of DNA damage response ...	96
4.4.3	NF- $\kappa$ B down-regulation delays cell cycle progression .....	97
4.5	The regulation of down-stream target genes of NF- $\kappa$ B after ionizing radiation exposure .....	98
4.5.1	NF- $\kappa$ B-dependent gene expression after X-irradiation .....	98
4.5.2	NF- $\kappa$ B-dependent gene expression after heavy ion exposure .....	101
4.6	The effect of LET on the up-regulated NF- $\kappa$ B target genes .....	103
4.6.1	Heavy ions induce expression of chemokine and cytokine genes most efficiently at LET-values relevant for NF- $\kappa$ B activation .....	103
4.7	Conclusion and outlook .....	104
4.8	Summary .....	106
5	Abbreviations .....	107
6	References .....	113
7	Acknowledgments .....	129
8	Curriculum Vitae .....	130



## 1 Introduction

Radiation, a double-edged sword, is part of nature. It is an effective therapeutic modality for the treatment of many types of tumors and it is a well-known human carcinogen. Human beings are exposed to ionizing radiation either from natural sources (e.g. cosmic or terrestrial radiation) or man-made sources (e.g. radiation used in radiotherapy) and the biological effects are strongly influenced by the radiation quality. The cellular radiation response, especially survival and cell cycle arrest after exposure to various radiation qualities resulting in different DNA damage profiles such as clustered DNA damage (combination of strand breaks and base damages), is incompletely understood. Furthermore, details of survival regulation and especially the role of Nuclear Factor  $\kappa$ B (NF- $\kappa$ B) in the survival and cell cycle regulation after exposure to different radiation qualities are unknown.

Exposure to ionizing radiation occurs in several contexts. People undergoing radiotherapy for treatment of cancer or inflammatory or degenerative diseases are exposed to X-rays,  $\alpha$ -,  $\beta$ - or  $\gamma$ -rays, neutrons, protons or carbon ions. The cosmic radiation that astronauts experience during spaceflight contains highly energetic protons,  $\alpha$ -particles and heavy ions. Currently, the uncertainty of space radiation exposure may result in radiation risks beyond the accepted range (Cucinotta and Durante 2006). The high uncertainty is mainly caused by the insufficient understanding of the biological effects of heavy ions which is critical in the carbon ion therapy settings as well. Therefore, the study of the biological effects of heavy ions, which is a topic of great importance for both tumor therapy and space radiobiology, is necessary.

### 1.1 Radiation exposure during tumor therapy

During tumor radiotherapy, patients experience high dose exposure at the targeted area to eliminate all cells of a tumor. Some cells in the surrounding tissue experience an acute low dose as well as the whole body receives a very low dose from leakage radiation (Purdy 2008). Ionizing radiation comprises electromagnetic radiation and charged particles including protons (hydrogen nuclei),  $\beta$ -particles (electrons and positrons),  $\alpha$ -particles (helium nuclei), heavy ions, uncharged neutrons,  $\gamma$ -rays and X-

rays. In conventional low linear energy transfer (LET<sup>1</sup>) radiotherapy, X-rays and  $\gamma$ -rays are applied to the tumor. Currently, protons and heavy ions (especially carbon ions) are used for radiotherapy at different heavy ions radiation research and tumor radiotherapy centers worldwide (see 1.1.1). The benefits of the use of accelerated heavy ions over conventional low-LET radiotherapy are precise energy and thereby dose deposition, maximum dose-on-target, and higher biological effectiveness. Some other ions, like helium, oxygen, neon, silicon and argon have also been used but carbon ion therapy was proved to be effective for different tumor types such as adenocarcinoma, adenoic cystic carcinoma, hepatocellular carcinoma, hepatoma, malignant melanoma and bone/soft tissue sarcomas (Okada *et al.* 2010; Purdy 2008) due to its higher relative biological effectiveness (RBE<sup>2</sup>) of  $\sim 3$  (Ando *et al.* 2006; Kanai *et al.* 1997) and distinct Bragg peak<sup>3</sup> (**Figure 1 A**).

The high and narrow Bragg peak of carbon ions is beneficial for precise energy deposition in the tumor. Heavy ions such as iron and silicon deposit high numbers of ionizations due to fragmentation processes along their microscopically small track (**Figure 1 B**) resulting in a very inhomogeneous dose distribution. The track diameter depends on the atomic size of the charged particle which results in different energy deposition pattern. This energy deposition pattern of high LET radiation is considered to account for different cellular effects compared to low LET radiation.

Beyond the Bragg peak, a very small physical dose delivered by secondary charged particles and neutrons of very high RBE (Kraft *et al.* 1999) may induce late effects in the surrounding cells and in bystander cells<sup>4</sup>. The data from clinical studies about risk of late effects for heavy ion therapy are too diverse for a definite conclusion (Suit *et al.* 2007).

---

<sup>1</sup> LET is described as the average energy deposition ( $\Delta E$ ) on the beam path ( $\Delta S$ ) of the ion in matter,  $\Delta E / \Delta S$  (keV/ $\mu\text{m}$ ).

<sup>2</sup> The RBE is the ratio of absorbed dose of a reference radiation ( $D_{\text{Ref}}$ ) which triggers a defined biological effect compared to the dose of a radiation quality under investigation ( $D_{\text{Test}}$ ) that is necessary for inducing the same biological effect. The  $D_{\text{Ref}}$  is usually 200 - 250 kV X-rays or  $\gamma$ -rays.  $\text{RBE} = D_{\text{Ref}} \text{ in Gy} / D_{\text{Test}} \text{ in Gy}$

<sup>3</sup> Bragg peak: Along the heavy ion track, the maximum energy is deposited before the heavy ion comes to rest. Therefore an extreme peak is observed at the end of the heavy ion track that is known as Bragg peak (named after the British physicist Sir William Bragg).

<sup>4</sup> Bystander cells are not directly exposed or traversed by radiation, but are in the neighborhood of a cell that had been hit or are incubated with medium from irradiated cells, and show responses (Mothersill *et al.* 2004).



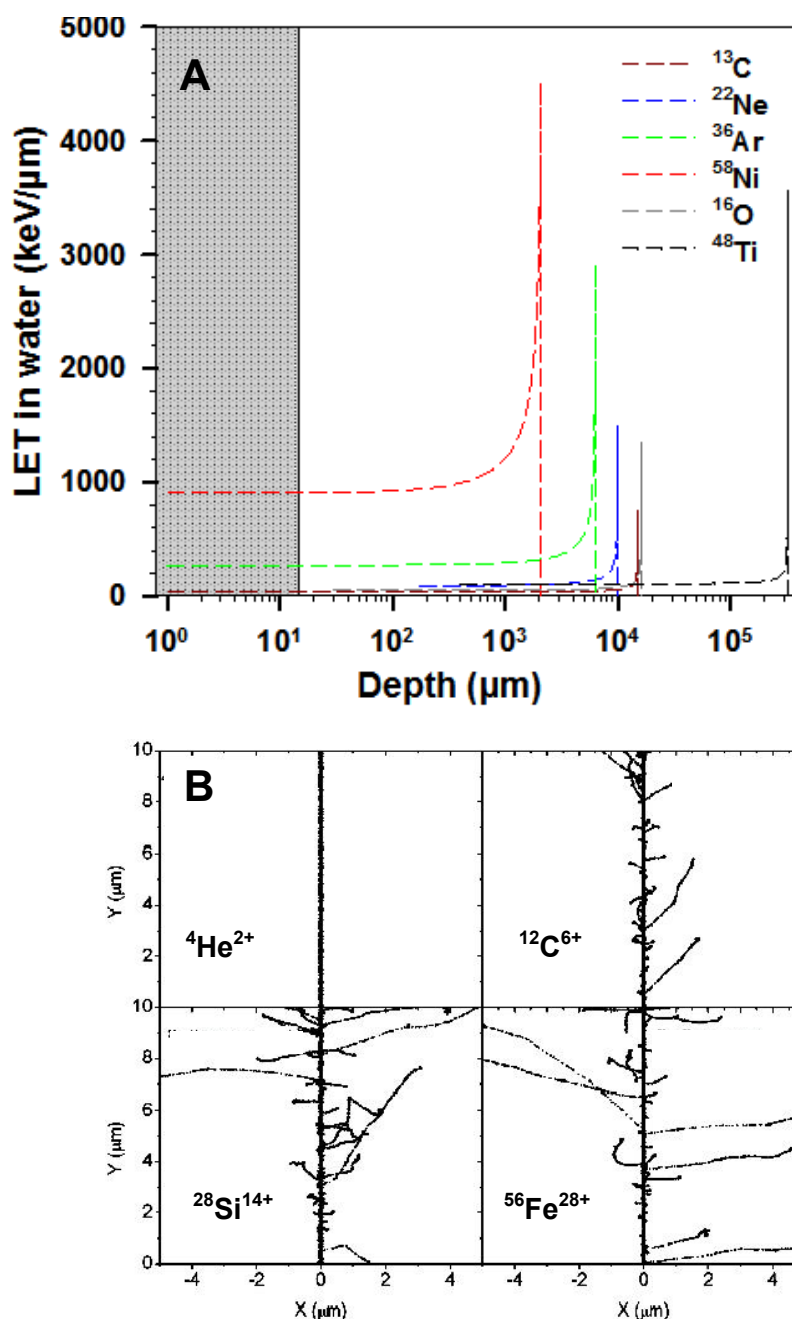


**Figure 1** Energy loss of energetic charged particles travelling through liquid water

A: Bragg curves of accelerated heavy ions <sup>13</sup>C (71 MeV/n, LET 33 keV/μm), <sup>22</sup>Ne (75 MeV/n, LET 92 keV/μm), <sup>36</sup>Ar (85 MeV/n, LET 272 keV/μm), <sup>58</sup>Ni (56 MeV/n, LET 905 keV/μm), <sup>16</sup>O (91 MeV/n, LET 51 keV/μm), and <sup>48</sup>Ti (996 MeV/n, LET 108 keV/μm) that were used in this study. The shaded area indicates the average thickness of a human cell. LET in water was calculated for the location of the cell and initial beam energies were chosen to achieve uniform LET distribution within the irradiated cell. Modified from (Hellweg 2012).

B: Heavy charged particle simulated track segments are projected two-dimensionally (for comparable LET 150-175 keV/μm). The tracks of an α-particle (<sup>4</sup>He<sup>2+</sup> 0.45 MeV/n), <sup>12</sup>C<sup>6+</sup> (10 MeV/n), <sup>28</sup>Si<sup>14+</sup> (90 MeV/n) and <sup>56</sup>Fe<sup>26+</sup> (1 GeV/n), were calculated using Monte Carlo track structure codes. The locations of energy deposition are shown in black and define the tracks of primary and secondary particles. Each dot represents a radiolytic species. Modified from Plante and Cucinotta (Plante and Cucinotta 2008).

### 1.1.1 Radiation research and tumor radiotherapy centers

There are several institutes world wide performing radiation research and radiotherapy. Some of them perform space radiation research at the same accelerators where patients are treated with heavy ions.

**HIMAC:** The Heavy Ion Medical Accelerator in Chiba (HIMAC) was constructed in 1993 at the National Institute of Radiological Sciences (NIRS) in Japan. In this facility, both radiation research and advanced radiotherapy treatment are performed.

**GSI:** The Gesellschaft für Schwerionenforschung mbH (GSI) was founded in 1969 and, renamed Helmholtz Centre for Heavy Ion Research in 2008. Carbon ion therapy started with the project Heavy Ion Therapy at GSI (HITAG). GSI offers three heavy ion facilities including heavy ion synchrotron SIS 18, universal linear accelerator (UNILAC) and storage ring ESR. SIS 18 offers beam energies in the range of 50-1000 MeV/n. Since 2009, cancer patients are treated at the newly opened Heidelberg Ion-Beam Therapy Center (HIT) at the University Clinics in Heidelberg, Germany.

**GANIL:** The synchrotron located in Caen, France, is called Grand Accélérateur National d' Ions Lourds (GANIL). The beam energies at GANIL are between 5 and 95 MeV/n, resulting in medium to high LET in water. Heavy ions from carbon ( $^{12}\text{C}$ ) to uranium ( $^{238}\text{U}$ ) can be accelerated at this facility. This facility is not yet open for tumor therapy. For radiation research, beam time proposals have to be submitted and accepted by the Program Advisory Committee (PAC) before any experiment can be performed.

### 1.2 Radiation exposure and risk estimation during space missions

Long stays in space, whether on the International Space Station (ISS) or on return flights to the Moon or Mars, are not only a physical and mental challenge for the astronauts because of microgravity ( $\mu \times g$ ), but are also associated with increased radiation exposure. The protection of humans from radiation hazards has been identified as one of the biggest problems in manned space missions (Pissarenko 1992; Setlow 2003).

The Earth is protected by the magnetic field and the atmosphere around it, but there is no such protection in outer space. The radiation field in Low Earth Orbit (LEO) not only consists of solar particle radiation (SPR) but also galactic cosmic rays (GCR) and the particles of the inner proton radiation belt. During solar particle events (SPE),

highly energetic protons (~89%),  $\alpha$ -particles (~10%) and heavy ions are emitted (~1%).

The ISS is partly shielded by the Earth's magnetic field, but the protective effect of the ISS walls or space suits are  $10^3$ - $10^4$  times lower than the air masses and the magnetic field on Earth (Reitz 2006; Reitz and Berger 2006). On board the ISS, the daily radiation dose is around 0.8 mSv (Apathy *et al.* 2003; Reitz *et al.* 2005; Reitz *et al.* 2009) and that dose increases as much as three times the daily dose during extra-vehicular activities. Therefore, astronauts receive a dose equivalent of about 0.3 Sv per year which is hundreds time more than on Earth (Townsend and Fry 2002). This continuous exposure to low doses (less than 1 Sv per year) can lead to late stochastic effects such as radiation-induced tumors and cataracts after a latency period of several years to decades (Brooks 2003; Gordon *et al.* 1995). The probability of tumor occurrence is proportional to the total absorbed dose<sup>5</sup>. During interplanetary missions, exposure to GCR at low dose rates is expected to result in accumulated doses of up to 1 Sv for a Mars mission.

The risk of high dose exposure in a short time period increases during SPE. Acute effects such as erythema in the case of a high skin dose, or prodromal symptoms, such as nausea and vomiting can be caused by SPE. They are followed by dose-dependent organ manifestation of the acute radiation syndrome (hematopoietic, gastrointestinal or central nervous system syndrome) and even death. A brief overview of radiation effects at different doses and the consequences that are to be expected after acute or chronic exposure is shown in **Table 1**.

Careful planning of space missions with respect to the solar cycle and considering the proper shelter and early warning system for SPEs can greatly reduce the risk of acute high dose radiation exposure. SPEs are still unpredictable; therefore early warning can be achieved only by signals from satellites closer to the Sun. The astronauts can protect themselves from high dose exposure by moving to a shelter room with stronger shielding. On the contrary, shielding of GCR results in secondary radiation that increases the dose behind the shield. Therefore, a closer look at the uniqueness of space environmental conditions (especially the radiation field in

---

<sup>5</sup> Absorbed dose is defined as the absorbed energy of ionizing radiation per unit mass. The unit of absorbed dose is Gray (Gy). 1 Gy = 1 J/kg

space), and cellular radiation response pathways (especially for exposure to densely ionizing radiation) is necessary. Better understanding of the cellular radiation response will help to reduce this uncertainty in risk assessment, and will allow development of countermeasures against deterministic, immediate, and stochastic effects that occur during long-term space missions.

**Table 1 Radiation effects in humans after whole body irradiation (Hellweg and Baumstark-Khan 2007)**

Dose	Risk and consequences
<b>Chronic dose</b>	
~ 0.4 Sv	First indication of increased cancer risk
2 - 4 Sv / year	Chronic radiation syndrome with complex clinical symptoms
<b>Acute single dose</b>	
~ 0.1- 0.3 Sv	Cancer risk as a late effect
> 0.5 Sv	Nausea and vomiting expected but no early death
(> 0.7) 3 - 5 Sv	Bone marrow syndrome: Symptoms include internal bleeding, fatigue, bacterial infections and fever. Maximum death rate after 30 days and increased to about 60 days, death from sepsis
5 to 12 Sv	Gastrointestinal syndrome: Symptoms include nausea, vomiting, diarrhea, dehydration, electrolyte imbalance, loss of digestive function and bleeding ulcers. Death after 3 - 10 days by sepsis
> 20 Sv	Central nervous system syndrome: Symptoms include loss of coordination, confusion, coma, convulsions, shock, gastrointestinal syndrome and hematopoietic symptoms. No survivors expected

### 1.3 Biological consequences of exposure to ionization radiation

To understand the impact of ionizing radiation on the human body, the radiation response processes have to be investigated on the molecular level. The DNA is considered as major target for the subsequent radiation effects (targeted effects). The radiation response is divided into different phases: physical, physicochemical, chemical, biochemical and biological (Herrmann *et al.* 2006). The physical phase

encompasses the ionization of atoms and molecules (time after exposure in seconds:  $10^{-18}$  -  $10^{-12}$ ) and is followed by the physicochemical phase, where ionized molecules recombine ( $10^{-12}$  -  $10^{-9}$ ). In the chemical phase ( $10^{-9}$  -  $10^0$ ), free radicals and reactive oxygen species (ROS) are formed which can cause DNA damage and bio-membrane damage. Ionizing radiation can cause a variety of DNA damages such as single and double strand breaks (SSB, DSB, respectively), ribose damages, and base modifications (Maynard *et al.* 2008). Cellular radiation responses are predominantly a result of DNA damage and include detection of DNA strand breaks and promotion of DNA repair (Jackson and Bartek 2009). Signaling pathways are subsequently activated in the biochemical phase ( $10^0$ - $10^3$ ), and represent an active cellular response to the radiation exposure. The following biological phase may last from minutes to several decades, if DNA damage is not repaired successfully, it could result in tumorigenesis or cell death (Herrmann *et al.* 2006).

The biological effects of ionizing radiation depend on its ability to ionize atoms or molecules, which can also result in the induction of mutations and chromosomal aberrations in affected cells (Durante *et al.* 2003; George *et al.* 2007; George *et al.* 2010; Horstmann *et al.* 2005a; Horstmann *et al.* 2005b). High-energy particles most often damage both strands of the DNA helix, which results in different biological consequences in the cell e.g. activation of DNA repair pathways, cell cycle arrest, and activation of transcription factors or cell death (**Figure 2**).

### 1.3.1 Ionizing radiation-induced DNA damages

The most critical target of ionizing radiation within a cell is the cell nucleus, particularly DNA, which encodes information required for the cell to perform its function. Ionizing radiation creates DNA damage either by a direct or an indirect effect (**Figure 3**).

The direct effect of radiation occurs predominantly by densely ionizing radiation, such as  $\alpha$ -radiation<sup>6</sup> and heavy ions<sup>7</sup>, which causes ionization of the relevant biomolecules, mostly DNA. For the indirect effects, radiation energy results in

---

<sup>6</sup>  $\alpha$ -radiation consists of the nucleus of helium ion.

<sup>7</sup> A heavy ion is the nucleus of any element with an atomic mass larger than 4 amu (atomic mass unit), excluding hydrogen and helium.

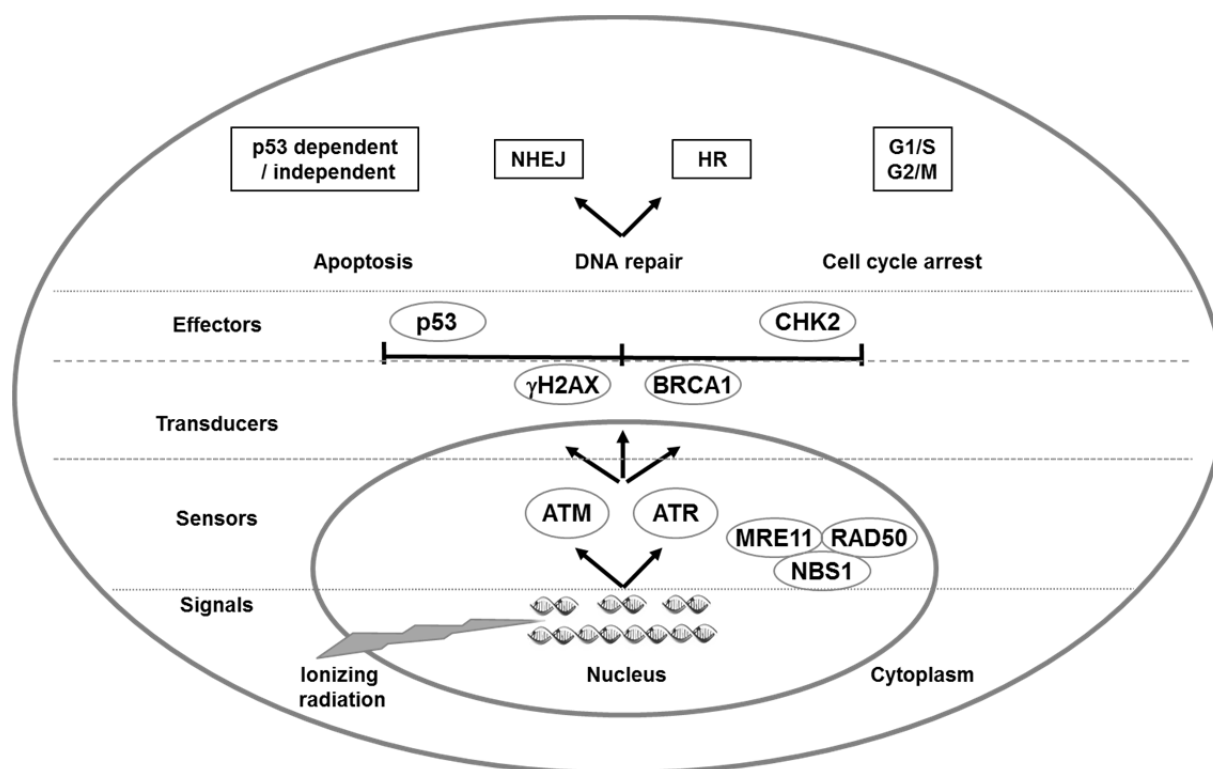


**Figure 2 Ionizing radiation causes DNA double-strand breaks (DSBs).**

DNA damage is recognized by the MRN sensor complex (MRE11-RAD50-NBS1) which recruits ATM and/or ATR kinases to activate ATM and/or ATR pathways. ATM/ATR signals the activation of BRCA1 and H2AX and also p53 and effector kinases such as CHK2. DSBs detected by the sensor proteins followed by transducer and effector proteins result in cell cycle arrest, DNA repair and/or apoptosis. For repairing the damaged DNA, one of the two major DSB repair mechanisms, homologous recombination (HR) or non-homologous end joining (NHEJ), is activated (Nagaria *et al.* 2013).

ionization of water molecules and the generated radicals can subsequently damage different DNA sites. It is assumed that two thirds of hydroxyl radicals ( $\cdot\text{HO}$ ) generated by sparsely ionizing radiation (X-rays) lead to indirect DNA damage by causing oxidation of DNA (Tjong 2009). Sparsely ionizing radiation (X-rays and  $\gamma$ -rays) creates four times more non-DSB (e.g., base lesions, abasic sites and SSBs) than prompt DSB (Eccles *et al.* 2011). In presence of atmospheric oxygen during X-ray exposure, peroxide radicals and peroxides formed in oxygenated tissue also cause DNA damage.

Densely ionized radiation (heavy ions) causes DNA damage mainly by direct ionization. Production of SSBs and DSBs depends on the type, dose and energy of the heavy ions. High LET heavy ions can produce both SSBs and DSBs directly by damaging the sugar phosphate backbone of DNA and also by generating clusters of

base damage (Ward 1994) which are converted to strand breaks during repair processes (**Figure 3**). It was suggested by microdosimetric considerations that high-LET heavy ions deposit considerable energy and form multiple sites of damage within DNA strands through their tracks (Brenner and Ward 1992). Heavy ions, depending upon the dose and LET, produce more DSBs by direct actions than by indirect action (Hirayama *et al.* 2009). High-LET induced damage is thought to be much more difficult for cells to repair accurately (Fakir and Hofmann 2006).

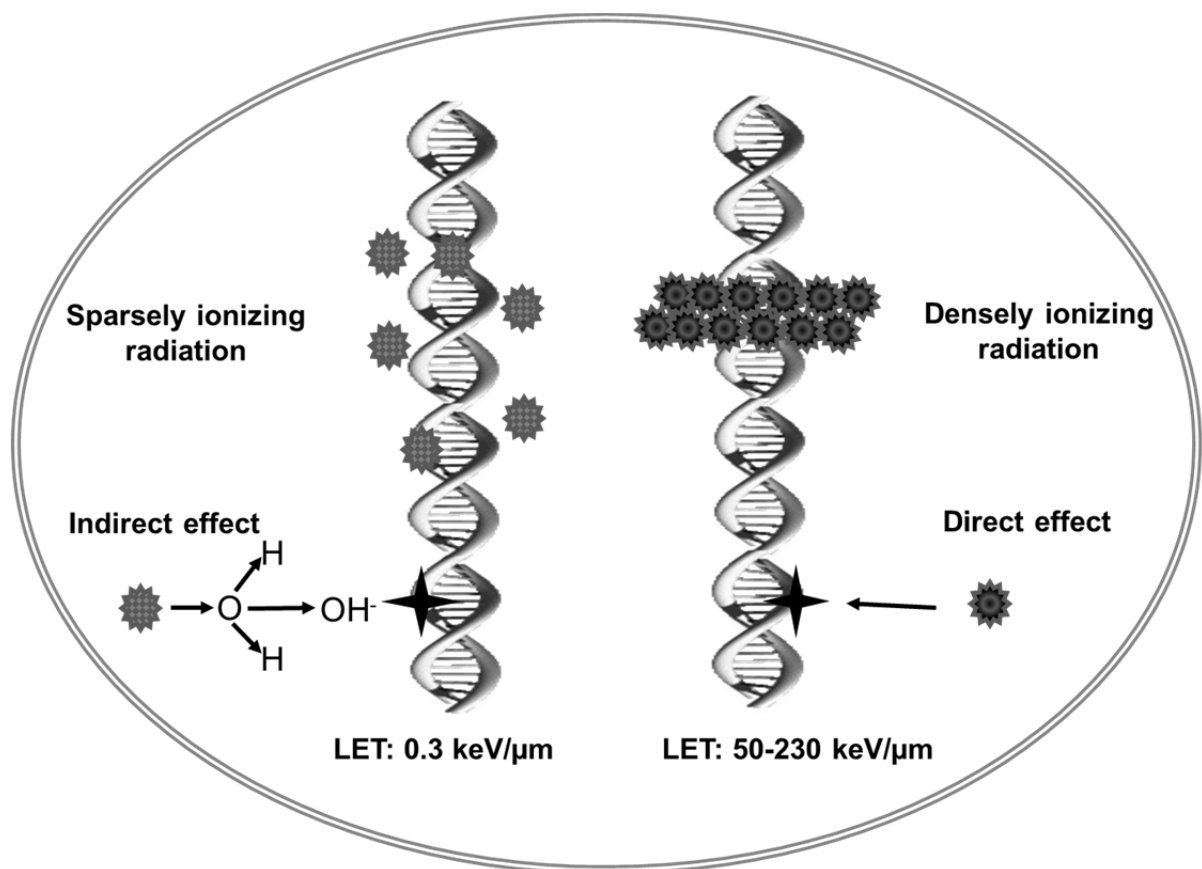


**Figure 3: Direct and indirect radiation effects on DNA**

Low LET and high LET radiation exposure produces direct and indirect effects at the molecular level (Pouget *et al.* 2011).

### 1.3.2 Ionizing radiation-induced DNA damage repair response

The mechanisms to repair various forms of DNA damage induced by ionizing radiation, like SSBs, DSBs, base damages, base loss, and cross-linkage of bases, are very important for cellular survival. DNA repair protects cells from undergoing mutations, thus it is crucial that the damage is repaired before the next cell division.

If DNA damage is not repaired properly, the cell may undergo tumor induction or die. There are several ways for repairing DNA damage in living cells including homologous recombination (HR), non-homologous end joining (NHEJ), base excision repair (BER), nucleotide excision repair (NER) and mismatch repair (MMR) (Mostoslavsky 2008). The genes involved in these five repair mechanisms are mentioned in **Table 2**. Among these five repair mechanisms only NHEJ and HR play important role in radiation-induced DNA DSB repair. NHEJ repairs DNA mainly in G1- and early S-phase, whereas HR takes place in late S; the G2-phase. NHEJ process is more error-prone compared to HR because HR uses the homologue DNA sequence of the sister chromatid to repair the DNA breaks. NER and BER are responsible for repair of base damage, whereby BER can remove some specific base damage, and NER acts generally on base damages that result in deformation of the DNA strand. Both repair pathways can be recruited for repair of complex damages that include base damages. The MMR can remove repair errors.

Ionizing radiation activates enzymes from the phosphatidylinositol-3-kinase-related (PIKK) family, including ATM (ataxia telangiectasia mutant), ATR (ataxia telangiectasia and Rad3-related protein) and DNA-PK (DNA-dependent protein kinase) (Tichy *et al.* 2010). Activation of ATM results in phosphorylation of several key proteins including p53 and Chk2 which initiate activation of the DNA damage checkpoint, leading to cell cycle arrest, DNA repair or apoptosis (Warmerdam and Kanaar 2010). ATM is not only involved in initiation of the NHEJ repair mechanism but also plays an important role in HR repair mechanism. ATM responds mainly to DNA DSB, whereas ATR is involved mostly in sensing SSBs and activating the DNA damage checkpoint. ATM and ATR respond to DNA SSBs and DSBs in a combined and complementary fashion to sense and repair damaged sites. The third kinase, DNA-PK, is required for NHEJ and plays a very important role in activating various cellular signaling pathways including the epidermal growth factor receptor (EGFR), ATM and NF- $\kappa$ B pathways (Kotula *et al.* 2013).



**Table 2 Essential genes of the five major DNA repair mechanisms, adopted from (Dexheimer 2013)**

DNA repair mechanism	Genes responsible for repair in respective mechanism
Base excision repair (BER)	DNA glycosylase, APE1, XRCC1, PNKP, Tdp1, APTX, DNA polymerase $\beta$ , FEN1, DNA polymerase $\delta$ or $\epsilon$ , PCNA-RFC, PARP
Mismatch repair (MMR)	MutS $\alpha$ (MSH2-MSH6), MutS $\beta$ (MSH2-MSH3), MutL $\alpha$ (MLH1-PMS2), MutL $\beta$ (MLH1-PMS2), MutL $\gamma$ (MLH1-MLH3), Exo1, PCNA-RFC
Nucleotide excision repair (NER)	XPC-Rad23B-CEN2, UV-DDB (DDB1-XPE), CSA,CSB, TFIIH, XPB, XPD, XPA, RPA, XPG, ERCC1-XPF, DNA polymerase $\delta$ or $\epsilon$
Homologous recombination (HR)	Mre11-Rad50-Nbs1, CtIP, RPA, Rad51, Rad52, BRCA1, BRCA2, Exo1, BLM-TopIII $\alpha$ , GEN1-Yen1, Slx1- Slx4, Mus81/Eme1
Non-homologous end-joining (NHEJ)	Ku70-Ku80, DNA-PKc, XRCC4-DNA ligase IV, XLF

### 1.3.3 Regulation of cell cycle as part of DNA damage response

After the recognition of ionizing radiation-induced DNA damage, it is necessary for the cell cycle to slow down or stop in cell cycle progression until the damage is fixed. Initial signaling by ATM/ATR is associated with activation of p53-dependent and -independent pathways to the cell-cycle regulatory check-points (G1, S or G2/M arrest) at various places in the cell cycle, which is regulated by cyclin-dependent kinases (CDKs) (Cude *et al.* 2007; Lodish H *et al.* 2000). CDKs are also required for cell cycle transition and regulation of cyclin genes that contribute to the transition of different cell cycle phases (Wilson 2004) shown in **Figure 4**.

It was shown that cells from ataxia telangiectasia (AT) patients show defective G1, S, and G2 arrest after ionizing radiation (Beamish and Lavin 1994). Therefore, it was concluded that ATM participates in governing the cell cycle checkpoints in response to genotoxic stress. Many tumor cells are also reported to be deficient in the G1/S checkpoint due to a non-functional p53 pathway and a non-effective G1 or S phase

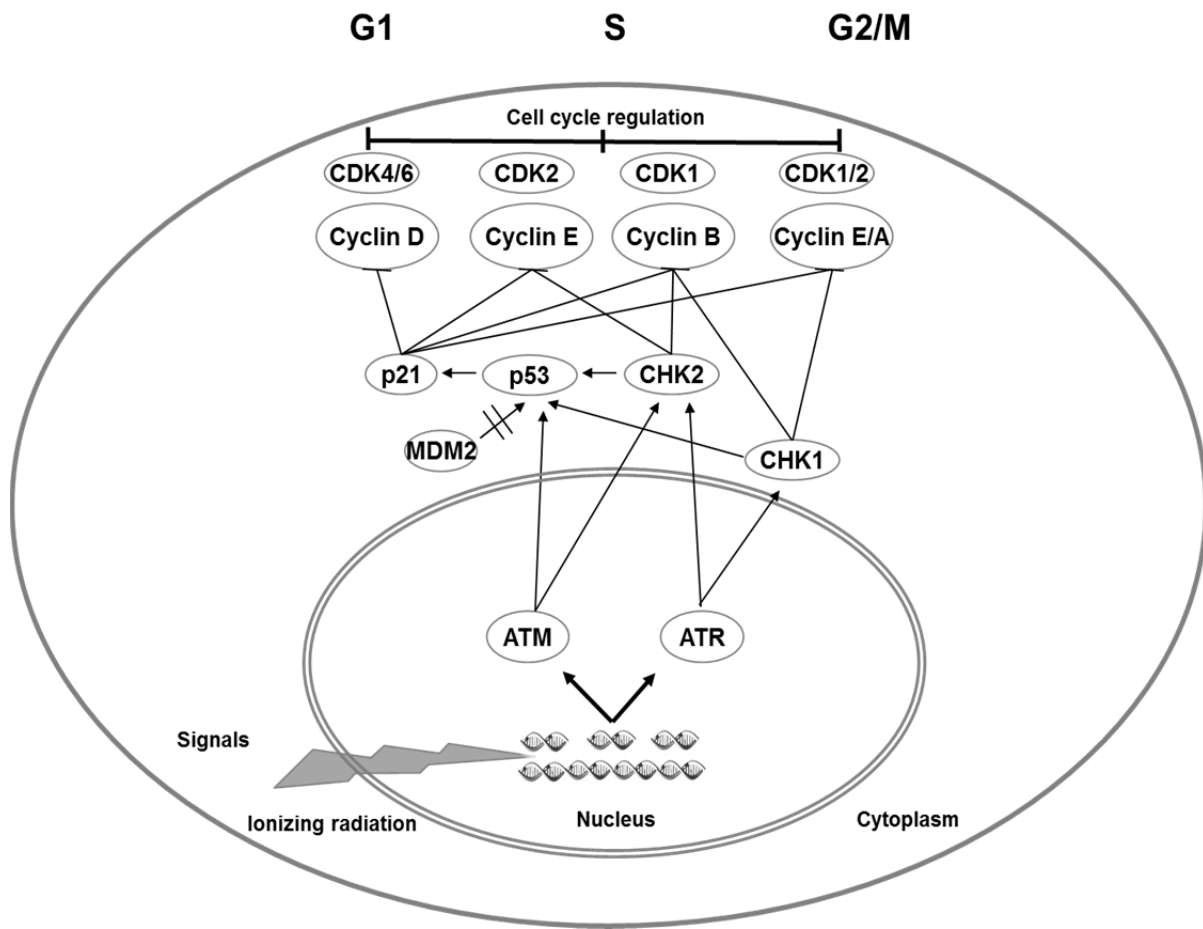


**Figure 4 Overview of cell cycle checkpoints that block cell cycle progression and lead to G1, S, G2/M arrest**

As a consequence of SSB and DSB, ATM and ATR phosphorylate p53, and the checkpoint kinases CHK1 and CHK2. p53 can also be phosphorylated by these checkpoint kinases. Phosphorylated p53 is released from its binding to MDM2 and up-regulates the transcription of the p21 gene (CDKN1A). p21 inhibits the CDK2-Cyclin E complex that normally induces the entry of the cell into the S-phase of the cell cycle, thereby initiating the G1 arrest. The passage from G2 to mitosis is normally enabled by the active CDK1-Cyclin B1 complex Adapted from (Iliakis *et al.* 2003; Pawlik and Keyomarsi 2004).

arrest induction. Once the damaged DNA is repaired, cyclin-CDK complexes enable further cell cycle progression. DNA repair takes place in different cell cycle phases; therefore, cell cycle progression either slows down or stops until the damage is repaired. The principles of the signaling cascades of individual checkpoints are very similar to each other, but there is still a great need for a better understanding of these processes (Cude *et al.* 2007).

### 1.3.4 Ionizing radiation-induced cell death

DNA damage induced by ionizing radiation may lead to cell death if the DNA damage is not properly repaired. In the case of error-free DNA repair, cellular survival is expected, but if repair is error-prone, it may lead cells to mutations, chromosomal aberrations, and delayed cell death. Ionizing radiation can cause different types of cell death and reduce cellular survival, which depends on the quality and quantity of exposed radiation. Radiation-induced cell death is functionally classified into reproductive death and interphase death (Kondo 2013). Reproductive death is the clonogenic failure or loss of proliferative ability of a cell caused by non- or mis-repaired DNA damage and measured by its colony forming ability (CFA) after radiation exposure. The CFA test is also a useful tool to examine radiosensitivity of cancer cells during radiation therapy. Reproductive cell death does not distinguish between the actual death and irreversible growth arrest. Apoptosis, necrosis, autophagy, or mitotic catastrophe lead to actual cell death whereas accelerated cellular senescence or premature differentiation are accompanied by irreversible growth arrest (Hellweg 2012). High dose exposure to low LET radiation ( $> 10$  Gy X-rays) or low doses of high LET radiation ( $< 2$  Gy neon ions) can lead to cell death after an arrest of  $\sim 24$  hours in the G2 phase of the cell cycle, and, without cellular attempts to divide, it is called interphase death (Mehnati *et al.* 2005; Sasaki *et al.* 1997). There are several mechanisms that lead cells to different types of cell death after DNA damage including impaired function of p53 regulation, loss of membrane integrity, up-regulation of CDK inhibitors p16<sup>INK4A</sup>, defects in G2/M and spindle checkpoint responses, telomere dysfunction, chromatin instability, and oncogene activation. Recently the Nomenclature Committee on Cell Death (NCCD) proposed seven additional functional classifications of regulated cell death modes including anoikis, cornification, entosis, necroptosis, netosis, parthanatos, and pyroptosis (Galluzzi *et al.* 2012). The involvement of such types in radiation-induced cell death is unknown.

### 1.3.5 Ionizing radiation-induced non-targeted effects

Ionizing radiation induces both targeted and non-targeted effects. Non-targeted effects occur when genomic instability is observed in the progeny of irradiated cells or if unirradiated cells receive signals either from nearby irradiated cells (Prise *et al.*

1998; Zhou *et al.* 2000) via gap-junction and medium-mediated diffusion or are cultured in medium transferred from cell cultures that had previously been irradiated (Mitchell *et al.* 2004a; Mitchell *et al.* 2004b). The latter non-targeted effects are known as bystander effects. There are two different bystander effects in mammalian cells. In one type, radiation exposure to a cell leads to damaging, and mutagenic events in adjacent, unhit cells. In the other type, radiation exposure to one cell leads to an adaptive response in bystander cells by increasing resistance to radiation-induced events (Mitchel 2004). Bystander effects direct cells to induce mutation and chromosome rearrangements, modulate gene expression and cell killing (Little 2006). There are multiple intracellular transducers, signaling pathways and factors involved to a particular endpoint associated with non-targeted effects including connexin mediated cell-to-cell gap junction communication (Autsavapromporn *et al.* 2011); reactive oxygen/nitrogen species (Azzam *et al.* 2003); inducible nitric oxide (NO) synthase (iNOS) (Matsumoto *et al.* 2011); cytokines and chemokines (Facoetti *et al.* 2006) and the enzymes COX-2 or NADPH oxidase (Azzam *et al.* 2003). Some studies suggest that effects in non-targeted cells might be controlled by DNA repair capacity (Nagasawa *et al.* 2003); epigenetic factors (Aypar *et al.* 2011); and/or mitochondrial dysfunction (Kim *et al.* 2006). The results from these studies suggest that degree of response and mode of transmission depend on cell type, cell density, biological endpoint assessed, radiation dose and dose rate, and radiation quality. Radiation-induced non-targeted effects in a biological system are variable and may not be observed in all experimental model systems (Schwartz 2007). Astronauts exposed to GCR in deep space missions are at higher risk as bystander effects are dominant in case of low dose of high-LET radiation exposure (Brenner and Ward 1992).

### **1.3.6 Ionizing radiation-induced transcription factors and signaling pathways**

Ionizing radiation activates multiple genotoxic stress-inducible signaling pathways that play critical roles in cellular survival. The pathways converge in the modulation of the activity of multiple transcription factors that alter expression of multiple target genes. ATM-mediated phosphorylation of c-Abl increases the transcription of stress response genes via activation of jun kinase (Karagiannis and El-Osta 2004). Ionizing radiation as well as growth factors and mitogens activate mitogen-activated protein

kinase (MAPK) pathways which then lead to activation of transcription factor activated protein 1 (AP-1). Other pathways activated by ionizing radiation include those downstream of death receptors, including pro-caspases and the transcription factor NF- $\kappa$ B. ROS are produced as a result of the indirect effects of ionizing radiation and may play an important role in activation of the transcription factor nuclear erythroid-derived 2-related factor 2 (Nrf2) and in induction of cellular antioxidant defense systems (McDonald *et al.* 2010). Gene expression and transcription factor activation varies among different cell types and also depends on ionizing radiation dose. In some cell types, radiation-induced signaling through growth factor receptors such as EGFR may provide radioprotective signals through multiple downstream pathways. In other cells, radioprotective signals are provided through NF- $\kappa$ B or MAPK pathways (Dent *et al.* 2003).

### **1.3.7 Activation of NF- $\kappa$ B as part of DNA damage response**

NF- $\kappa$ B is an activatable transcription factor which is involved in a wide variety of functions such as immune system regulation, inflammation, cellular survival, proliferation, differentiation, and apoptosis (Baichwal and Baeuerle 1997; Beg and Baldwin 1993; Ghosh 2007; Ghosh and Hayden 2012; Ghosh and Hayden 2008; Verma *et al.* 1995). NF- $\kappa$ B plays a key role in regulating gene expression that gives cells a survival advantage and resistance to a variety of chemotherapeutic agents and radiation therapy (Baldwin 2001). NF- $\kappa$ B signaling consists of a complex network of positive and negative gene regulation that leads to phosphorylation, ubiquitination, post-translational modification, translocation and degradation of several proteins and their subunits.

Previously, activation of NF- $\kappa$ B was supposed to be initiated from the ligand-receptor interactions on the cell membrane via canonical/classical and non-canonical/alternative pathways. In the last decade, it was discovered that NF- $\kappa$ B is also activated in response to DNA damage via genotoxic stress induced pathways (Hadian and Krappmann 2011; Miyamoto 2010). Several studies suggested that the DNA damage by ROS activates NF- $\kappa$ B signaling. Various chemicals that inhibit topoisomerase activity, including actinomycin D (ActD), etoposide (VP16), bleomycin, daunomycin (Dauno), amsacrine, doxorubicin (Dox), and camptothecin (CPT), were

reported to create DNA strand breaks and activate NF- $\kappa$ B (Huang *et al.* 2000; Piret and Piette 1996).

Activation of the DNA damage induced NF- $\kappa$ B pathway depends strongly on the genotoxic stimulus, timing of stimulus, dose and specially the cell type. In tissue culture based assays, the central component of DNA-damage response is the PI3-like kinase ATM (**Figure 5**). ATM deficient cells are no longer able to activate NF- $\kappa$ B in response to ionizing radiation or CPT (Durocher and Jackson 2001). Furthermore, ATM is needed for ubiquitination of NEMO, which in response to DNA damage, translocates to the nucleus. SUMOylation by the sumo ligase PIASy, in a complex with PIDD and RIP1, promotes nuclear localization of NEMO. Activated ATM phosphorylates and mono-ubiquitinates NEMO and triggers release of it from the nucleus back to the cytoplasm. The protein ELKS associates with the ATM-NEMO cytoplasmic complex and facilitates ATM-dependent cytoplasmic/canonical IKK complex activation (Huang *et al.* 2003; Janssens *et al.* 2005; O'Dea and Hoffmann 2009). Activation of IKK complex results in degradation of Inhibitor of NF- $\kappa$ B (I $\kappa$ B $\alpha$ ) and activation of NF- $\kappa$ B. The canonical p50:p65 heterodimer then translocates to the nucleus and initiates transcription of cell survival genes that inhibit apoptosis. Thus NF- $\kappa$ B activation by DNA damage helps cells to escape from lethal effects of DNA damage.

After the discovery of NF- $\kappa$ B, the focus of subsequent studies was to unravel the role of NF- $\kappa$ B in immune and inflammatory responses. Later on this focus was shifted towards the role of NF- $\kappa$ B in carcinogenesis, and radiotherapy resistance.

Many studies have suggested that NF- $\kappa$ B signaling is regulated by the PI3K pathway whereas others have suggested MAPK signaling can regulate this transcription factor through autocrine mechanisms (Bhat-Nakshatri *et al.* 2002; Jung and Dritschilo 2001; Leonore 1999; Troppmair *et al.* 1998). Now the focus of the research about NF- $\kappa$ B is to understand the molecular processes involved in NF- $\kappa$ B-dependent gene expression by ionizing radiation and NF- $\kappa$ B mediated DNA repair mechanism. Recent results of the Cellular Biodiagnostics group suggested an LET dependence of NF- $\kappa$ B activation, with stronger activation when LET increases (Hellweg 2012). The mechanisms of this stronger activation and the effects on cellular radiation response are completely unknown.

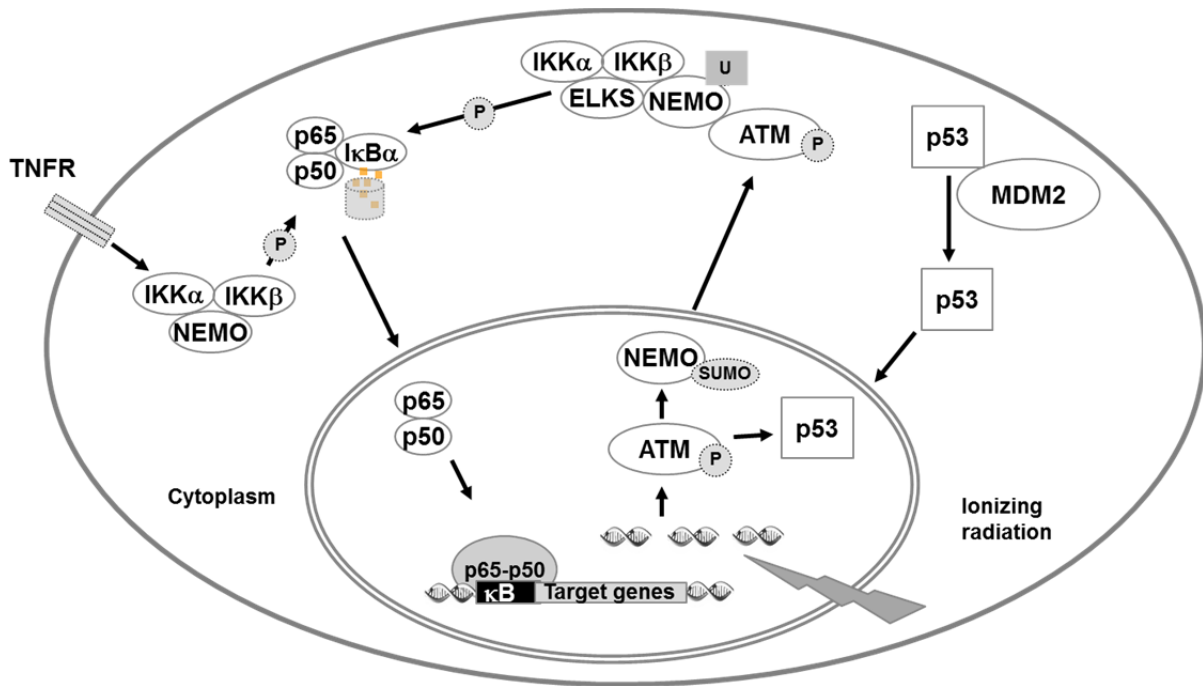


**Figure 5 Classical and genotoxic stress induced NF- $\kappa$ B pathway**

Ionizing radiation (e.g. X-rays,  $\gamma$ -radiation) or chemical (e.g. CPT, VP16) induced double stranded breaks (DSB) trigger the phosphorylation of ATM, which associates with SUMOylated NEMO in the nucleus, causing subsequent phosphorylation and ubiquitination of NEMO, and export it to the cytoplasm. In the cytoplasm, the complex of NEMO and phosphorylated ATM associates with the ELKS protein (essential regulatory subunit of IKK) and stimulates the activity of IKK $\beta$  containing complexes, causing degradation of I $\kappa$ B $\alpha$  and subsequent NF $\kappa$ B translocation to the nucleus. The binding of TNF- $\alpha$  to TNF-R also leads to the rapid activation of IKK and subsequent translocation of NF- $\kappa$ B sub-units p50:p65 to the nucleus. The p50:p65 complex binds to the  $\kappa$ B binding sites and regulates the transcription of downstream genes. The classical pathway starts with binding of the corresponding ligands to surface cytokine receptors, such as TNF- $\alpha$  to TNFR and results via adaptor proteins in activation of the IKK complex. At this stage, genotoxic stress induced and classical pathways converge (Ghosh and Hayden 2012; Ghosh and Hayden 2008).

### 1.3.8 Down-stream events after NF- $\kappa$ B activation

The nuclear translocation of NF- $\kappa$ B dimers is a critical step in NF- $\kappa$ B signaling cascades and can provide information on the reaction kinetics and damage response. The NF- $\kappa$ B activity is also essential for p53-mediated apoptosis and initiation of cell cycle arrest in response to DNA damage. The possible down-stream events of NF- $\kappa$ B pathway activation following DNA damage are binding of NF- $\kappa$ B to  $\kappa$ B or  $\kappa$ B-like DNA motifs (NF- $\kappa$ B-responsive elements, NREs) with the consensus sequence GGGRNNN(N)YCC<sup>8</sup> and initiating NF- $\kappa$ B target gene transcription. NREs

<sup>8</sup> N, any nucleotide, R, purine, Y, pyrimidine

have been identified in the promoter or enhancer regions of more than 200 genes including growth factors, pro-inflammatory enzymes (COX-2, iNOS), pro-inflammatory cytokines (TNF- $\alpha$ , IL-1, IL-6), chemokines (IL-8/CXCL8; monocyte chemoattractant cytokine 1, MCP-1/CCL2), angiogenic factors (vascular endothelial growth factor, VEGF), degradative enzymes (matrix metalloproteinases, MMPs) and adhesion molecules (intercellular adhesion molecule-1, ICAM-1; vascular cell adhesion molecule-1, VCAM-1; E-selectin), pro- or anti-apoptotic gene products (e.g. Bcl-2, bcl-XL) and a number of I $\kappa$ Bs. These target genes are involved in inflammation, innate immune responses, angiogenesis, tumor progression and metastasis in various cancers, and fibrosis (Duffey *et al.* 1999; Habelhah 2010; Shen and Tergaonkar 2009). Moreover, the regulation of MMPs plays an important role through degradation of extracellular matrix proteins, which protects the integrity of cell membranes and promotes the proliferation and migration of tumor cells. Furthermore, up-regulation of NFKBIA, encoding I $\kappa$ B $\alpha$ , initiates a negative feedback loop. Up to now, it is not clear to what extent the different target genes are activated in response to different doses and qualities of ionizing radiation.

### **1.3.9 Role of NF- $\kappa$ B and cytokines in the bystander effect**

Ionizing radiation induces signals that alter the survival and the response of un-irradiated cells. Since NF- $\kappa$ B is an important transcription factor for expression of many genes, it might participate in the bystander response. There is evidence suggesting a role of ionizing radiation in inducing NF- $\kappa$ B activation in both directly and indirectly (not exposed to radiation) irradiated cells (Aravindan *et al.* 2014). Down-regulating NF- $\kappa$ B by using inhibitors of I $\kappa$ B kinase (IKK) also efficiently down-regulates expression of bystander markers COX-2 and iNOS in both directly and indirectly irradiated fibroblasts providing evidence for the role of NF- $\kappa$ B in the bystander effect (Zhou *et al.* 2008).

However, p53 does not play a role in bystander effects since cells without functional p53 show large bystander response in CHO cells (Zhou *et al.* 2005). Activation of NF- $\kappa$ B, c-Jun N-terminal kinase (JNK) and extracellular signal-related kinase (ERK) in the exposed population suggests activation of these stress-inducible signaling pathways in bystander cells (Azzam *et al.* 2002). Furthermore, ionizing irradiation



exposure to fibroblasts induces TNF- $\alpha$  and IL-1 $\beta$  which also controls COX-2 expression (Zhou *et al.* 2008).

#### **1.4 Aim of the study**

NF- $\kappa$ B is a ubiquitous transcription factor that is activated by ionizing radiation exposure and was shown to play a role in cellular survival. A specific subpathway, the genotoxic stress induced pathway, was demonstrated to be responsible for this activation. While low LET radiation activates NF- $\kappa$ B only at high doses, it was recently revealed that NF- $\kappa$ B is activated by much lower doses in a specific range of LET (~100-300 keV/ $\mu$ m) which is relevant for carbon ion tumor therapy and to which astronauts are exposed in space. The role of this strong NF- $\kappa$ B activation in the cellular radiation response to heavy ions is unknown, specifically the profile of up-regulated NF- $\kappa$ B target genes.

This study is conducted to investigate, for the first time, the expression of downstream target genes of NF- $\kappa$ B in human embryonic kidney (HEK) cells after exposure to heavy ions, including  $^{36}\text{Ar}$ ,  $^{208}\text{Pb}$ ,  $^{13}\text{C}$ ,  $^{22}\text{Ne}$ ,  $^{58}\text{Ni}$ ,  $^{16}\text{O}$ , and  $^{48}\text{Ti}$ , of different radiation qualities and broad LET range (0.3 - 10000 keV/ $\mu$ m). To understand this gene expression regulation in the context of cellular radiation response, it was necessary to determine the effect of LET in different cellular responses (cell survival, cell cycle and DNA damage response including NF- $\kappa$ B activation). The role of NF- $\kappa$ B in the cellular radiation response leading to cell cycle arrest or cell death was investigated by knock down of the NF- $\kappa$ B subunit p65 and NF- $\kappa$ B activation prior to irradiation.

This study contributes to the understanding of the cellular radiation response to heavy ions and thereby helps to develop protective countermeasures for astronauts during long term space missions and to mitigate radioresistance of tumors in cancer radiotherapy.

## 2 Materials and methods

### 2.1 Materials

#### 2.1.1 Equipment

The equipments used for this study are listed up in **Table 3**.

**Table 3** Equipments and suppliers

Equipment	Supplier
Autoclave	Systec 2540-EL, Systec GmbH, Wetzlar, Germany
Centrifuge	Multifuge 3 S-R, Thermo Scientific, Schwerte, Germany
CO <sub>2</sub> incubator	Heraeus Jubilee Edition, Thermo Fisher Scientific, Germany
Digital camera	Mrc5, Carl Zeiss AG, Oberkochen, Germany
Dosimeter	UNIDOSwebline, PTW, Freiburg, Germany
Flow cytometer	FACScan, BD Biosciences, Heidelberg, Germany
Fluorescence microscope	Zeiss Axio Imager M2, Göttingen, Germany
Fuchs-Rosenthal counting chamber	Brand, Wertheim, Germany
Inverse microscope	Axiovert 35, Carl Zeiss AG, Oberkochen, Germany
Laminar flow hood type 2	Herasafe, Thermo Fisher Scientific, Schwerte, Germany
Microelectrophoresis unit	Bioanalyzer 2100r, Agilent Technologies, Karlsruhe, Germany
Microplate Fluorescence Reader	Lambda Fluoro 320, Eurofins MWG Operon, Ebersberg, Germany
Pipette devices (10, 100, 1000 µl)	Eppendorf Ltd, Hamburg, Germany
Real-time thermocycler	DNA Engine Opticon2 System, BioRad Ltd., Munich, Germany
Shaking incubator	Multitron Infors Ltd, Einsbach, Germany
Spectrophotometer	Thermo Scientific, Schwerte, Germany
X-ray tube	Gulmay RS225, X-strahl, Surrey, United Kingdom

### 2.1.2 Consumables

Consumable materials are shown in **Table 4**.

**Table 4 Consumables and manufacturers**

Vessel	Manufacturer
96-well plate for qPCR	4titude Ltd, Berlin, Germany
96-well strip plate (1x8 well strips)	Corning Costar, New York, USA
Tissue culture flasks 80 cm <sup>2</sup> and 25 cm <sup>2</sup>	Nunc, Wiesbaden, Germany
Cell scraper	TPP, Trasadingen, Switzerland
Centrifuge tubes 15 ml and 50 ml (Falcon)	Nunc, Wiesbaden, Germany
Cryotubes 1.8 ml	Nunc, Wiesbaden, Germany
Petri dishes Ø 3, 6, 10, 14 cm	Nunc, Wiesbaden, Germany
Pipet tips (10, 100, 1000 µl)	Eppendorf Ltd., Hamburg, Germany
Powder-free Latex Exam Gloves	Kimberly Clark, Neenah, WI, USA
qPCR adhesive seal sheets	4titude Ltd, Berlin, Germany
Safe-Lock tubes 0.5 ml; 1.5 ml; 2.0 ml	Eppendorf Ltd., Hamburg, Germany
Sterile filter 0.22 µm	Millipore Corp., Bedford, USA
Syringe, sterile, 10 ml	Terumo Syringe, Leuven, Belgium
Tissue culture plates with 6 and 24 wells	Nunc, Wiesbaden, Germany

### 2.1.3 Kits and assays

**Table 5** displays the kits used in this study.

**Table 5 Reagent kits**

Kit	Manufacturer
Human RT2 Profiler™ PCR Arrays	SABiosciences, Frederick, MD, USA
RT2 RNA Quality Control (QC) PCR Array	SABiosciences, Frederick, MD, USA
Iscrip cDNA synthesis kit	Bio-Rad, Munich, Germany
Platinum® SYBR®Green qPCR SuperMix-UDG kit	Invitrogen, Carlsbad, California, USA
QIAprep Miniprep	QIAGEN, Hilden, Germany
RNA 6000 Nano Assay	Agilent Technologies, Böblingen, Germany
RNeasy Plus Mini Kit	QIAGEN, Hilden, Germany
RT2 First strand kit	SABiosciences, Frederick, MD, USA

### 2.1.4 Chemicals

Chemicals for routine use were ordered by Sigma-Aldrich Steinheim, Germany, unless otherwise stated (**Table 6**).

**Table 6 Chemicals and suppliers**

Chemical	Supplier
4',6-Diamidino-2-phenylindole	Sigma Aldrich, Steinheim, Germany
Amphotericin B (250 µg/ml)	PAN Biotech, Aidenbach, Germany
Ampicillin-Sodium-Salt	Sigma-Aldrich, Steinheim, Germany
Betaine	Sigma-Aldrich, Steinheim, Germany
Bisbenzimidazole ( $C_{27}H_{28}N_6O \cdot 3HCl \cdot 3H_2O$ )	Sigma Aldrich, Steinheim, Germany
Bovine Serum Albumin	Sigma Aldrich, Steinheim, Germany
Crystal violet	Merck, Darmstadt, Germany
Ethanol 99,8 % vol	Merck, Darmstadt, Germany
Fetal Bovine Serum (FBS)	Biochrom AG, Berlin, Germany
Formaldehyde 37 %	Merck, Darmstadt, Germany
Helipur H plus, disinfectant	B. Braun, Melsungen, Germany
Isopropanol	VWR, Darmstadt, Germany
Kanamycin	Biochrom AG, Berlin, Germany
LB-agar	Biochrom GmbH, Berlin, Germany
LB-broth	Biochrom GmbH, Berlin, Germany
L-Glutamine	PAN Biotech, Aidenbach, Germany
Magnesium chloride	Merck, Darmstadt, Germany
Mounting medium	Invitrogen, California, USA
Neomycin / Bacitracin	Biochrom AG, Berlin, Germany
One-Step RT-PCR Kit	Invitrogen, Carlsbad, USA
Penicillin / Streptomycin	PAN Biotech, Aidenbach, Germany
Potassium chloride	Merck Darmstadt, Germany
Propidium iodide	Invitrogen, Carlsbad, USA
Ribonuclease (RNase)	Calbiochem, La Jolla, USA
RNase-Free DNase Set	QIAGEN, Hilden, Germany
Sodium chloride	Merck Darmstadt, Germany
Sodium dihydrogenphosphate	Merck Darmstadt, Germany
β-Mercaptoethanol	Sigma Aldrich, Steinheim, Germany

**Table 6 Chemicals and suppliers (continued)**

Chemical	Supplier
Triton X-100	Sigma Aldrich, Steinheim, Germany
Trypsin/EDTA	PAN Biotech, Aidenbach, Germany
$\alpha$ -MEM medium	PAN Biotech, Aidenbach, Germany
$\beta$ -D-Glucose-Monohydrate	Merck, Darmstadt, Germany

### 2.1.5 Cell lines and plasmids

The cell lines used in this work are listed in **Table 7**. The parental cell line HEK/293 used for generation of the reporter assays was derived from human embryonic kidney cells (Graham *et al.* 1977).

HEK/293 cells were stably transfected with the vector pNF $\kappa$ B-DD-tdTomato (**Figure 6 A**) carrying the destabilized variant of the reporter gene tdTomato to generate the HEK-pNF $\kappa$ B-DD-tdTomato reporter cell line for reporting NF- $\kappa$ B activation. DD-tdTomato expression is controlled by a synthetic promoter, made up of four NF- $\kappa$ B binding sites (5'-GGGAATTTCC-3') and the RNA polymerase binding site from the thymidine kinase promoter. The vector pNF $\kappa$ B-DD-tdTomato contains the kanamycin/neomycin resistance gene under the control of a bacterial promoter and the SV40 enhancer for enabling clonal selection.

**Table 7 Cell lines**

Cell line	Origin
HEK/293	American Tissue Culture Collection (ATCC), CRL-1573, LGC Standards, Wesel, Germany
HEK-pNF- $\kappa$ B-DD-tdTomato-C8	Current project
HEK-pNF- $\kappa$ B-d2EGFP/Neo L2	(Hellweg <i>et al.</i> 2003)
HEK shRNA RelA	(Koch 2013)

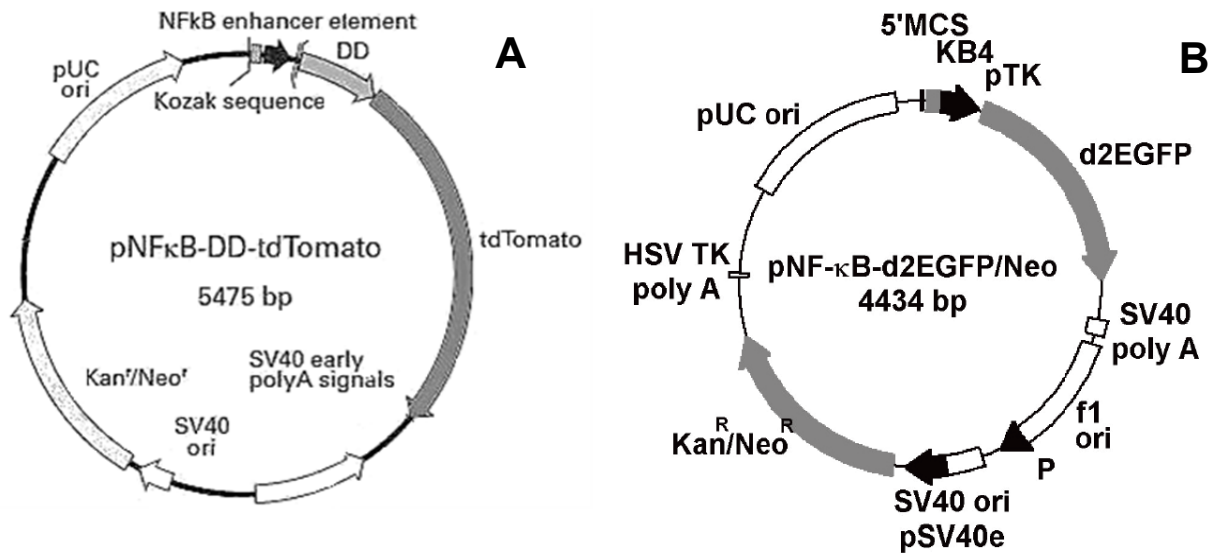


**Figure 6** Vector maps of pNF $\kappa$ B-DD-tdTomato (A) and pNF- $\kappa$ B-d2EGFP/Neo (B)

The pNF $\kappa$ B-DD-tdTomato and pNF- $\kappa$ B-d2EGFP/Neo reporter plasmids were used for stable transfection of HEK/293 cells. The reporter genes (DD-tdTomato, d2EGFP) are under control of an NF- $\kappa$ B-dependent promoter to report NF- $\kappa$ B activation. The promoter contains 4x NF- $\kappa$ B response elements ( $\kappa$ B4). The pNF- $\kappa$ B-d2EGFP/Neo plasmid was constructed by Hellweg *et al.* (2003) and carries the destabilized EGFP (d2EGFP) reporter gene whereas pNF $\kappa$ B-DD-tdTomato was obtained from Clontech and carries the destabilized tdTomato (DD-tdTomato) reporter gene.

The cell line HEK-pNF- $\kappa$ B-d2EGFP/Neo L2 carrying the vector pNF- $\kappa$ B-d2EGFP/Neo (Figure 6 B), containing four NF- $\kappa$ B binding sites that control destabilized Enhanced Green Fluorescent Protein (d2EGFP) expression, was already constructed (Hellweg *et al.* 2003) and used in heavy ion experiments.

The HEK shRNA RelA cell line was constructed by transfecting HEK-pNF- $\kappa$ B-d2EGFP/Neo L2 cells with a SureSilencing™ shRNA plasmid targeting RelA (p65) subunit of NF- $\kappa$ B with a RelA knockdown (KD) level of 83.1 % (Koch 2013). This cell line was used to determine the role of NF- $\kappa$ B in cellular survival and cell cycle experiments.

### 2.1.6 Media, buffers and solutions

Media, buffers, fixation solutions and other solutions were prepared as described in **Table 8** to **Table 13**.

**Table 8 Media for bacterial growth**

Item	Reagent
Luria Bertani (LB)-medium	20 g LB powder 1000 ml <i>Aqua dest.</i> Autoclaved Stored at 4 °C.
Luria Bertani (LB)-agar	35 g LB agar 1000 ml <i>Aqua dest.</i> Autoclaved 50 µg / ml Kanamycin Stored at room temperature.

Cell culture medium, which is shown in **Table 9**, was completed by adding fetal bovine serum (FBS) and glucose in order to provide growth factors and antibiotics to reduce the risk of contamination with bacteria and fungi.

For use, PBS 5x (**Table 10**) was diluted 1:5 with autoclaved deionized water. PBS 1x was stored at 4 °C.

**Table 9 Media for cell culture**

Item	Reagent
Culture Medium α-MEM	500 ml α-MEM 10 % (v/v) FBS 5 % (v/v) Penicillin / Streptomycin 5 % (v/v) L-Glutamine 5 % (v/v) Amphotericin 5.5 mmol/l Glucose Stored at 4 °C.
Selection Medium α-MEM	500 ml Culture Medium α-MEM 0.6 mg/ml G418 Stored at 4 °C.
Freezing Medium	Culture Medium α-MEM 20 % (v/v) FBS 10 % (v/v) Dimethyl sulfoxide (DMSO) Freshly prepared for use.

**Table 10 Buffers**

Item	Reagent
Phosphate buffered saline (PBS) 5x	80 g NaCl 2 g KCl 14.4 g Na <sub>2</sub> HPO <sub>4</sub> × 2H <sub>2</sub> O 2 g KH <sub>2</sub> PO <sub>4</sub> 2000 ml A. dest. pH 7.2 Stored at -20 °C.
Tris/Borate/EDTA (TBE) buffer 10x	1 mol/l TRIS (hydroxymethyl) amino ethane 0.97 mol/l Boric acid 0.02 mol/l EDTA pH 8.3 Stored at room temperature.

**Table 11 Fixation solutions**

Item	Reagent
Formaldehyde fixation solution	10 ml 37 % Formaldehyde stock solution 90 ml PBS Stored at 4 °C.
100 % Ethanol	100 ml Ethanol (100%) Stored at -20 °C.

**Table 12 Staining solutions**

Item	Reagent
Propidium iodide (PI) staining solution	50 µg/ml RNase A 0.1 % (v/v) Triton X-100 20 µg/ml PI in PBS Stored at 4 °C.
DAPI Staining solution	0.1 µg/ml DAPI in PBS Stored at -20 °C.
Crystal Violet staining solution	0.5 g Crystal violet 50 ml Formaldehyde 37% 500 ml Tap water Stored at room temperature.
Bisbenzimidide (Hoechst 33342) 10 µmol/l	12.5 µl Bisbenzimidide (8 mmol/l) 10 ml in PBS Stored at room temperature in dark.



**Table 13 Other solutions**

Item	Reagent
Trypsin/EDTA (0.5% trypsin, 0.2% EDTA)	10 ml Trypsin/EDTA (0.5 % trypsin, 0.2 % EDTA) 90 ml PBS, stored at 4 °C.
Poly-D-lysine (0.01 mg/ml)	100 µl Poly-D-lysin (1 mg/ml) 10 ml <i>Aqua dest.</i> , stored at 4 °C.
TNF- $\alpha$ stock solution (10 µg/ml)	Dissolved in 1% BSA Aliquots of 50 µl, stored at -80 °C.

### 2.1.7 Software

The computer programs used to edit and evaluate data are shown in **Table 14**.

**Table 14 Software and suppliers**

Item	Purpose / use	Supplier
2100 Expert Software for Bioanalyzer	Assessment of integrity of RNA	Agilent Technologies, Karlsbrunn, Germany
Axiovision	Measurement of the area of cell and cell nucleus	Carl Zeiss AG, Oberkochen, Germany
Basic Local Alignment Search Tool (BLAST)	Primer design	<a href="http://www.ncbi.nlm.nih.gov/tools/primer-blast">http://www.ncbi.nlm.nih.gov/tools/primer-blast</a>
CFA_DOSE V1.04 and CFA_AllData V1.04	Dose effect curve analysis	Excel macrosheets developed by Dr. Christa Baumstark-Khan
Flowing Software version 2.5.1	Cellular DNA content calculation in different cell cycle phases	Free online software, <a href="http://www.flowingsoftware.com">http://www.flowingsoftware.com</a>
Image Processing and Analysis in Java (ImageJ)	Image analysis	Free online software, <a href="http://rsbweb.nih.gov/ij/download.html">http://rsbweb.nih.gov/ij/download.html</a>
Opticon 2	For real-time PCR detection	Bio-Rad, Munich, Germany
Relative Expression Software Tool - Multiple Condition Solver (REST-MCS©) - version 1	Determination of relative expression levels of investigated genes	W. Pfaffl and G.P. Horgan, Technical University (TU) Munich, Germany
Sigma Plot 12.0	Data analysis software	SPSS, Munich, Germany

## **2.2 Methods**

### **2.2.1 Routine tissue culture methods**

#### **2.2.1.1 Cell culture conditions**

Cell culture work was conducted in a biosafety level 1 (BSL-1) laboratory under sterile conditions in a laminar flow hood. The laminar flow hood was cleaned with isopropanol (70 %) before and after use. The solutions and media used were stored at 4 °C and were warmed to 37 °C in a water bath prior to use. The cell lines were propagated as monolayer cultures in 75 cm<sup>2</sup> tissue culture flasks and grown by incubating in a CO<sub>2</sub>-gassed incubator under standard conditions (37 °C, 5 % CO<sub>2</sub>, 95 % air and saturated humidity).

The cell lines were screened regularly for Mycoplasma contamination by collecting 500 µl supernatant from every cell line. The frozen supernatant was sent to the Leibniz-Institute DSMZ-German Collection of Microorganisms and Cell Cultures (Deutsche Sammlung von Mikroorganismen und Zellkulturen, Braunschweig, Germany) where a polymerase chain reaction (PCR) was performed to amplify the 16S RNA of mycoplasma, if present. Only mycoplasma-free cells were used for experiments.

#### **2.2.1.2 Cell line propagation**

The HEK/293 cells were cultured according to standard procedures in 75 cm<sup>2</sup> flasks in  $\alpha$ -medium (modified MEM, Pan-Biotech, Germany) with 10 % FBS under standard conditions. Consequently, cell lines were washed with PBS before detaching with 0.05% trypsin in 0.02% EDTA solution. After detachment, cells were suspended in culture medium. For determining the number of cells, they were diluted 1:20 in PBS and counted in a Fuchs-Rosenthal counting chamber.

Seeding was subsequently performed at a density of  $3 \times 10^4$  cells/cm<sup>2</sup> in new flasks every week. Medium change was performed every 4 days with 15 ml of medium.

#### **2.2.1.3 Poly-D-lysine coating of cell culture vessels**

For irradiation experiments and transporting cells to the heavy ion accelerator laboratories, the tissue culture vessels (Petri dishes, tissue culture flasks, 96- and 24-well plates) were coated with poly-D-lysine which facilitates the attachment of cells to surfaces and inhibits detachment of HEK cells that usually occurs at temperatures

below 37 °C. The stock solution of poly-D-lysine (1 mg/ml) was diluted to 0.01 mg/ml poly-D-lysine with sterile H<sub>2</sub>O and pipetted into tissue culture vessels (1.6 µg/cm<sup>2</sup>) covering the whole surface. After 10 minutes (min) of incubation at room temperature the tissue culture vessels were washed three times with autoclaved *A. dest.* and stored at 4 °C until seeding of cells (no longer than 10 days).

#### **2.2.1.4 Cryopreservation of cells**

Cell lines or transfected cell clones were preserved in liquid nitrogen at -196 °C in presence of cryoprotective medium. Cell lines were trypsinized and centrifuged for 5 min at room temperature and 80×g. The pellet was re-suspended in freshly prepared freezing medium with a cell concentration of 1×10<sup>6</sup> cells/ml and 1 ml cell suspension was aliquoted into each cryotube. To minimize cell damage by formation of ice needles which predominate at freezing temperature around -5 °C, cells were cooled down to -80 °C with a speed of -1 °C/min, in a box containing 100 % isopropanol, before storage in liquid nitrogen.

#### **2.2.1.5 Thawing cells from liquid nitrogen stocks**

The cryotubes were taken out from liquid N<sub>2</sub> following standard safety procedures and thawed at 37 °C. With disappearance of the last ice in the cryotube, the contents from vials were immediately transferred into 75 cm<sup>2</sup> flasks filled with 20 ml warm culture medium, thereby diluting DMSO to 0.5 %. Cells were allowed to attach to the surface for 18 h and medium was exchanged afterwards to remove residual DMSO.

### **2.2.2 Radiation exposure**

#### **2.2.2.1 Exposure to sparsely ionizing X-rays**

Irradiation with low-LET X-rays (0.3-3.0 keV/µm) was performed at DLR by using the X-ray exposure facility Xstrahl RS 225 Molecular Research System (Gulmay Medical, Surrey, United Kingdom) operated at a voltage of 200 kV and a current of 15 mA (**Figure 7**). The distance of the sample from the X-ray source was set to 450 mm to provide a constant dose rate of 1.0 Gy/min. To eliminate soft X-rays, a copper (Cu) filter (Filter No. 5) with a thickness of 0.5 mm was used. The temperature inside the irradiation chamber was set to 37 °C. Cells in exponential growth phase (at day 4) were directly exposed either in flasks or in plates, the cell layer being perpendicular to the X-rays. After X-irradiation cells were further incubated at standard conditions

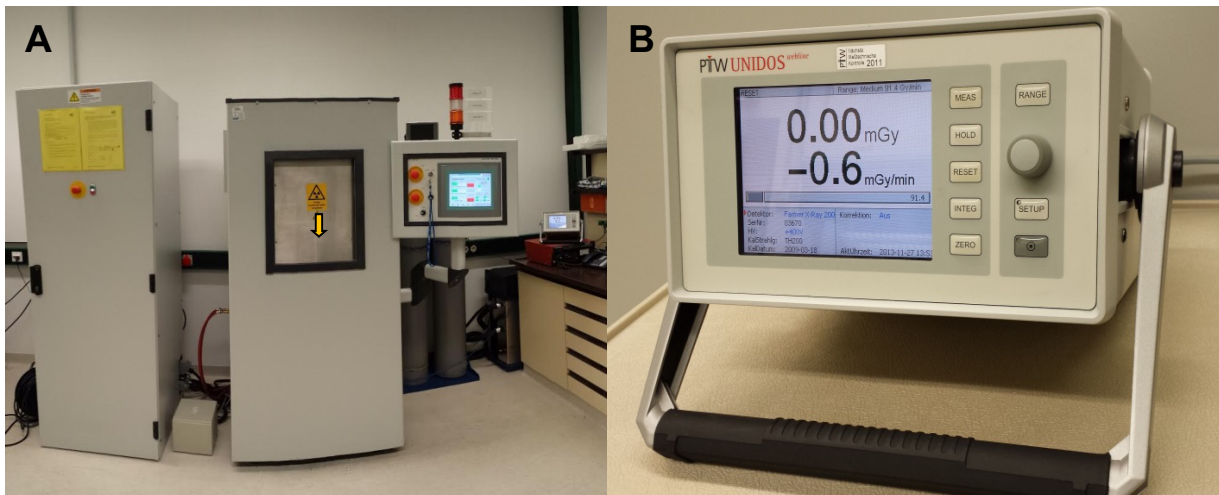


**Figure 7 X-ray exposure facility**

The Gulmay XStrahl RS 225 consists of a generator element, an exposure element and a control panel (A, from left to right). The UNIDOS weblin dosimeter was used for dose and dose rate determination (B). The ionization chamber of the dosimeter was positioned in the center of the irradiation table in the irradiation chamber (A, yellow arrow, indicates also the irradiation direction).

and harvested for analyses at various time points according to experimental requirements mentioned below.

#### 2.2.2.2 Exposure to densely ionizing heavy ions

The exposures to the heavy ions  $^{36}\text{Ar}$ ,  $^{208}\text{Pb}$ ,  $^{13}\text{C}$ ,  $^{22}\text{Ne}$ ,  $^{58}\text{Ni}$ ,  $^{16}\text{O}$ , and  $^{48}\text{Ti}$  (Table 15) were performed at GANIL in Caen, France and at the GSI facility in Darmstadt, Germany (Figure 8). Two days before irradiation, the cells were seeded into Nunc 25 cm<sup>2</sup> flasks (GSI) or Iwaki 25 cm<sup>2</sup> flasks (GANIL) at a density of  $3 \times 10^4$  cells/cm<sup>2</sup>. Cell lines were allowed to reach to a density of about 50% at the time of irradiation.

At GANIL, the samples were placed in an upright position in a multiple sample holder in front of the beam line. At GSI, the samples were positioned in equal distance on a conveyor belt in front of the beam exit window.

In order to prevent desiccation of the cells during exposure the flasks were filled with 50 ml  $\alpha$ -MEM culture medium. After irradiation, samples were brought back to the laboratory in a box filled with prewarmed coolpacks, medium was removed and 5 ml  $\alpha$ -MEM culture medium was added. Cells were incubated again in the incubator until harvested at different time points for analysis of radiation response.

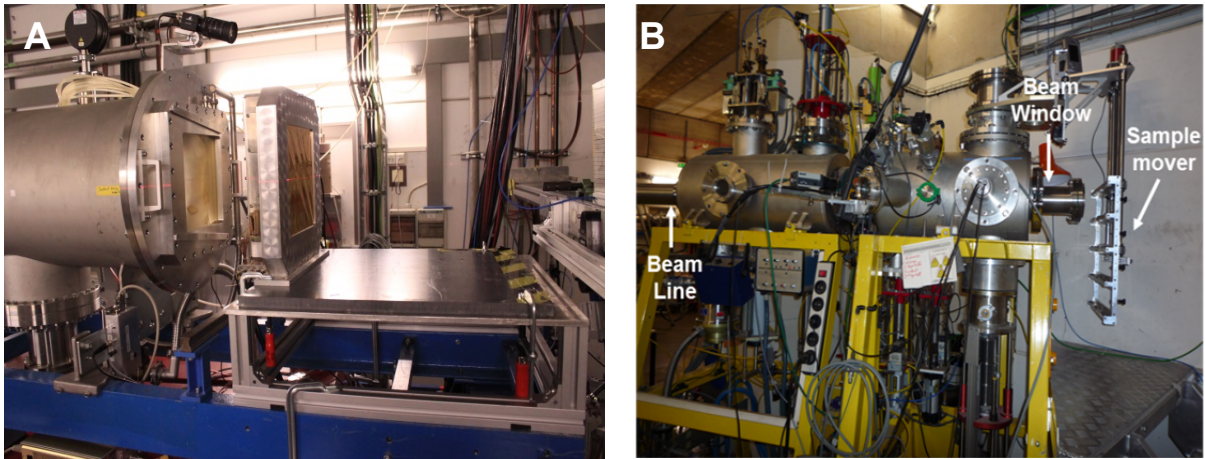


**Figure 8** Heavy ion beam lines at GSI (A) and GANIL (B)

For heavy ion exposure, cells were grown in 25 cm<sup>2</sup> tissue culture flasks and arranged in front of the ion beam upright on a conveyor belt (A) or a specially designed sample mover (B).

Dosimetry was performed by the staff at the accelerator facilities. Each flask was irradiated with a fixed dose rate (~1 Gy/min). The fluence for heavy ions (P/cm<sup>2</sup>) was converted to dose (Gy) by **Equation 1** (Wulf *et al.* 1985):

$$\text{Dose [Gy]} = 1.6 \times 10^{-9} \times \text{LET [keV/\mu m]} \times F [\text{P/cm}^2] \quad \text{Equation 1}$$

#### 2.2.2.2.1 Calculation of average heavy ions hits per cell nucleus

To calculate the average hits per cell nucleus, the area of the HEK cell nucleus was determined in bisbenzimidazole-stained cells (0.5 μmol/l for 45 min). Photographs of the stained nuclei were taken by means of the digital camera Mrx5 which was adapted to the fluorescence microscope Axiovert 135 (Carl Zeiss, Oberkochen, Germany). The nucleus area (A) of HEK cells was measured using the software Axiovision and yielded an average area of 142 ± 23 μm<sup>2</sup> (Hellweg *et al.* 2011b). The expected fluence (F<sub>e</sub>) per cell nucleus was calculated according to the **Equation 2**:

$$F_e [\text{P/cell nucleus}] = 10^{-8} * A [\mu\text{m}^2] * F [\text{P/cm}^2] \quad \text{Equation 2}$$

The Poisson distribution of the heavy ion hits in the cell nuclei was calculated according to the **Equation 3** and the fractions of un-hit and hit cell nuclei were summed up:

$$f_x(x) = \frac{F_e^x}{x!} e^{-F_e}, \quad x = 0, 1, 2, 3, \dots \quad \text{Equation 3}$$

**Table 15 Heavy ions used in this study**

Ion	Location	Energy (MeV/n)	Energy on target <sup>a</sup> (MeV/n)	LET (keV/μm)	Dose range (Gy)
X-rays	DLR	0.2	0.2	0.5 - 3	0.5 - 32.0
<sup>13</sup> C	GSI	100	95	10	0.5 - 5.0
<sup>13</sup> C	GANIL	75	71	33	0.5 - 16.0
<sup>16</sup> O	GANIL	95	91	51	0.2 - 30.0
<sup>13</sup> C	GANIL	35	28	75	0.2 - 16.0
<sup>22</sup> Ne	GANIL	80	75	92	0.2 - 12.0
<sup>48</sup> Ti	GSI	1000	996	108	0.5 - 4.0
<sup>58</sup> Ni	GSI	1000	985	175	0.5 - 16.0
<sup>36</sup> Ar	GANIL	95	85	272	0.2 - 34.0
<sup>58</sup> Ni	GANIL	75	56	905	1.0 - 23.6
<sup>209</sup> Pb	GANIL	29	20	9674	1.0 - 62.0

<sup>a</sup> Effective irradiation energy at the cell monolayer after losing of primary beam energy by passage through two detector foils, the exit window, air (GANIL: 1 cm, GSI: 100 cm) and the bottom of the culture vessel (1200 mm polystyrene).

## 2.2.3 Analysis of cellular radiation response

### 2.2.3.1 Colony forming ability test

The colony forming ability (CFA) assay is the gold standard method for determining the colony forming ability (Puck and Marcus 1956). Cells were seeded in 25 cm<sup>2</sup> tissue culture flasks and irradiated with different doses (2.2.2). Two different protocols were followed: Cells were plated in 6 cm petri dishes either immediately after radiation exposure (**immediate plating**) or after a 24 h recovery period (**late plating**). During this recovery period cells have the chance to repair DNA damage and to recover from potentially lethal damage. This would result in a better survival for the late plated cells compared to early plated cells.

Cells were trypsinized, counted and a defined number of cells were transferred in 50 ml centrifuge tubes containing 30 ml culture medium. The seeding density was calculated by the plating efficiency (PE) and the anticipated lethal effects per dose. For statistical reasons, plating was performed with six Petri dishes (6 cm<sup>2</sup>) per dose. After 14-21 days of incubation, medium was aspirated, petri dishes were gently washed with PBS, and grown colonies were fixed and stained with 5 ml of 3.7 %

formaldehyde containing crystal violet staining solution. After 30-60 min, the staining solution was removed and the colonies were gently washed with tap water. The Petri dishes were dried overnight, colonies were counted and survival was calculated as described below.

### 2.2.3.1.1 Calculation of dose effect curves

A dose response curve (**Figure 9**) is a plot of an observed biological effect versus dose. For the dose effect curve of survival after radiation exposure, the dose is plotted on a linear scale and the surviving fraction on a logarithmic scale. Excel macrosheets (CFA\_DOSE V1.04 for analyzing single experiments, CFA\_AllData V1.04 for calculating dose-effect curves from repeated experiments and comparing different dose-effect curves, both developed by Dr. Christa Baumstark-Khan) were used to calculate plating efficiency (PE), relative cellular survival (S) and its natural log (ln S).

The PE was obtained from the ratio of the colony number and the number of seeded cells as shown in **Equation 4**

$$PE = \frac{\text{Colonies counted}}{\text{Cells seeded}} \quad \text{Equation 4}$$

The relative survival ( $S_{\text{dose}}$ ) was calculated by dividing the PE of irradiated cells ( $PE_{\text{dose}}$ ) by the PE of the mock irradiated control cells ( $PE_{\text{dose}=0}$ ) according to **Equation 5**.

$$S_{\text{dose}} = \frac{PE_{\text{dose}}}{PE_{\text{dose}=0}} \quad \text{Equation 5}$$

In the CFA macrosheets, the relative survival and its natural logarithm (ln S) from the plating efficiencies for each colony count was calculated according to the single-hit multi-target model (Kiefer 1971).

$$S = 1 - \left( 1 - e^{-\frac{D}{D_0}} \right)^n \quad \text{Equation 6}$$

The equation can be simplified to the following regression line equation for higher doses as shown in **Equation 7**:

$$\ln(S) = \frac{-D}{D_0} + \ln(n) \quad \text{Equation 7}$$

where  $D$  represents dose,  $D_0$  is the reciprocal value of the slope within the linear part of the curve and  $n$  is extrapolation number obtained by extrapolating the exponential part of the curve to the 100% survival line.

The slope  $v$  is also represented as shown in **Equation 8**.

$$v = -1/D_0 \quad \text{Equation 8}$$

To compare survival curves of different cell lines or exposure conditions, several parameters were used.  $D_0$ ,  $D_q$ , and  $n$  were calculated by using the following mathematical formula which was derived from the single-hit multi-target model as shown in **Equation 9**.

$$D_q = D_0 \times \ln n \quad \text{Equation 9}$$

$D_q$  is the quasi threshold dose which represents the width of the shoulder of the curve.

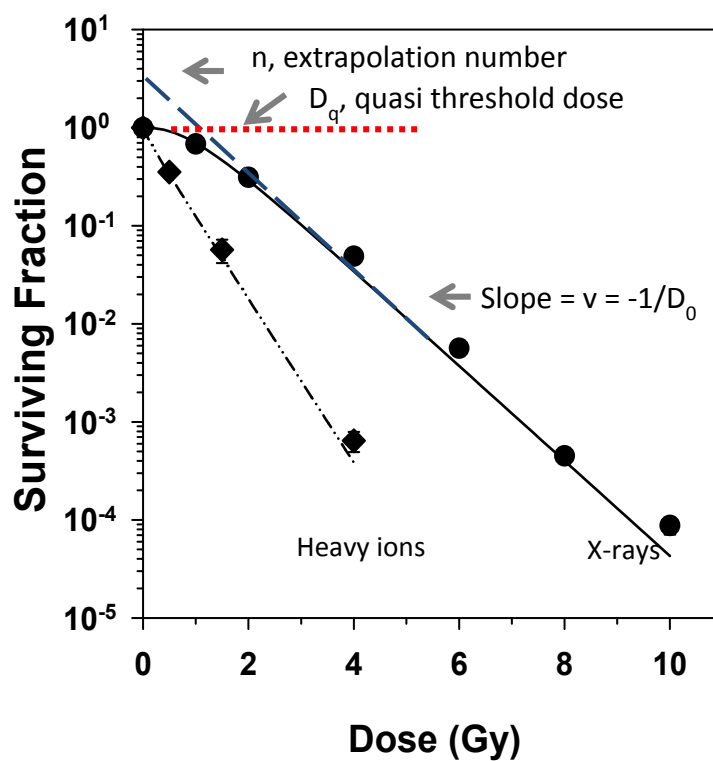


**Figure 9** Dose-effect curves calculated according to the single-hit multi-target model and their descriptive parameters slope  $v$ ,  $D_0$ ,  $D_q$  and  $n$

A dose-effect curve for low LET radiation (e.g. X-rays) shows a "shoulder" while a dose-effect curve for high LET radiation (e.g. heavy ions) shows a purely exponential decrease with increasing dose in a semi-logarithmic plot (survival fraction plotted on a logarithmic scale against dose on a linear scale).  $D_0$  is the negative reciprocal of the slope ( $v$ ) in the exponential part of the curve ( $D_0 = -1/v$ ). The intersection of this extrapolated curve with the 100% survival line (surviving fraction = 1) is the quasi threshold dose  $D_q$ . The extrapolation number  $n$  is calculated by extrapolation of the exponential part of the survival curve to dose = 0 (intercepts of the regression line with the y-axis).



### 2.2.3.1.2 Calculation of Relative Biological Effectiveness

The Relative Biological Effectiveness (RBE) of different radiation qualities is calculated by dividing the doses assumed to cause the same biological effect of the reference radiation (X-rays) and the test radiation. The RBE of survival reduction for each heavy ion species was calculated by dividing the  $D_0$  value for X-rays by the  $D_0$  value for the respective heavy ion (test radiation) (**Equation 10**).

$$\text{RBE}_{\text{Survival reduction}} = \frac{D_{0(\text{x-rays})} [\text{Gy}]}{D_{0(\text{test radiation})} [\text{Gy}]} \quad \text{Equation 10}$$

The RBE for NF- $\kappa$ B activation was calculated by the doses initiating a duplication of the reporter protein fluorescence 18 hours after irradiation in reporter cell lines. Doses initiating duplication ( $D_{2x}$ ) were derived from the regression line in the dose-effect curves of NF- $\kappa$ B activation. The RBE for NF- $\kappa$ B activation (RBE ( $D_{2x\text{NF-}\kappa\text{B}}$ )) was then calculated by dividing the absorbed dose of X-rays (reference radiation) by the absorbed dose of heavy ions (test radiation) inducing doubling of NF- $\kappa$ B activation (**Equation 11**).

$$\text{RBE}(D_{2x\text{NF}\kappa\text{B}}) = \frac{\text{Dose of reference radiation inducing biological effect} [\text{Gy}]}{\text{Dose of test radiation inducing biological effect} [\text{Gy}]} \quad \text{Equation 11}$$

### 2.2.3.2 Flow cytometry of fluorescent proteins

NF $\kappa$ B-dependent d2EGFP and DD-tdTomato expression was measured by flow cytometry. Cells were seeded in a density of  $3 \times 10^4$  cells/cm<sup>2</sup> and grown for 2 days to reach the exponential growth phase. At defined time points, cells were detached from the surface using trypsin and fixed with 3 ml cold 3.7% formaldehyde in PBS for 30 min at 4 °C. The FA was then diluted with PBS (1:3) and cells were stored at 4 °C. Prior to flow cytometric analysis, cells were centrifuged at 500×g for 5 min at room temperature and resuspended cells (in 1 ml PBS) were transferred to round-bottom tubes for flow cytometry.

Flow cytometry was performed in a fluorescence activated cell scanner (FACScan). Forward and sideward scatter (FSC, SSC) and fluorescence of the samples were measured with an argon laser (488 nm) as excitation source.  $2 \times 10^4$  cells were analyzed at a rate of 200–600 cells per second. Fluorescence was measured in fluorescence channels (FL-1: emission filter 530/30, FL-2: emission filter 585/42) and

depicted using Flowing software (V 2.5.1). FSC and SSC of the samples were displayed in a dot plot as a measure of cell size and granularity. In the FL-1 histogram, the markers d2EGFP<sup>(+)</sup> and d2EGFP<sup>(-)</sup> were set when the HEK-pNF- $\kappa$ Bd2EGFP/Neo L2 cell line was used. In FL-2 histogram, the markers DD-tdTomato<sup>(-)</sup> cells and DD-tdTomato<sup>(+)</sup> cells were set when the HEK-pNF $\kappa$ B-DD-tdTomato-C8 cell line was used. The population fractions displaying fluorescence intensities in the zone of marker DD-tdTomato<sup>(+)</sup> cells were used here as an example to show the analysis of the fluorescent cell population (**Figure 10**).

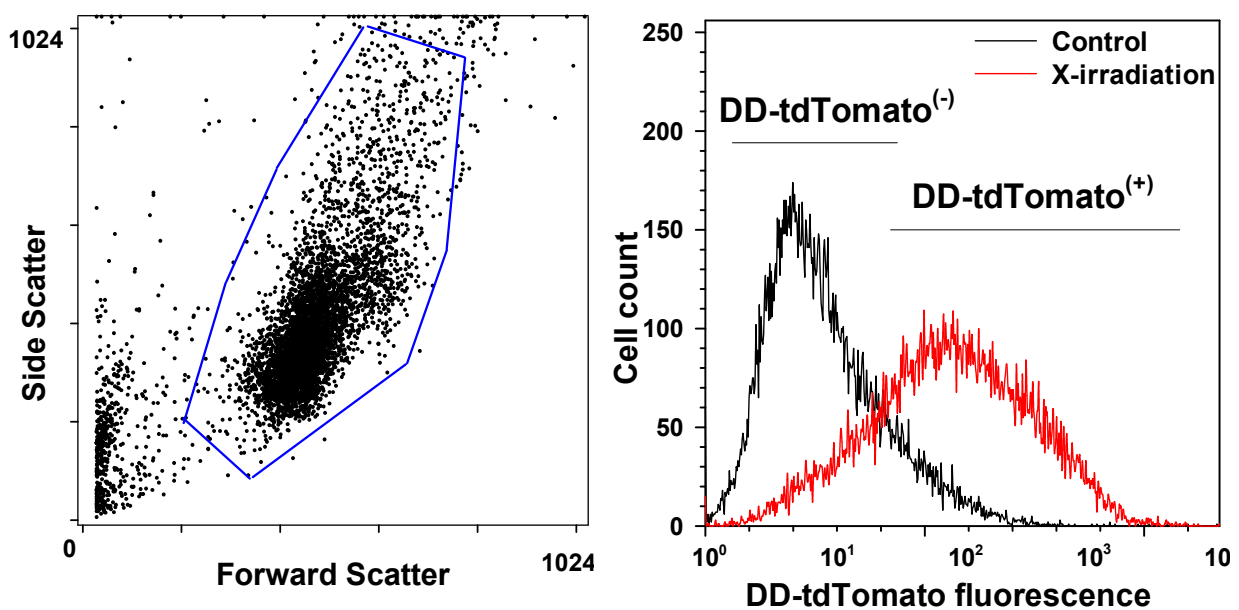


**Figure 10** Flow cytometry data analysis of NF- $\kappa$ B activation. Dot plot (A) and histogram (B) analyzed by Flowing software (V 2.5.1).

The dot plot (A) of a cell population was used to manually define a region (blue line) in respect to cell size (forward scatter) and granularity (side scatter). Events outside this region are not taken into account for further analysis. A threshold for the forward scatter was set in order to eliminate the debris.

The histogram (B) shows the DD-tdTomato fluorescence of the gated cell population. In the control sample, markers for DD-tdTomato<sup>(-)</sup> and DD-tdTomato<sup>(+)</sup> cells are set. The percentage of DD-tdTomato<sup>(+)</sup> cells was used as a measure of NF- $\kappa$ B activation. The red line in the graph represents a typical histogram of HEK-pNF- $\kappa$ B-DD-tdTomato-C8 cells 18 hours after X-irradiation (16 Gy).

### 2.2.3.3 Cell cycle analysis

For cell cycle analysis, cells were seeded in a density of  $3 \times 10^4$  cells/cm<sup>2</sup> and grown for 2 days until they reach the exponential growth phase. After X-irradiation samples were trypsinated with 1 ml trypsin and fixed in 3 ml ice-cold ethanol (100%) at specific time points. The fixed cell suspensions were stored at -20 °C for at least 24 h. Fixed samples were prepared for flow cytometry by adding two volumes of PBS (1:3 dilution of ethanol) and pelleted by centrifugation (500×g, 5 min). Pelleted cells were re-suspended in 1 ml of propidium iodide staining solution (**Table 12**) for 1 h at 37 °C. The flow cytometric analysis was performed by counting 10,000 to 20,000 events at a flow rate of 200-500 cells/s. Data were collected using the CellQuest Software from the cytometer.

The data files were opened in Flowing software (V 2.5.1). A dot plot of FSC and SSC was created, and the region of intact cells was defined as already described for flow cytometry of fluorescent protein DD-tdTomato analysis (**Figure 10 A**). A second dot plot displayed the width of the fluorescence signal in channel FL-2 (FL2-W) on the x-axis versus the area of the fluorescence signal in FL-2 (FL2-A) on the y-axis (**Figure 11 A**). A region around cells of low FL-2W was generated. Cells with higher FL-2W were regarded as doublets. Only defined single cells were displayed in a histogram showing the height of the fluorescence signal in the PI measuring FL-2 channel (FL2-H, **Figure 11 B**).

This histogram plot was used for semi-automated cell cycle analysis using the Module “Cell Cycle Control” of the flowing software, which, after manual defining the G1-phase markers (**Figure 11 B**, G1-markers) and setting of G2-peak multiplier and peak width multiplier, finds G2-phase and S-phase markers and writes the calculated numbers of events, and numbers of G1, S, and G2 phase cells in an exportable table for further statistical analyses. Graphs were plotted by using Sigma Plot™ software package and statistics was done with Microsoft Excel.

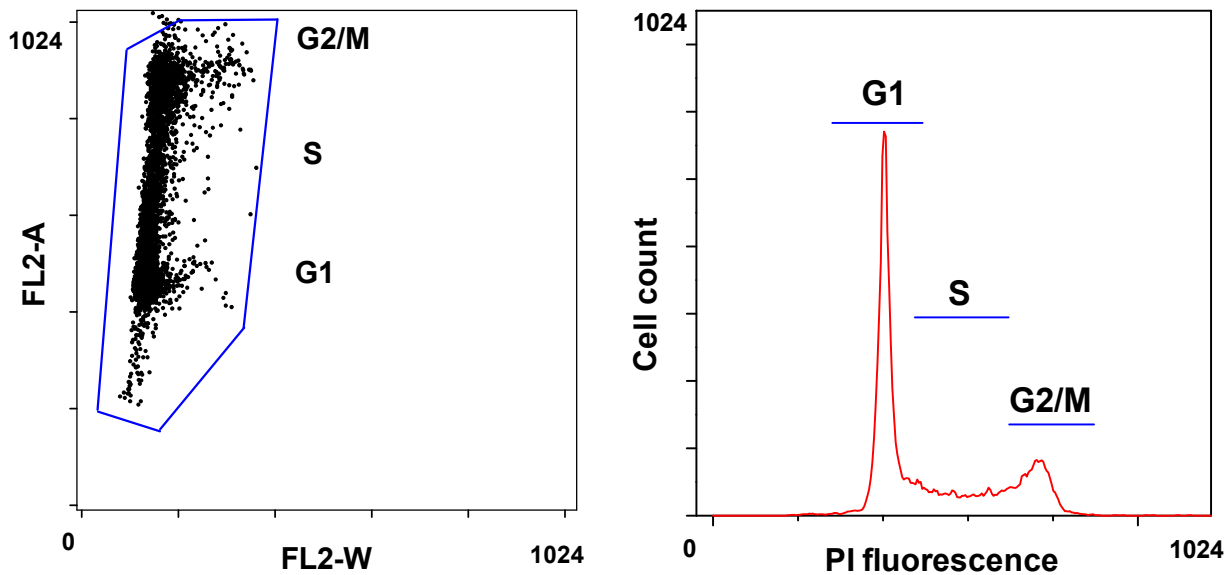


**Figure 11 Analysis of cell cycle phase using flow cytometry dot plot (A) and histogram (B).**

The dot plot (A) of a cell population allows to manually define a region in respect to width (FL2-W) and area (FL2-A) of the fluorescence signal and thereby excluding cell doublets. Events outside this region are not taken into account for further analysis.

The histogram (B) shows the PI fluorescence of the gated cell population. PI fluorescence intensity is directly proportional to the DNA content and was therefore used to draw conclusions regarding the distribution of cells within the cell cycle phases.

## 2.2.4 Gene expression analysis by reverse transcriptase RT-qPCR

The amount of mRNA of selected NF- $\kappa$ B target genes was quantified by reverse transcriptase real-time quantitative polymerase chain reaction (RT-qPCR). NF- $\kappa$ B target genes were selected from a previous study (Koch 2013) and primers for these target genes were designed. RNA was isolated from irradiated cells, and its amount, integrity and quality was determined. RNA was reverse transcribed to cDNA and quantified by real-time qPCR.

### 2.2.4.1 RNA isolation

After X-irradiation (2.2.2.1) and heavy ion exposure (2.2.2.2), RNA was collected at different incubation times according to experimental requirements. Before RNA collection, syringes, cell scrapers and microcentrifuge tubes were pre cooled at  $-20^{\circ}\text{C}$  to minimize RNA degradation by RNAases or heat shock. For RNA isolation, the cell culture medium was completely removed and cells were lysed by adding  $600\ \mu\text{l}$  RLT-lysis buffer (from the RNeasy Plus Mini Kit, containing  $14.3\ \text{mol/l}$   $\beta$ -mercaptoethanol). The lysed cells were collected with a cell scraper and transferred

to microcentrifuge tubes using 2 ml syringes. Syringes and needles were used not only for collection but also to homogenize the sample by moving it up and down several times before transferring it into RNase-free microcentrifuge tubes. Samples were immediately frozen and stored at -80 °C until further processing.

Total RNA isolation was performed with the RNeasy Plus Mini Kit according to the manufacturer's instructions. Genomic DNA was effectively removed by on-column DNA digestion using the RNase-Free DNase Set. The RNA was eluted with 50 µl RNase free water. The RNA concentration was measured by spectrophotometry (Nanodrop).

#### **2.2.4.2 Integrity of RNA**

The integrity of the isolated RNA was assessed by micro-electrophoresis using the RNA 6000 Nano Assay in the Bioanalyzer. The electrophoretic analysis on the chip is based on capillary gel electrophoresis and uses a fluorescent dye that binds to RNA to determine both RNA concentration and integrity.

Before running the 6000 Nano Assay on the Bioanalyzer, electrodes were cleaned by placing a washing chip filled with 350 µl RNaseAway in the Bioanalyzer for 1 min. Another washing chip filled with 350 µl RNase free water is placed for 30 sec to rinse the electrodes. The lid was left open for 10 sec to allow the electrodes to dry.

130 µl of the filtered RNA gel matrix was mixed with 2 µl of fluorescent dye in an RNAase-free Eppendorf tube and vigorously vortexed for mixing of gel and dye. 9.0 µl of the gel-dye mix was dispensed in the well of a NanoChip marked with a black circle "G". The chip priming station was used for gel distribution on the chip which served as a sieving polymer and helped in creating integrated electrical circuits. 5 µl of the RNA 6000 Nano Marker was dispensed in the well marked with the ladder symbol and each of the 12 sample wells. 1 µl of heat denatured (70 °C for 1 min) RNA samples and RNA ladder were added in the ladder and sample wells, respectively. After vortexing, the chip was placed in the Agilent 2100 Bioanalyzer and the user manual protocol was followed for operating the machine and to analyze data. The RNA 6000 ladder contains six RNA fragments which are 0.2 to 6 kb in size at a total concentration of 150 ng/µl. Therefore six peaks of different sizes 0.2, 0.5, 1.0, 2.0, 4.0 and 6.0 kb are observed in the electropherogram (**Figure 12**). The quality of RNA and protein contamination was assessed by the 28S/18S rRNA ratio.

A 28S/18S ratio of two was considered as the best quality RNA and a ratio of 0 indicated the poor quality (indicating degradation of RNA in the sample). The samples with a 28S/18S ratio of around 2 and high RNA integrity (RIN) number above 9 were considered for cDNA synthesis and further analysis.

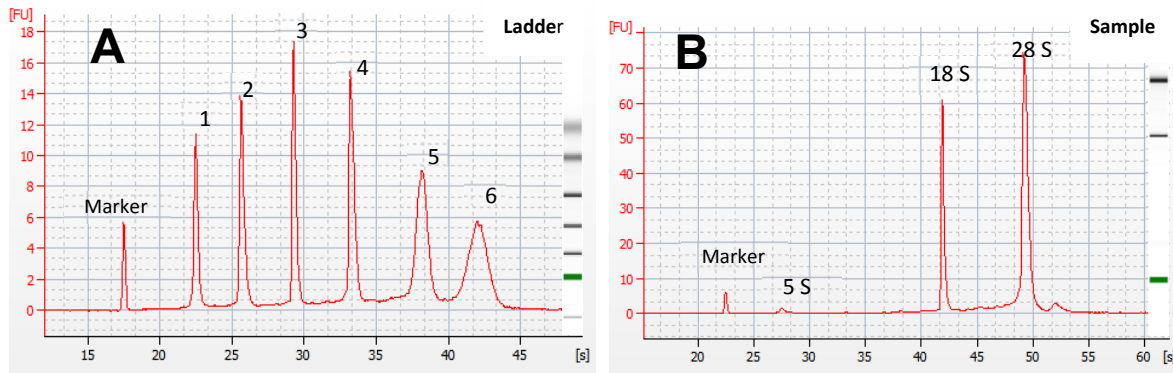


**Figure 12 Electropherogram of RNA ladder (A) and RNA Sample (B)**

The electropherograms result from micro-electrophoresis of a RNA ladder (A) and an intact RNA sample with the 5S, 18S and 28S peaks (B) using the Agilent 2100 Bioanalyzer. FU represents fluorescence units and s represents seconds. The seven characteristic regions of the ladder and 3 regions in the sample are marked (Schroeder *et al.* 2006).

### 2.2.4.3 cDNA synthesis

RNA was reverse transcribed to first-strand cDNA using the iScript cDNA Synthesis Kit. The iScript kit contains a recombinant RNase H<sup>+</sup> MMLV reverse transcriptase which is supplied with an RNase inhibitor mix. The reactions were set up according to the instructions of the kit. RNA concentration was measured in the Nanodrop spectrophotometer and samples were diluted to 200 ng/μl. For cDNA synthesis 1 μg of RNA (5 μl of 200 ng/μl) was mixed with the kit components as described in **Table 16**. The reaction mixture was incubated in a thermocycler according to the iScript protocol: 5 min at 25 °C (Annealing), 30 min at 42 °C (Elongation), 5 min at 85 °C (Deactivation) and 4 °C (Overnight storage).

The expected yield of cDNA was considered to be 50 ng/μl. The obtained cDNA samples were stored at -20 °C for further use in qPCR analysis and the remaining RNA at -80 °C.

**Table 16 Reaction mix for cDNA synthesis**

Reagents	Volume
Nuclease-free water	10 $\mu$ l
5x iScript select reaction mix	4 $\mu$ l
RNA sample (1 $\mu$ g total RNA)	5 $\mu$ l
iScript reverse transcriptase	1 $\mu$ l
Total	20 $\mu$ l

#### 2.2.4.4 Primer design

Primers were designed to avoid internal secondary structures, repetitive sequences, intron-exon border overlaps, pseudo genes, big differences in melting temperature ( $T_m$ ) value of primer pairs and complementation. Primers consisted of 14-24 base pairs in length and 40-60 % guanine (G) and cytosine (C) with a G or C at 3' ends. Guanine/cytosine (G/C) and adenine/thymine (A/T) were uniformly distributed to maintain  $T_m$  and annealing temperature ( $T_a$ ) of 55-65°C (normally 5°C below primer- $T_m$ ). The sequence of the primer and corresponding gene were retrieved and tested by the BLAST tool at NCBI website. Two to three primer pairs per gene of interest were ordered from Invitrogen.

#### 2.2.4.5 Primer optimization

Primers were received in lyophilized form in an amount of 25 nmol. All primers were diluted according to the supplier's protocol by reconstituting in DNase free H<sub>2</sub>O to make 1 mmol/l stock solutions. Primers were further diluted 1:100 to the 10  $\mu$ mol/l working solution and 0.2  $\mu$ mol/l was used in the PCR (0.5  $\mu$ l primer in 25  $\mu$ l reaction mix). All stock and working dilutions were stored at -20 °C.

Primers were optimized for real-time RT-qPCR by using the gradient calculator tool of Opticon Monitor software version 3.0. The  $T_m$  of primer-DNA hybrids was calculated by the primer design software (NCBI / Primer BLAST) and ranged from 55 to 65 °C. Therefore, real-time RT-qPCR was performed for each primer pair with temperatures from 55 to 61 °C with 5 ng cDNA per well. For each tested temperature, reaction mixes were also prepared with betaine (N, N, N-trimethylglycine, 5 mol/l solution) and also without template (NTC = no template control). Betaine is a PCR additive which can reduce secondary structure formation in G/C rich regions and therefore improves DNA amplification. Optimal PCR conditions (annealing temperature, addition of

betaine) were set for each primer individually with respect to the crossing point (CP) value and melting curve. CP values should be as small as possible indicating the best possible amplification efficiency. More than one peak in the melting curve indicates primer-dimers or unspecific products. Therefore primers with a high  $T_m$  value deviation were excluded. A list of optimized primers used is given in **Table 17**.

**Table 17** Primer sequences, annealing temperature ( $T_a$ ), amplicon length and NCBI database codes (NCBI) of the designed primers used for gene expression analysis

Gene name	Primer sequence 5' - 3'	Optimized $T_a$	Length (bp)	NCBI
<b>Housekeeping genes</b>				
GAPDH	fwd: CAATGACCCCTTCATTGACC rev: GATCTCGCTCCTGGAAGATG	60.0	146	NM_002046
HPRT	fwd: TGACACTGGCAAACAATGCA rev: GGCCTTTTCACCAGCAAGCT	62.0	120	NM_000194
PBGD	fwd: CAGCTTGCTCGCATACAGAC rev: GAATCTTGTCCCCTGTGGTG	60.4	106	NM_000190
<b>Target genes</b>				
NFKBIA*	fwd: AACCTGCAGCAGACTCCAC rev: TGCTCACAGGCAAGGTGTAG	61.0	137	NM_020529
CXCL1 / GRO- $\alpha$	fwd: AGGGAATTCACCCCAAGAAC rev: TAACTATGGGGGATGCAGGA	60.1	132	NM_001511
CXCL2 / GRO- $\beta$	fwd: CTCAAGAATGGGCAGAAAGC rev: TCAGGAACAGCCACCAATAA	60.1	132	NM_002089
CXCL8	fwd: TCTGCAGCTCTGTGTGAAGG rev: AATTTCTGTGTTGGCGCAGT	60.1	153	NM_000584
CXCL10	fwd: GAACTGTACGCTGTACCTGCA rev: TTGATGGCCTTCGATTCTGGA	60.1	172	NM_001565
CD83	fwd: TTGAGAGTGACAGGATGCC rev: AGCCGTGCAAAACAAGTGA	56.0	131	NM_001040280
CDKN1A (p21/WAF)	fwd: GGAAGACCATGTGGACCTGT rev: AAATCTGTCATGCTGGTCTGC	61.9	129	NM_000389
GADD45 $\alpha$	fwd: GAGAGCAGAAGACCGAAAGGA rev: CACAACACCACGTTATCGGG	61.9	145	NM_001924

\*Betain (5 mol/l) was added to reduce the formation of secondary structure in G-C rich regions.



#### 2.2.4.6 Real-time quantitative PCR (qPCR)

Real-time PCR was performed in the Opticon<sup>®</sup>2 by using Platinum<sup>®</sup> SYBR<sup>®</sup> Green qPCR SuperMix-UDG kit. The cDNA samples stored at -20 °C were thawed on ice. All the steps from thawing samples till preparing plates were performed on ice to reduce evaporation and condensation of the reaction mixture.

For determination of qPCR efficiency, 2 µl cDNA from each sample was collected to a pool of combined samples of 72 µl containing 3600 ng cDNA. A dilution series of standards (25-0.008 ng/µl cDNA) was prepared from the cDNA pool. The remaining cDNA samples (50 ng/µl) were diluted 1:4 with nuclease-free water, resulting in cDNA concentrations of 12.5 ng/µl. RT-qPCR reaction mixtures were prepared according to the Platinum<sup>®</sup> SYBR<sup>®</sup> Green qPCR SuperMix-UDG protocol. The SYBR<sup>®</sup> Green qPCR SuperMix contained pre-blended 2×buffer, *Taq* DNA polymerase, nucleotides and bivalent cations. The composition of the reaction batch per well is listed below in **Table 18**.

Each well of a 96-well plate was loaded with 25 µl reaction mix including 2 µl sample or efficiency dilutions. Samples, controls, blanks and efficiencies were loaded in triplicates on the 96-well plates accordingly.

**Table 18** The composition of a single real-time qPCR reaction mix

Reagents	Volume
SYBR Green Mix	12.5 µl
Primer fwd, 0.2 µmol/l	0.5 µl
Primer rev, 0.2 µmol/l	0.5 µl
DNA 5 ng/µl	2.0 µl
<i>A. bidest.</i>	9.5 µl
Total volume	25.0 µl

The plates were sealed with an adhesive film and the amplification protocol for qPCR reaction was followed.

**Table 19 Amplification protocol for real-time qPCR**

No.	Step	Incubation time	Temperature
1	Pre-heating	2 min	50°C
2	Pre-denaturation <sup>a</sup>	2 min	95°C
3	Denaturation	15 sec	95°C
4	Annealing	30 sec	<b>Table 17</b>
5	Elongation	30 sec	72°C
6	Plate read		
7	Final extension	20 sec	78°C
8	Reading fluorescence		
9	Repeat (3-8) 44 times		
10	Melting curve analysis		60-95°C
11	Plate reading	hold 3 sec	every 0.2 °C
12	Cooling down the heat block	1min	29°C

<sup>a</sup>Pre-denaturation was performed to activate the *Taq* DNA polymerase.

#### 2.2.4.7 Relative quantification of gene expression levels

Opticon Monitor Software version 2.02 was used in qPCR analysis. This software creates a standard graph of the arithmetic means of the number of cycles against the amount of cDNA in the cDNA pool dilution series (25, 5, 1, 0.2, 0.04, 0.008 ng/μl). The slope of a standard curve was used to estimate the PCR amplification efficiency (*E*) of a real-time PCR reaction by using the equation **Equation 12**.

$$E = 10^{-1/\text{slope}} \quad \text{Equation 12}$$

A value of PCR efficiency in between 1-2 is considered significant. A slope of -3.32 is considered to be the best, because it indicates PCR efficiency of 2 which is the exact doubling of PCR product in each cycle.

The threshold for the determination of the threshold cycle ( $C_t$ ) is the only parameter that was changed manually in these experiments. The  $C_t$  is the cycle number at which the fluorescence generated in the reaction crosses the threshold line.

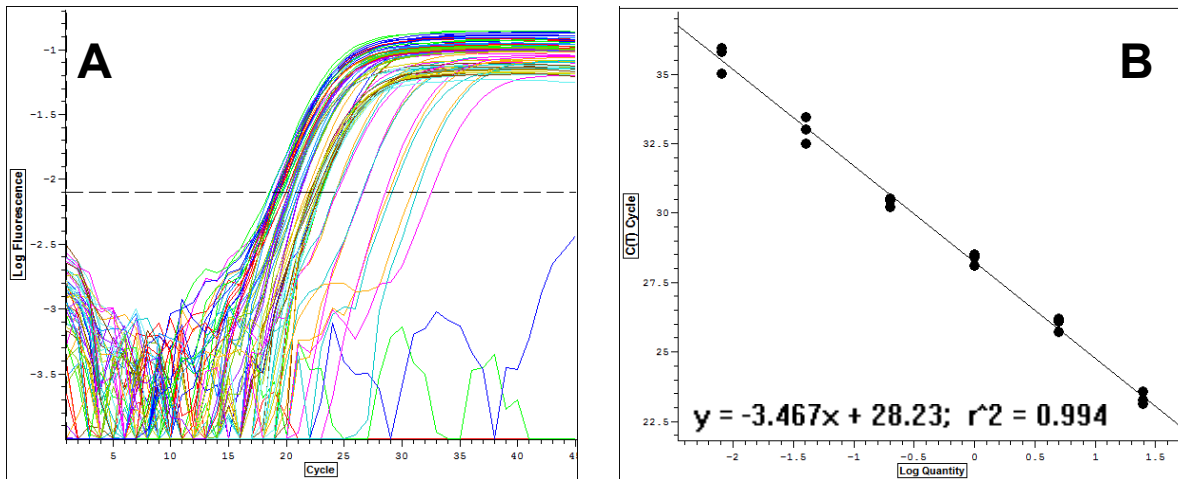


**Figure 13 Real-time PCR amplification plots (A) and standard curve (B)**

Real-time qPCR amplification plot (all heavy ions, LET 0.3-9674 keV/ $\mu\text{m}$ ) (A): The fluorescence is increasing with the PCR cycle. The number of the cycle during which the threshold was crossed is the  $C_t$  value. The threshold was set manually in the early exponential phase of the DNA amplification plots, above the background fluorescence of the first 10-15 PCR cycles (dotted line). Real-time qPCR standard curve (B): The slope of the standard curve is -3.5, and the regression coefficient  $r^2$  is 0.994.

In the standard curve, the threshold was set in the exponential part of the amplification plots (**Figure 13 A**), resulting the highest correlation coefficient of the efficiency curve (**Figure 13 B**). To determine the reproducibility of a run, the variation coefficient  $C_V$  was used (%) for the measurement of the  $C_t$  values in triplicate. The inter-assay reproducibility was determined by repeating the RT-qPCR run on different days. A coefficient of variation  $\leq 5\%$  was used as a quality standard.

#### 2.2.4.8 Statistical evaluation of qPCR data by REST Software

The Relative Expression Software Tool REST<sup>®</sup> MCS software (Pfaffl *et al.* 2002) was used for statistical evaluation of the target genes' expression in relation to the studied reference genes. The difference in expression of the target and reference genes was calculated according to formula given below ( **Equation 13**).

$$\text{Regulation} = \frac{(E_{\text{target}})^{\Delta C_{t \text{ target}} (\text{Mean}_{\text{control}} - \text{Mean}_{\text{sample}})}}{(E_{\text{reference}})^{\Delta C_{t \text{ reference}} (\text{Mean}_{\text{control}} - \text{Mean}_{\text{sample}})}} \quad \text{Equation 13}$$

$E_{\text{target}}$	=	Amplification efficiency of the target gene
$E_{\text{reference}}$	=	Amplification efficiency of the reference gene
$\Delta C_{t \text{ target}}$	=	Difference in $C_t$ of target gene in control and sample
$\Delta C_{t \text{ reference}}$	=	Difference in $C_t$ of the reference gene in control and sample

### 2.2.5 Gene expression analysis by target gene array

Human RT<sup>2</sup> Profiler™ PCR Arrays (SABiosciences) were used for expression profiling of 89 NF-κB target genes per sample. For performing RT<sup>2</sup> Profiler™ PCR Arrays, RNA was isolated as described in section 2.2.4.1 and reverse transcribed into cDNA by using RT<sup>2</sup> First strand kit as described in section 2.2.5.1. RT<sup>2</sup> RNA QC PCR arrays were used to assess RNA quality. The RNA samples were finally examined by RT<sup>2</sup> Profiler™ PCR Array (2.2.5.4).

#### 2.2.5.1 RT<sup>2</sup> First Strand cDNA Synthesis

Reverse transcription of the isolated, purified and intact RNA into cDNA was performed by using the RT<sup>2</sup> First strand kit (SABiosciences).

To eliminate any residual genomic DNA contamination, 4.0 µl of 5×gDNA Elimination buffer was added to each RNA sample and the volume was adjusted to 10 µl with RNase-free water and the mixture was incubated at 42 °C for 5 min. The reaction was stopped by chilling the samples on ice immediately for at least one minute.

For the “First Strand cDNA Synthesis Reaction” 10 µl of reverse-transcription mix (4 µl 5× BC3 buffer, 1 µl Primer and External Control Mix P2, 2 µl RT Enzyme MixRE3 and 3 µl RNase-free water) was added to each sample. After incubating at 42 °C for exactly 15 min, the reaction was immediately stopped by incubating at 95 °C for 5 min. After addition of 90 µl RNase free water to each reaction, the solution was mixed by pipetting up and down several times before storing them at a -20 °C freezer.

#### 2.2.5.2 RNA quantification and quality control

The RT<sup>2</sup> RNA QC PCR was performed after checking integrity of RNA (2.2.4.2) to further assess the quality of the RNA samples. This quality control array analyzes HK1 (ACTB) and HK2 (HPRT1) housekeeping gene expression levels, reverse transcription (RTC), positive PCR control (PPC), genomic DNA contamination (GDC), no reverse transcription (NRT) and no template (NTC) controls (**Figure 14**).

After thawing the samples of the RT<sup>2</sup> First Strand Kit, the PCR components mix was prepared. For each assay, 8 µl of cDNA synthesis reaction was mixed with 110 µl 2× RT<sup>2</sup> SYBR Green Mastermix, and 110 µl RNase free water. 25 µl of this PCR components mix were pipetted into wells A to H of the quality plate for up to 6 samples. After sealing the plates with optical thin wall strips, and transfer of the plate

into the DNA Engine Opticon<sup>®</sup>2 System, the PCR cycling program was set up according to **Table 20**.

After completing the RT-qPCR reaction, a dissociation (melting) curve analysis was performed to verify the PCR specificity. The threshold cycle ( $C_t$ ) for each well was calculated by using the cycler software.

### 2.2.5.3 NF- $\kappa$ B-dependent target gene expression

The RT-qPCR reaction was performed in Human RT<sup>2</sup> Profiler<sup>™</sup> PCR Arrays. The array enables the simultaneous quantification of both rare and abundant genes in the same sample (96-well layout), by using the DNA Engine Opticon<sup>®</sup>2 System. For the expression of genes, one RT<sup>2</sup> Profiler<sup>™</sup> plate was used per sample. Accordingly, 2.7 ml PCR components mix was prepared as mentioned in **Table 21**.

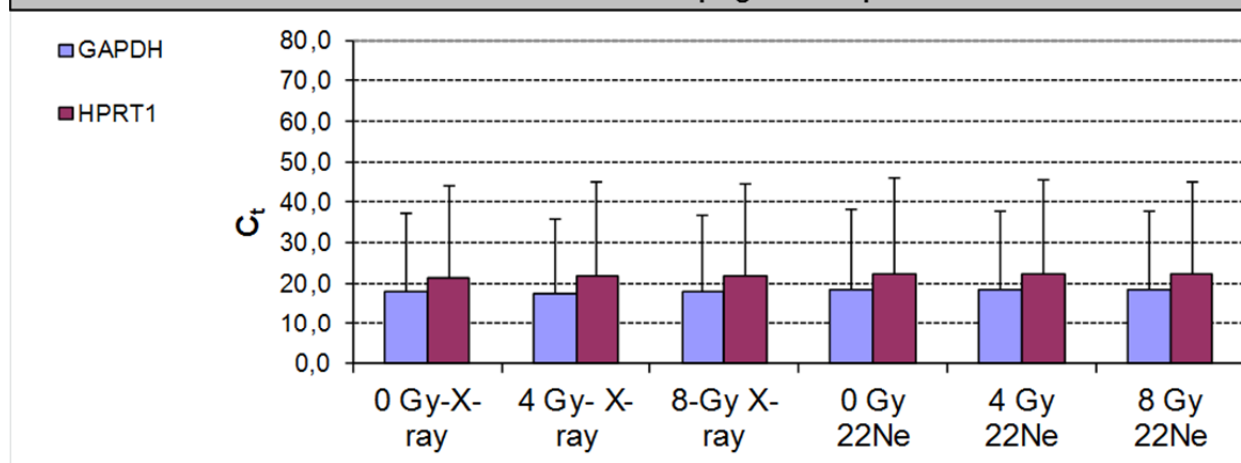
25  $\mu$ l of this PCR components mix were pipetted into each well of the plate. Before adding each plate to the cycler, the plates were sealed and centrifuged for 1 min at 1000 $\times$ g at room temperature. Quantitative real-time analysis was performed in the Opticon<sup>2</sup> thermocycler according to **Table 20**.

**Table 20** Cycling conditions for real-time PCR according to the RT<sup>2</sup> Profiler<sup>™</sup> PCR array protocol

	Cycles	Time	Temperatures
Initial denaturation <sup>a</sup>	1	10 min	95 °C
Denaturation	40	15 s	95 °C
Annealing		35 s	55 °C
Elongation		30 s	72 °C
Plate Read			
Elongation		20 s	78 °C
Plate Read			
Final	1	1 min	95 °C
		2 min	65 °C
Melting curve		read every 0.2 °C	65-95 °C

<sup>a</sup>SYBR Green Mastermix contains, in addition to nucleotides and the fluorescein-coupled reference dye, a high-performance HotStart DNA Taq polymerase which is activated at 95 °C for 10 min.

	Sample Name	0 Gy-X-ray	4 Gy- X-ray	8-Gy X-ray	0 Gy 22Ne	4 Gy 22Ne	8 Gy 22Ne
Row	Control Name	Average Ct					
A	cDNA GAPDH	18,15	17,30	17,95	18,50	18,42	18,34
B	cDNA HPRT1	21,39	21,87	21,86	22,44	22,15	22,08
C	cDNA RTC (1/20 diluted)	35,00	35,00	35,00	35,00	35,00	35,00
D	cDNA PPC (CXCL10)	33,81	30,42	29,65	35,00	33,89	30,46
E	cDNA GDC (Contamina	35,00	35,00	35,00	35,00	35,00	35,00
F	mRNA NRT (GAPDH)	35,00	35,00	35,00	35,00	35,00	35,00
G	H2O PPC - H <sub>2</sub> O (CXCL	35,00	35,00	35,00	35,00	35,00	35,00
H	H2O NTC (GAPDH)	35,00	35,00	35,00	35,00	35,00	35,00



Reverse Transcription Control (RTC): Are RNA sample impurities affecting reverse transcription?							
$C_t^C - C_t^G$		0,00	0,00	0,00	0,00	0,00	0,00
Cut-off	5	NO	NO	NO	NO	NO	NO
Positive PCR Control (PPC): Are RNA sample impurities affecting PCR?							
$C_t^D - C_t^G$		-1,19	-4,58	-5,35	0,00	-1,11	-4,54
Cut-off	3	NO	N/A	N/A	NO	NO	N/A
No Reverse Transcription (NRT) control: Is genomic DNA contamination detectable?							
$C_t^F$		35,00	35,00	35,00	35,00	35,00	35,00
Cut-off	35	NO	NO	NO	NO	NO	NO
Genomic DNA Contamination (GDC) control: Will it affect the results?							
$C_t^E$		35,00	35,00	35,00	35,00	35,00	35,00
Cut-off	35	NO	NO	NO	NO	NO	NO
No Template Control (NTC): Is the PCR system clean?							
$C_t^H$		35	35	35	35	35	35
Cut-off	34	YES	YES	YES	YES	YES	YES

**Figure 14** Quality control of cDNA for further gene expression analysis with the RT<sup>2</sup> Profiler™ PCR array, using the analysis template of the RT<sup>2</sup> RNA QC PCR array.

This example displays the results of a real-time RT-qPCR plate investigating the quality of 6 cDNA samples, after irradiation with different doses of X-rays and <sup>22</sup>Ne ions. For each sample, the validation sheet (supplied by SABiosciences) reports the average C<sub>t</sub> value, quality of RNA (integrity and impurity) and genomic DNA contamination if any.

**Table 21 RT-qPCR master mix for one 96-well plate**

RT <sup>2</sup> -qPCR master mix	Quantity
RT <sup>2</sup> SYBR Green qPCR Master Mix	1350 $\mu$ l
DNase RNase free H <sub>2</sub> O	1248 $\mu$ l
Template cDNA (9 ng/ $\mu$ l)	102 $\mu$ l

#### 2.2.5.4 Relative quantification of gene expression levels in target gene array

After completing PCR amplification, the  $C_t$  values were entered into the Excel-based template provided by SABiosciences for calculating relative gene expression. The calculation of the gene expression levels is based on the efficiency corrected  $\Delta \Delta C_t$  method. In the first step, the  $C_t$  value of the reference gene subtracted from the  $C_t$  value of the respective target gene (given as  $\Delta C_t$ ) results in the target gene expression in relation to the housekeeper genes (**Equation 14**).

$$\Delta C_t = C_{t \text{ Target gene}} - C_{t \text{ Reference gene}} \quad \text{Equation 14}$$

Thereafter, the  $C_t$  value of the respective control is subtracted from the  $\Delta C_t$  value of the treated sample, giving the  $\Delta \Delta C_t$  (**Equation 15**).

$$\Delta \Delta C_t = \Delta C_{t \text{ Sample}} - \Delta C_{t \text{ Control}} \quad \text{Equation 15}$$

In case of a perfect doubling of the PCR template, meaning a maximal efficiency of 2 ( $E=2$ ), the relative expression of treated versus control sample was calculated by means of **Equation 16**.

$$\text{Rate}_{\text{Gene expression}} = 2^{-\Delta \Delta C_t} \quad \text{Equation 16}$$

### 3 Results

The activation of transcription factor NF- $\kappa$ B was shown to be an early step in the cellular radiation response of human cells. Since NF- $\kappa$ B activation by the genotoxic stress dependent sub-pathway after DNA damage and its role in cell-protective responses such as cell cycle arrests and survival have been evaluated to a limited extent, the current work focusses on the activation of NF- $\kappa$ B and the subsequent target gene expression after exposure to ionizing radiation (heavy ions) relevant to tumor therapy and spaceflight.

To visualize the activation of NF- $\kappa$ B via the canonical and the genotoxic stress induced pathways, sensitive reporter systems based on HEK cells were used. To evaluate the NF- $\kappa$ B dependent reporter gene expression, flow cytometry was performed after exposure to ionizing radiation (X-rays and heavy ions). Due to differences between the level of NF- $\kappa$ B activation after X-irradiation and heavy ions exposure, it was expected that LET might play an important role in different cellular responses. In addition, the relative biological effectiveness (RBE) of heavy ions having a broad range of LET (0.3 - 10000 keV/ $\mu$ m) was examined for NF- $\kappa$ B activation and cellular survival, because the NF- $\kappa$ B pathway is known to have pro-survival functions.

To understand the contribution of NF- $\kappa$ B signaling in the cellular radiation response, a knock down cell line was used and the role of NF- $\kappa$ B in cellular survival, DNA damage response and cell cycle progression was determined.

As this NF- $\kappa$ B down-regulation lead cells towards higher radiosensitivity, lower survival and delayed cell cycle progression, the expression of down-stream target genes of NF- $\kappa$ B were investigated by a target gene array. Furthermore, the effect of LET on the up-regulated NF- $\kappa$ B target genes was analyzed by quantitative real-time PCR.



### 3.1 Effect of ionizing radiation on NF- $\kappa$ B activation in HEK reporter cell lines

For analysis of the effect of LET on radiation-induced NF- $\kappa$ B activation, first the kinetics of NF- $\kappa$ B activation by X-rays were determined and compared to those of an inducer of the canonical pathway.

#### 3.1.1 Activation of NF- $\kappa$ B by the canonical pathway is quicker than by the genotoxic stress induced pathway

NF- $\kappa$ B is not only activated by ligands (e.g. TNF- $\alpha$ ) binding to TNF- $\alpha$  binding receptors (TNFR) on the plasma membrane surface but also by DNA damage induced by e.g. ionizing radiation. TNF- $\alpha$  plays a role in antitumor effects and exerts cytolytic and cytostatic action. It binds to the TNFR and activates the canonical NF- $\kappa$ B pathway. Ionizing radiation, however, activates the genotoxic stress induced NF- $\kappa$ B pathway by creating DSB. The HEK reporter cell line was used to analyze the activation of NF- $\kappa$ B after exposure to TNF- $\alpha$  and ionizing radiation (X-rays).

**Figure 15 A** demonstrates that NF- $\kappa$ B activation by the canonical pathway is quicker than by the genotoxic stress induced pathway. NF- $\kappa$ B activation kinetics was investigated up to 48 h after exposing HEK-pNF $\kappa$ B-DD-tdTomato-C8 cells to either 16 Gy of X-rays or 20 ng/ml TNF- $\alpha$ .

DD-tdTomato expression as a consequence of NF- $\kappa$ B activation was analyzed by flow cytometry (**Figure 15 A**). Strong DD-tdTomato signals were observed in ~60 % of the total cell population after 8 h and 16 h of TNF- $\alpha$  treatment and X-irradiation, respectively. Fluorescence microscopy revealed that HEK-pNF $\kappa$ B-DD-tdTomato cells express a strong red fluorescence inside the cell when NF- $\kappa$ B is activated (**Figure 15 B**).

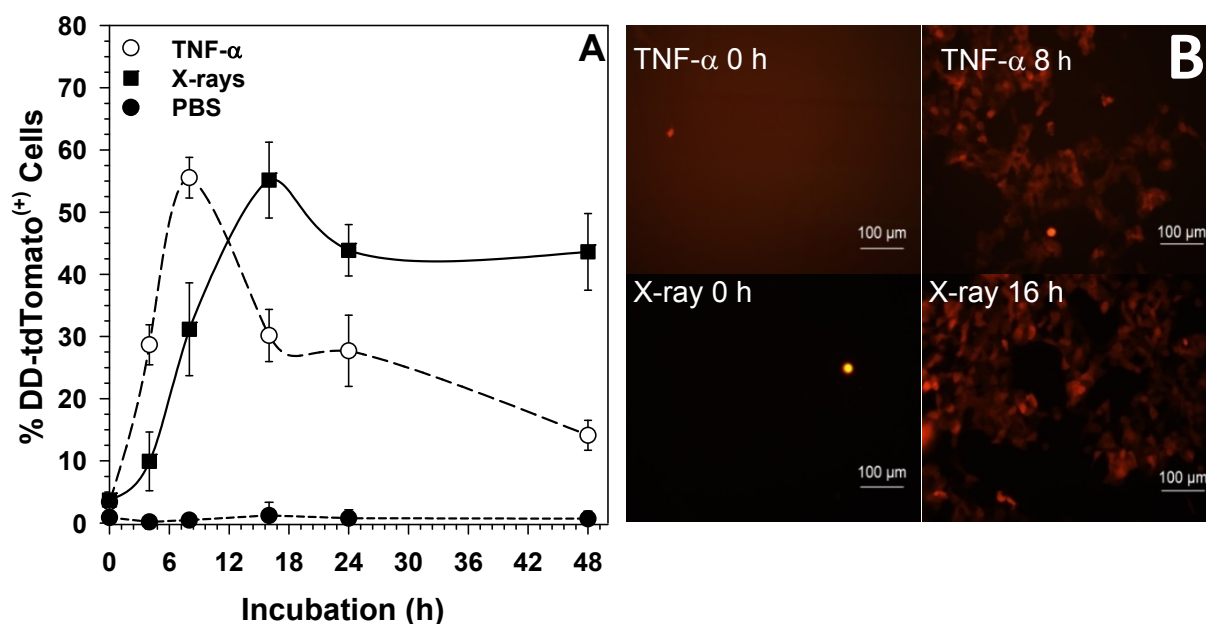


**Figure 15** NF- $\kappa$ B-dependent DD-tdTomato expression kinetics after TNF- $\alpha$  treatment (20 ng/ml) and X-irradiation (16 Gy).

HEK-pNF $\kappa$ B-DD-tdTomato-C8 cells were seeded in a density of  $3 \times 10^4$  cells/cm<sup>2</sup> and grown for 2 days before treatment. At different time points after induction, cells were fixed with 3.7% formaldehyde and DD-tdTomato expression was analyzed by flow cytometry (A) and by fluorescence microscopy (B). Maximal NF- $\kappa$ B-dependent DD-tdTomato expression was observed 8 h and 16 h after TNF- $\alpha$  treatment and X-irradiation respectively. Bars show standard errors of more than three individual experiments.

### 3.1.2 Activation of NF- $\kappa$ B in response to space-relevant radiation qualities

Low LET radiation (X-rays) activates NF- $\kappa$ B in a dose-dependent manner. In order to define the LET dependence of NF- $\kappa$ B activation in human cells, heavy ions of different LET in the range of 30 to  $\sim 10000$  keV/ $\mu$ m were used (Table 15). According to the kinetics of NF- $\kappa$ B activation reaching a maximum around 16 h after irradiation, NF- $\kappa$ B-dependent reporter gene (DD-tdTomato or d2EGFP) expression was determined in the HEK reporter cell lines HEK-pNF- $\kappa$ B-d2EGFP/Neo and HEK-pNF $\kappa$ B-DD-tdTomato-C8 16 h after exposure.

It was observed that NF- $\kappa$ B activation was much higher after heavy ion exposure compared to X-irradiation. All the heavy ions under investigation (Table 22) activated NF- $\kappa$ B-dependent reporter gene expression in a dose-dependent manner (Figure 16). Energetic heavy ions up to the LET 272 keV/ $\mu$ m were most effective in activating NF- $\kappa$ B-dependent gene expression in HEK cells. The lowest fluence that was shown to activate NF- $\kappa$ B-dependent reporter gene expression was two argon ions per cell

nucleus. Very high LET heavy ions,  $^{58}\text{Ni}$  (905 keV/ $\mu\text{m}$ ) and  $^{208}\text{Pb}$  (9674 keV/ $\mu\text{m}$ ), also induced NF- $\kappa$ B-dependent reporter gene expression but the extent of NF- $\kappa$ B activation was comparable to X-rays.

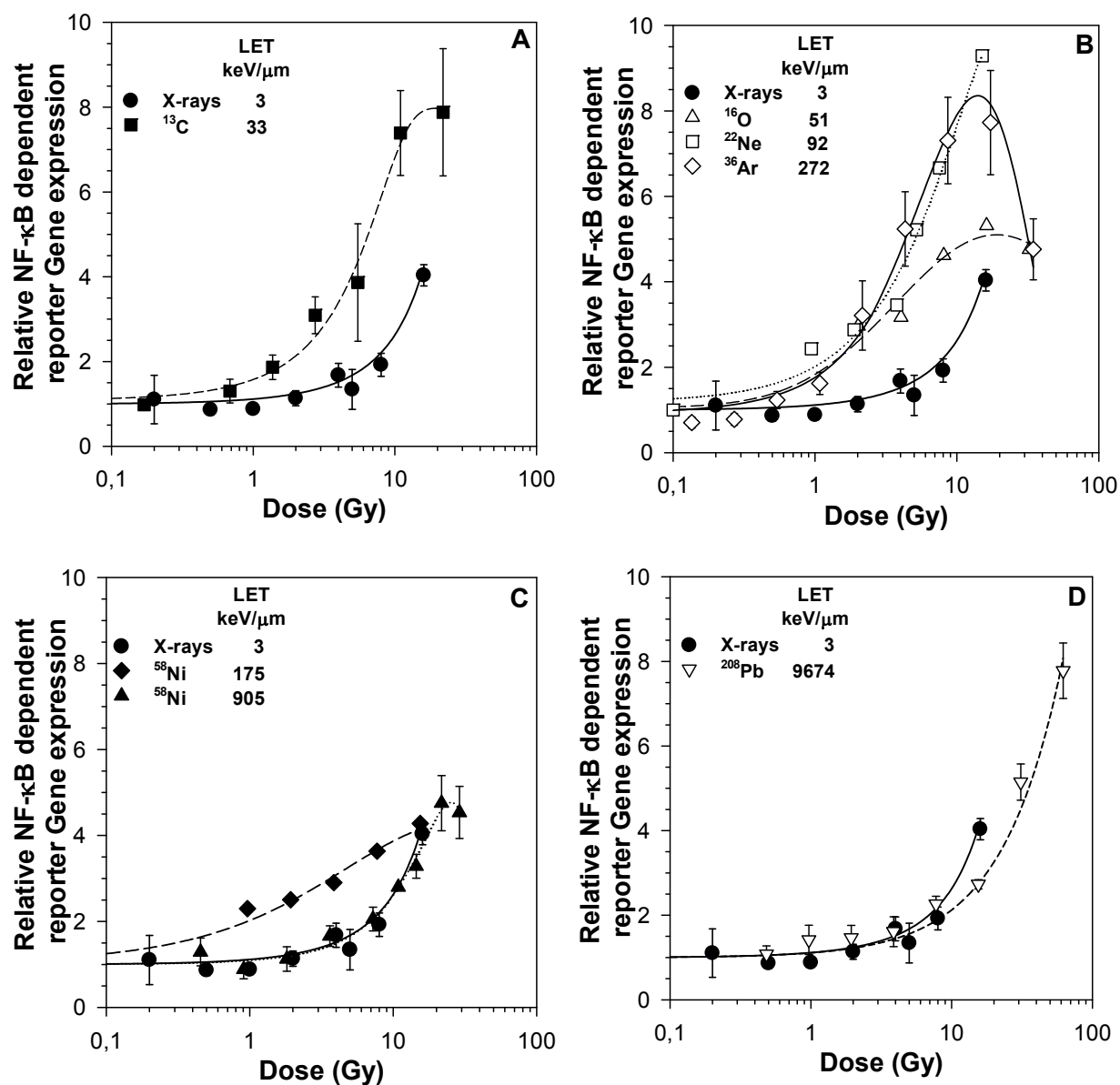


**Figure 16** NF- $\kappa$ B-dependent reporter gene expression after exposure to various energetic heavy ions (LET 3-9674 keV/ $\mu\text{m}$ ).

Dose-effect relationships for activation of NF- $\kappa$ B-dependent gene expression 16 h after exposure to low LET radiation (X-rays) was compared with high LET radiation (accelerated heavy ions). Heavy ions are very effective in activating NF- $\kappa$ B-dependent gene expression in HEK cells up to the LET of 272 keV/ $\mu\text{m}$  (A-C). Very high LET heavy ions  $\geq 900$  keV/ $\mu\text{m}$  induced NF- $\kappa$ B comparably to X-rays (C, D). Means and standard errors of independent experiments with three to six samples per dose are shown

A list of heavy ions and extent of NF- $\kappa$ B activation by average hits per cell nucleus is given in **Table 22**. As activation of NF- $\kappa$ B after exposure to ionizing radiation of different quality may play a major role in different cellular radiation responses, these responses are analyzed in the next subchapter.

## **3.2 Cellular responses to exposure with ionizing radiation**

Hallmarks of the cellular radiation response are reduced proliferation and induction of cell death or cell cycle arrest. Before determining the expression of several candidate genes that can regulate these responses, these endpoints had to be quantified after exposure to radiation with different LET.

### **3.2.1 Effect of ionizing radiation on cellular survival**

Cellular survival was determined using the colony forming ability. Dose effect curves were calculated according to the single-hit multi-target model. The parameters  $D_0$ ,  $n$  and  $D_q$  were calculated for the dose effect curve from the linear regression lines (section 2.2.3.1).

#### **3.2.1.1 Low LET radiation reduces cellular proliferation and survival**

To determine the effects of ionizing radiation on cellular proliferation, HEK-pNF $\kappa$ B-DD-tdTomato cells were exposed to different doses of X-rays. Relative cellular proliferation was analyzed over a period of 10 days (**Figure 17 A**). It was observed that the cellular proliferation was decreased in a dose-dependent manner. At low doses, 1 and 2 Gy, the cell proliferation was lower compared to the unirradiated cells and cells entered into stationary phase much earlier than non-irradiated cells. A delay in exit from lag phase followed by a steep log phase was observed at 4 Gy. The cellular survival also decreased significantly after exposure to 6-8 Gy and most of the cells were unable to emerge from lag phase to follow regular cell proliferation pattern (lag, log and stationary phase).

The survival curve showed a shoulder in the lower dose range (< 2 Gy) which represents the repair capacity of HEK-pNF $\kappa$ B-DD-tdTomato cells, whereas higher doses (> 4 Gy) resulted in exponential decrease in survival. At higher doses such as 6 and 8 Gy the cellular survival decreased up to 1000 times as compared to the low doses 1 and 2 Gy (**Figure 17 B**).

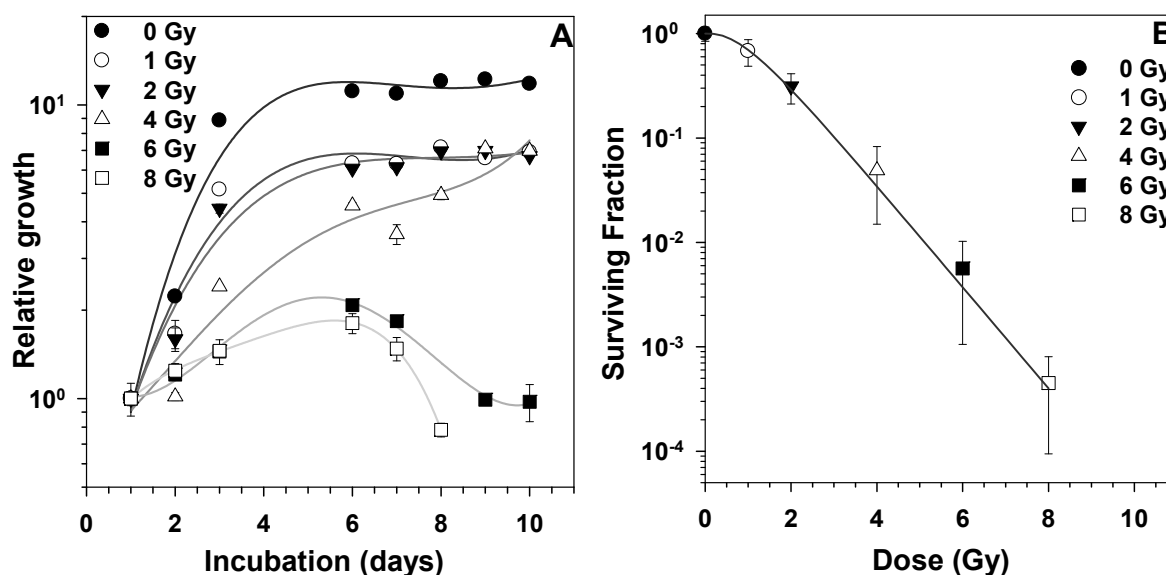


**Figure 17 Proliferation (A) and cellular survival (B) of HEK cells after exposure to low LET radiation (X-rays)**

(A) HEK cells were exposed to 1, 2, 4, 6 and 8 Gy X-rays. After radiation exposure, cells were subsequently cultured for up to 10 days in culture medium containing 10 % FBS. The relative cell number was evaluated by measuring the fluorescence of the DNA intercalating dye bisbenzimidazole at excitation/emission wavelengths of 360/460 nm, respectively. Data represent mean  $\pm$  SE of more than three independent experiments with 8 replicates each.

(B) The survival was determined by the colony forming ability test. The cells were seeded 24 hours before irradiation. Colonies were fixed and stained after 14-21 days incubation. Bars show the standard deviation of more than three individual experiments.

### 3.2.1.2 Cellular survival is LET-dependent

Exposure to low LET radiation results in a survival curve with a shoulder which indicates the cellular DNA damage repair capacity in the low dose range (0-2 Gy).

High LET radiation including  $^{13}\text{C}$  (10, 33 and 75 keV/ $\mu\text{m}$ ),  $^{16}\text{O}$  (51 keV/ $\mu\text{m}$ ),  $^{22}\text{Ne}$  (92 keV/ $\mu\text{m}$ ),  $^{58}\text{Ni}$  (175 keV/ $\mu\text{m}$ ) and  $^{36}\text{Ar}$  (272 keV/ $\mu\text{m}$ ) have a high damaging capacity as seen by reduced  $D_0$  values and exponentially decreasing survival curves without any shoulder. The steepness of the survival curves depends on the radiation quality (LET). For exposure to accelerated  $^{13}\text{C}$  ions it was observed that cell killing potential increased with increasing LET (**Figure 18 A**). Survival of HEK cells was decreased up to an LET of 272 keV/ $\mu\text{m}$  (**Figure 18 B**).

In case of the very high LET particles  $^{58}\text{Ni}$  (905 keV/ $\mu\text{m}$ ) and  $^{208}\text{Pb}$  (9674 keV/ $\mu\text{m}$ ), the  $D_0$  increased again, probably due to lower cell killing potential of very heavy ions caused by compacted ionizations within a very narrow track structure and overkill effect (**Figure 18 C and D**). It was concluded that cell killing caused by heavy ions

not only depends on the cell and ion type but also to the range of LET value. For HEK cells, heavy ions in the LET range of 33 to 272 keV/ $\mu\text{m}$  have maximum cell killing potential (**Table 23**).  $D_0$  was calculated from survival curves to determine the biological effectiveness of the heavy ion.

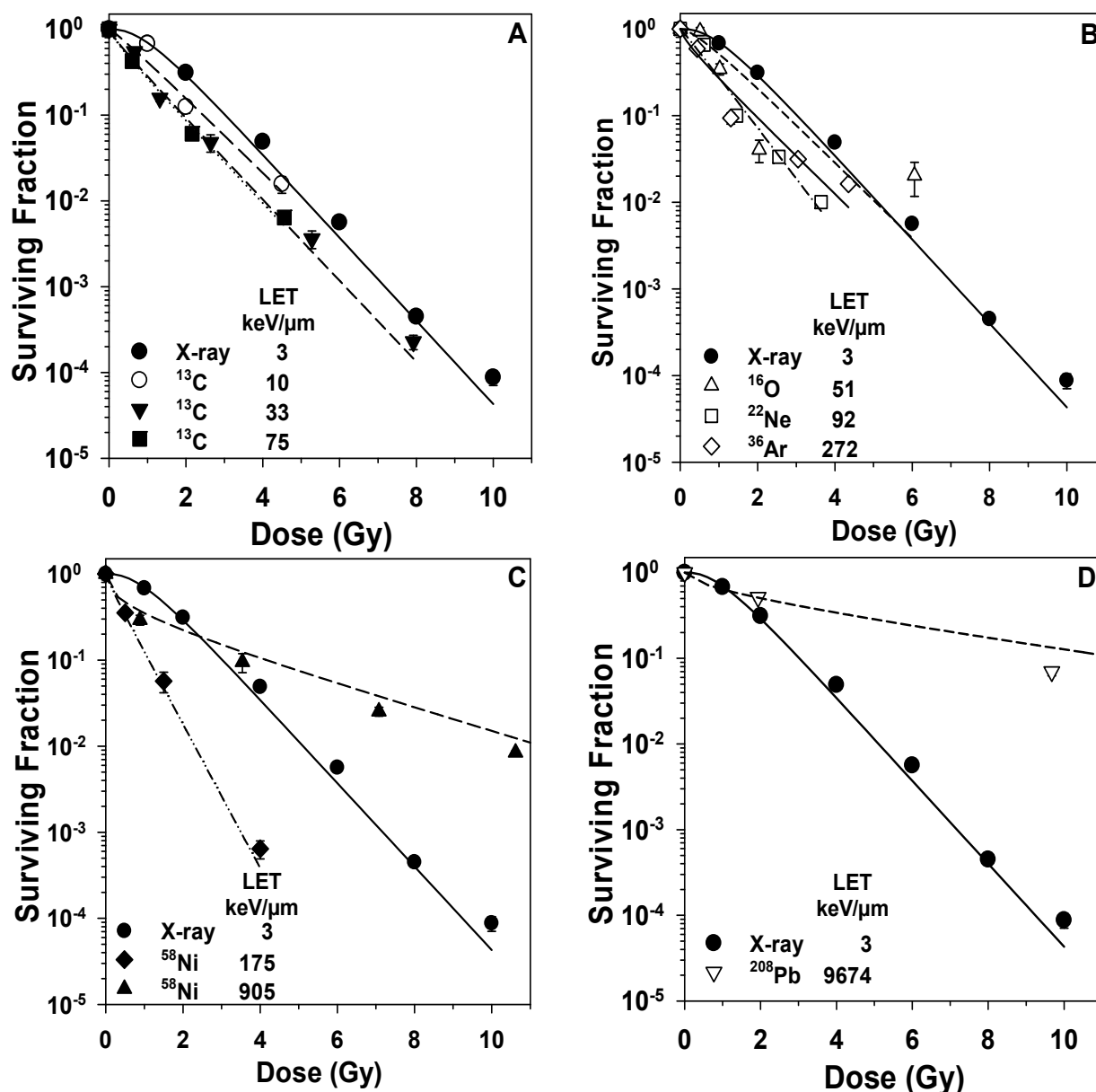


**Figure 18** Survival of HEK cells after exposure to heavy ions (LET 33-9674 keV/ $\mu\text{m}$ ).

Dose-effect curves for cellular survival after exposure to low LET radiation (X rays 0.3-3 keV/ $\mu\text{m}$ ) were compared with high LET radiation (10-9674 keV/ $\mu\text{m}$ ). HEK cells were seeded 24 hours before irradiation and colonies were fixed and stained after 14-21 days incubation. Heavy ions have an increasing killing effect up to the LET 272 keV/ $\mu\text{m}$ . Very high LET heavy ions (> 900 keV/ $\mu\text{m}$ ) showed a lower killing effect compared to X-rays. Bars indicate the standard error resulting from up to 10 independent experiments for X-rays and 1-2 independent heavy ion experiments with six replicates each. If the bars are not visible, they are smaller than the symbol.

**Table 22** Dose and average hits per cell nucleus that is required for doubling of NF- $\kappa$ B-dependent reporter gene expression

Ion	Energy (MeV/n)	LET in H <sub>2</sub> O (keV/ $\mu$ m)	Dose range (Gy)	Average hits per cell nucleus	Dose for 2x NF- $\kappa$ B activation	Average hits for 2x NF- $\kappa$ B activation	RBE (D <sub>2x</sub> ) <sup>a</sup>
X-rays	0.2	0.3-3	0.5 - 32.0	<sup>b</sup>	6.94	**	1.00
<sup>13</sup> C	75	33	0.2 - 29.8	2.8 – 363	1.70	~45	4.07
<sup>16</sup> O	95	51	0.2 - 15.9	2.9 – 279.2	1.21	~22	5.71
<sup>22</sup> Ne	80	92	0.2 - 12.0	2.3 – 109	0.99	~10	7.01
<sup>58</sup> Ni	1000	175	0.5 - 16.0	0.6 – 78	0.98	~5	7.05
<sup>36</sup> Ar	95	272	0.2 - 34.0	0.07 – 1.13	1.26	~4	5.50
<sup>58</sup> Ni	75	905	1.0 - 23.6	0.2 – 21	7.13	~7	0.97
<sup>208</sup> Pb	29	9674	1.0 - 62.0	0.009 – 5.6	8.87	~1	0.78

<sup>a</sup> D<sub>2x</sub> is the dose eliciting a doubling of the NF- $\kappa$ B-dependent fluorescence signal. Average hits per cell nucleus and average hits for 2x NF- $\kappa$ B activation were calculated from Poisson distribution for the respective heavy ion. The RBE was calculated for doubling of NF- $\kappa$ B-dependent fluorescence (RBE<sub>2x</sub>) by dividing D<sub>2x</sub> of X-rays by D<sub>2x</sub> of heavy ions.

<sup>b</sup> As X-rays are not considered to be of particulate nature, the number of hits cannot be calculated. However, it is known that 1 Gy of X-rays results in ~40 DSB/Gy, 800 SSB/Gy, and even more base damage.

**Table 23** Parameters of the survival curves ( $n$ ,  $D_q$ ,  $D_0$ ) and RBE for cell killing by different ion species in HEK cells (sorted from lowest to highest LET)

Ion species	Energy (MeV/ n)	LET in H <sub>2</sub> O (keV/ $\mu$ m)	$n$	$D_q$ (Gy)	$D_0$ (Gy)	RBE ( $D_0$ ) <sup>a</sup>
X-rays	0.2	0.3-3	$1.60 \pm 0.05$	$0.47 \pm 0.05$	$1.00 \pm 0.01$	1
<sup>13</sup> C	100	10	$0.16 \pm 0.18$	$-0.15 \pm 0.17$	$1.00 \pm 0.06$	1
<sup>13</sup> C	75	33	$0.81 \pm 0.10$	$-0.19 \pm 0.10$	$0.92 \pm 0.03$	1.09
<sup>16</sup> O	95	51	$1.10 \pm 0.67$	$0.10 \pm 0.57$	$1.03 \pm 0.14$	0.97
<sup>13</sup> C	35	75	$0.76 \pm 0.07$	$-0.23 \pm 0.07$	$0.91 \pm 0.02$	1.09
<sup>22</sup> Ne	80	92	$1.06 \pm 0.12$	$0.05 \pm 0.09$	$0.74 \pm 0.03$	1.35
<sup>58</sup> Ni	1000	175	$0.84 \pm 0.16$	$-0.08 \pm 0.09$	$0.52 \pm 0.03$	1.92
<sup>36</sup> Ar	95	272	$0.72 \pm 0.10$	$-0.32 \pm 0.11$	$0.97 \pm 0.06$	1.03
<sup>58</sup> Ni	75	905	$0.33 \pm 0.05$	$-3.62 \pm 0.29$	$3.23 \pm 0.20$	0.31
<sup>208</sup> Pb	29	9674	$0.50 \pm 0.09$	$-4.72 \pm 0.86$	$6.93 \pm 0.55$	0.14

<sup>a</sup> RBE was calculated from  $D_0$  by applying the equation  $RBE = D_{0 \text{ reference}}/D_{0 \text{ test}}$ . X-rays were used as reference radiation.



### 3.2.2 Relative biological effectiveness of the tested radiation qualities

In order to quantitatively compare the biological effects induced by the tested radiation qualities, the RBE for cell killing by heavy ion species was calculated by dividing the  $D_0$  value for X-rays by the  $D_0$  value for the respective heavy ion as shown in section 0. The RBE for cell killing was plotted as a function of LET (**Figure 19 A**). The RBE for cell killing increased with LET, showing peak values at around 100-300 keV/ $\mu\text{m}$  and decreased for heavy ions with a LET > 250 keV/ $\mu\text{m}$ . For the very heavy ions -  $^{58}\text{Ni}$  (905 keV/ $\mu\text{m}$ ) and  $^{208}\text{Pb}$  (9674 keV/ $\mu\text{m}$ ) - RBE values fall even below 1.

The doubling of reporter fluorescence above background seen 16 hours after irradiation was considered as relevant biological endpoint for calculation of the RBE of NF- $\kappa\text{B}$  activation. Doses leading to this doubling of reporter signal ( $D_{2x}$ ) were calculated from the initial slopes from the regression lines in **Figure 16**. RBE values for NF- $\kappa\text{B}$  activation by each heavy ion species were calculated by dividing the  $D_{2x}$  value for X-rays by the  $D_{2x}$  value for the respective heavy ion. The RBE for NF- $\kappa\text{B}$  activation was plotted as a function of LET (**Figure 19 B**). The RBE for NF- $\kappa\text{B}$  activation is shown to increase gradually with LET to a maximum in the range of 30-300 keV/ $\mu\text{m}$ . For radiation qualities with an LET > 300 keV/ $\mu\text{m}$ , the RBE for NF- $\kappa\text{B}$  activation decreases to 1.

While for reproductive cell death the RBE reaches maximal values of around 2, RBE for NF- $\kappa\text{B}$  activation is much higher with a maximum of at least 7.

Very high LET ions with an LET > 300 keV/ $\mu\text{m}$ , such as  $^{208}\text{Pb}$  (9674 keV/ $\mu\text{m}$ ) and  $^{58}\text{Ni}$  (906 keV/ $\mu\text{m}$ ), were less efficient for both, cell killing and NF- $\kappa\text{B}$  activation.

### 3.2.3 Effect of ionizing radiation on cell cycle progression

The previous subchapters described the dose and LET dependence of cellular survival as a late endpoint after exposure to different radiation qualities. NF- $\kappa\text{B}$  activation as early change after radiation exposure was also shown to be strongly dose- and LET-dependent. Here, alteration of cell cycle progression as an early step of the cellular response, integrating several signaling pathways, to different radiation qualities was determined.

### 3.2.3.1 X-irradiation leads to cell cycle arrest in G2/M-and S-phase

To investigate the time effect in DNA damage response, the progression of cells through the mitotic cell cycle was analyzed. The mitotic cycle is a tightly regulated and controlled process which gives cells the chance to verify the quality of the

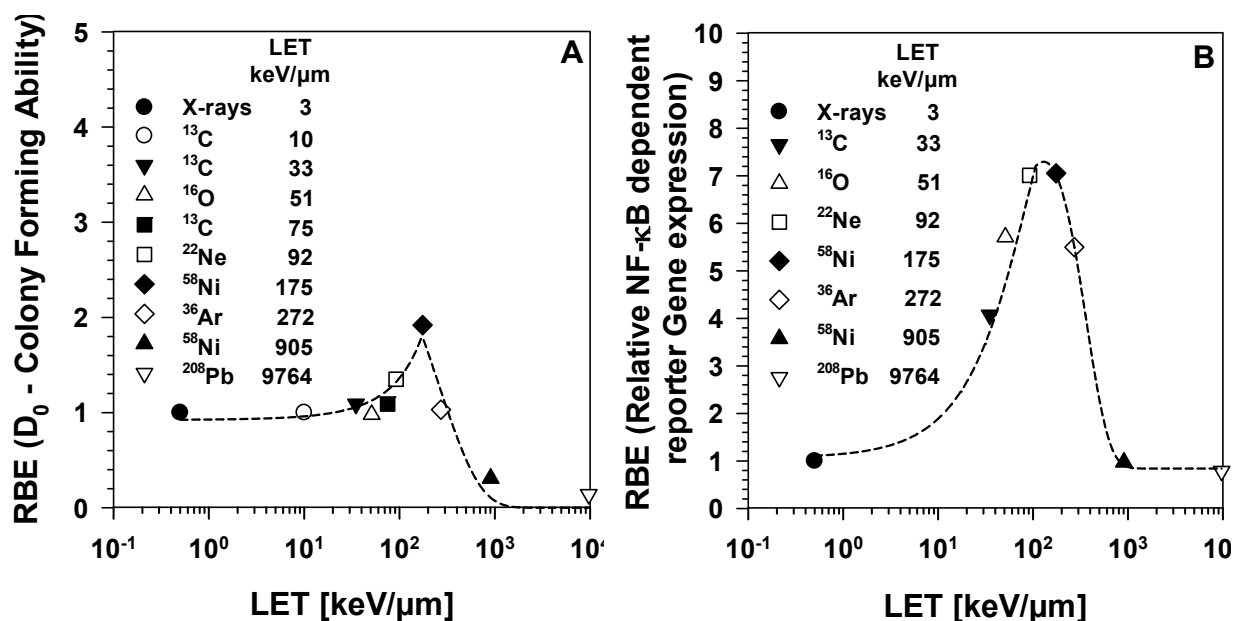


**Figure 19 Relative Biological Effectiveness (RBE) of different heavy ions for 0.37 survival fraction (A) and NF-κB activation (B).**

The RBE values for cell killing were calculated by dividing respective D<sub>0</sub> value of cellular survival after X-irradiation by D<sub>0</sub> value of cellular survival after heavy ions exposure according to Table 23. The RBE for NF-κB activation was calculated by dividing the reference radiation dose initiating a duplication of the reporter fluorescence (D<sub>2x</sub> of X-rays) by the absorbed dose of the test radiation (D<sub>2x</sub> of heavy ions) as described in Table 22. The maximum RBE for NF-κB activation is in the same range of LET value 100-300 keV/μm as for cell killing.

genetic material before critical steps take place. While in the S-phase DNA is being duplicated, in M-phase the duplicated DNA is evenly distributed to daughter cells. Overcoming of checkpoints at the ends of the preceding gap phases G1 and G2 requires a certain quality of the genetic material and in case of DNA damage the cell cycle phases can be delayed or blocked either in G1 or in G2/M phase. Such cell cycle blocks from X-rays-induced DNA damage, enables an efficient radiation response in form of DNA repair. The severity and amount of DNA damage determines the extent and duration of G2/M arrest.

A clear correlation between increasing X-ray dose and the distribution/progression of cells in the mitotic cycle can be seen in **Figure 20**. The normal distribution of cells in

different phases of cell cycle is represented by 0 h samples which is G1: ~60 %, S: ~25 %, G2: ~15 %. After exposure with 2 Gy of X-rays the cell cycle was arrested progressively in G2/M phase till 16 h and came back to the normal distribution of cells afterwards. After 4 Gy of X-irradiation, the cell cycle was arrested in G2/M phase for a longer period of time (16-24 h). After a dose of 8 Gy the arrest in G2/M phase was much more pronounced and lasted more than 48 h. At very high doses such as 16 Gy cells are arrested in the S phase of cell cycle. These results demonstrate that X-rays induce a time- and dose-dependent cell cycle arrest of HEK cells in G2/M and S-phase.

### **3.2.3.2 Effect of X-rays on expression of cell cycle regulating genes**

To determine the possible mechanisms underlying the effects of ionizing radiation on cell cycle progression, the expression of genes related to cell cycle regulation was evaluated. The mRNA levels of CDKN1A and GADD45 $\alpha$  were determined by real-time RT-qPCR. Exposure to low LET radiation doses of 2 and 4 Gy showed significant time-dependent up-regulation of CDKN1A which was more than 2 folds around 16 hours compared to basal level (**Figure 21 A**). The expression level of GADD45 $\alpha$  was 3 fold up-regulated around 16 hours and remained up-regulated up to 24 hours after 4 Gy exposure (**Figure 21 B**).

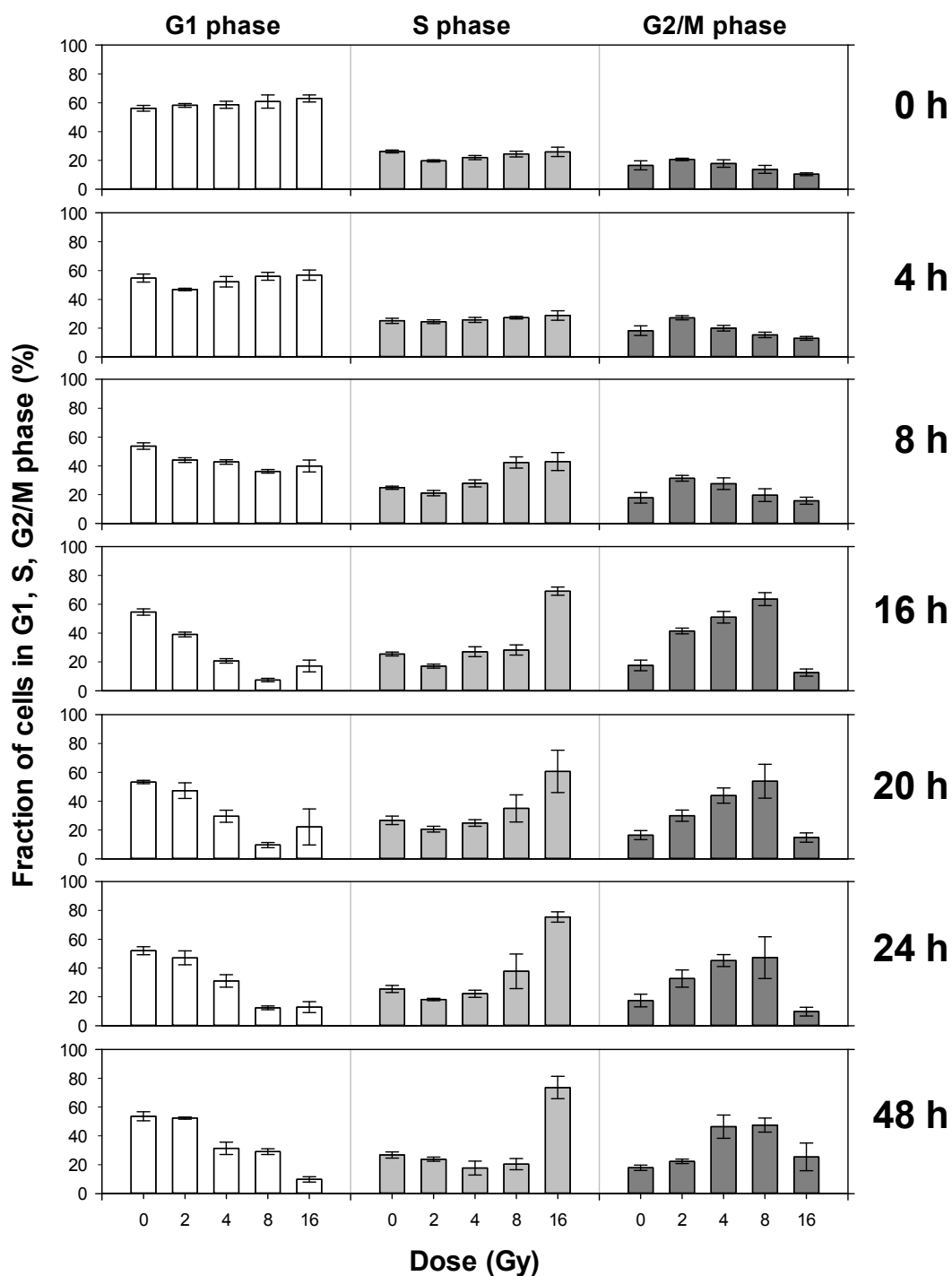


**Figure 20 Cell cycle progression in HEK-pNF $\kappa$ B-DD-tdTomato-C8 cells after X-ray exposure**

HEK-pNF $\kappa$ B-DD-tdTomato-C8 cells were exposed to X-rays (up to 16 Gy). For cell cycle determination cells were fixed in 70% ethanol, stained with propidium iodide and analyzed by flow cytometry. Cell cycle phases G1, S and G2 were determined by the intensity of propidium iodide fluorescence which corresponds to the DNA content of cells. The fraction of cells in G1, S and G2/M phases in 0 h samples show the normal distribution of cells in cell cycle phases. Cells accumulate in G2/M phase maximally 16-24 h after exposure to X-ray ( $\leq 8$  Gy). The duration of G2/M block increased respectively to the dose. As the dose increases up to 16 Gy, the fraction of cells in the S phase increases and lasted for more than 48 h. Bars represent the standard error of more than three individual experiments.

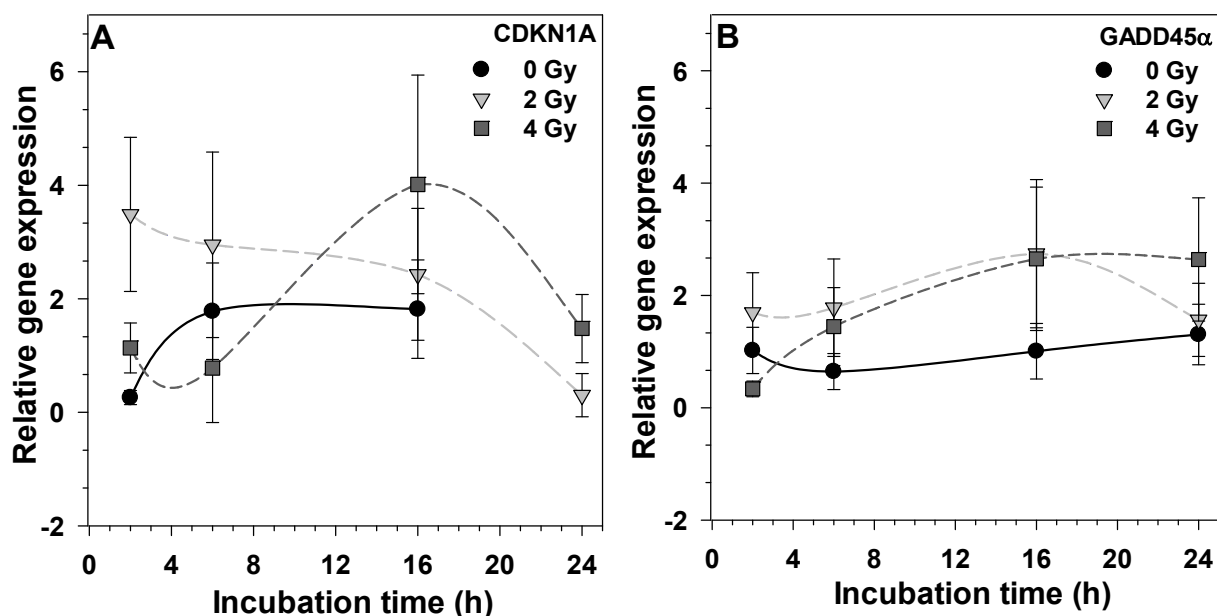


**Figure 21 Expression of CDKN1A (A) and GADD45α (B) after X-irradiation**

HEK cells were exposed to 0, 2 and 4 Gy of X-rays and harvested at the indicated time points. Target gene (CDKN1A and GADD45α) expression was normalized against the expression of the optimal combination of the housekeeping genes PBGD, HPRT and GAPDH. The 0 Gy is the control and shows basal expression of target genes. Means and standard error of three independent experiments with each three technical replicates are shown.

### 3.2.3.3 Heavy ions arrest the cell cycle in G2/M and S phase dependent on LET range and dose

To determine the cell cycle behavior after exposure to radiation with increasing LET values, heavy ions of different LET values (**Table 15**) were used. The kinetics of cell cycle arrest after X-irradiation indicated that a peak response is reached 16-20 h after radiation exposure. Therefore, the cell cycle distribution 18 h after exposure with different radiation qualities was analyzed (**Figure 22**).

After X-ray exposure cells were arrested gradually in G2/M phase till 8 Gy. The S-phase arrest was more pronounced after exposure to heavy ions of LET 30-175 keV/μm, compared to X-ray exposure. At very high doses such as 16 Gy, cells got arrested in S phase due to higher damage. At an LET of 33 keV/μm the cells accumulated in G2/M phase at low dose ( $\leq 2$  Gy) but after 4 Gy cells were arrested in S phase. It was observed that at doses below 4 Gy, the cell cycle was arrested

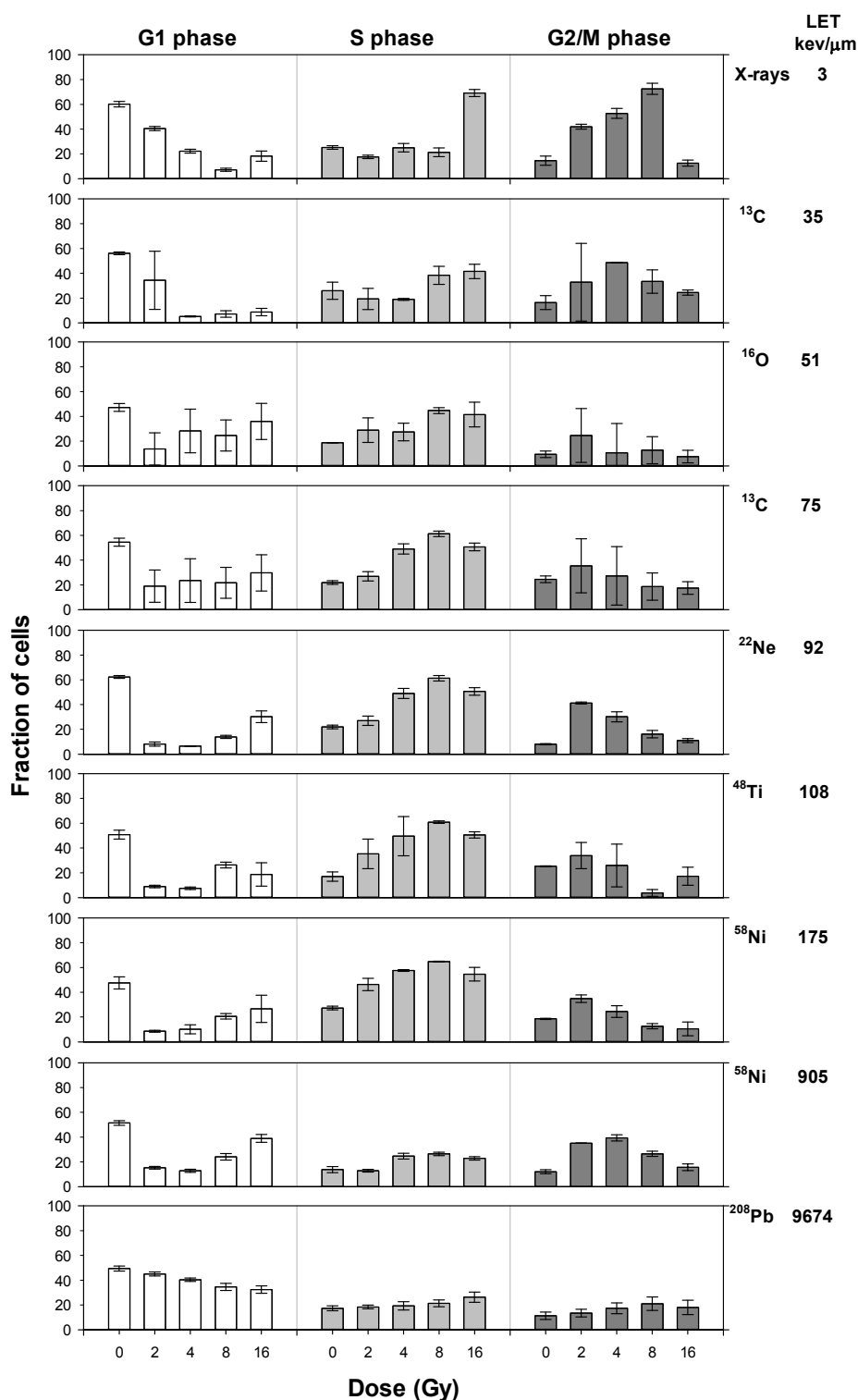


**Figure 22 Cell cycle distribution after exposure to heavy ions of different LET values (3-9674 keV/μm)**

HEK reporter cells were exposed to defined doses of X-rays and heavy ions listed in Table 15. For cell cycle determination cells were fixed in 100% ethanol 18 h after irradiation, stained with propidium iodide and analyzed by flow cytometry. The fraction of cells in G1, S and G2/M phases shows the distribution of cells in different phases of cell cycle. After low dose and low LET exposure cells accumulated stronger in G2/M phase. The fraction of cells in S phase increased after exposure to heavy ions in the LET range of 30-175 keV/μm. Cell cycle experiments with heavy ions were performed once due to their limited availability therefore no standard errors bars are shown.

in G2/M phase but as LET and dose is increased the cells started arresting in the S phase. The HEK reporter cells exhibited a higher S-phase arrest after  $^{16}\text{O}$  ion (51 keV/ $\mu\text{m}$ ) exposure and a G2/M phase arrest after  $^{13}\text{C}$  ion (75 keV/ $\mu\text{m}$ ) exposure compared to X-irradiation at low and high doses both. The accumulation of cells in S-phase increased dose-dependently after irradiation with  $^{22}\text{Ne}$  (80 keV/ $\mu\text{m}$ ),  $^{48}\text{Ti}$  (108 keV/ $\mu\text{m}$ ) and  $^{58}\text{Ni}$  (175 keV/ $\mu\text{m}$ ) ions, compared to the fraction of cells in S-phase after X-irradiation. Maximum S phase arrest was observed at 16 Gy of  $^{48}\text{Ti}$  (108 keV/ $\mu\text{m}$ ). At very high LET values such as  $^{58}\text{Ni}$  (175 and 905 keV/ $\mu\text{m}$ ) and  $^{209}\text{Pb}$  (9674 keV/ $\mu\text{m}$ ) cells seemed to accumulate in G1 phase and no S phase or G2 arrest was observed after  $^{209}\text{Pb}$  (9674 keV/ $\mu\text{m}$ ) irradiation even at very high doses till 16 Gy.

### 3.2.3.4 Effect of LET on expression of cell cycle regulating genes

To determine the possible mechanisms underlying the effects of LET on cell cycle progression, the expression of CDKN1A and GADD45 $\alpha$  was evaluated at mRNA level. The expression of GADD45 $\alpha$  was quicker compared to CDKN1A after high LET irradiation. The GADD45 $\alpha$  gene showed early expression at 6 h after irradiation that decreased at 24 h, whereas CDKN1A showed a higher expression 24 h after irradiation compared to the 6 h values (Figure 23 A).

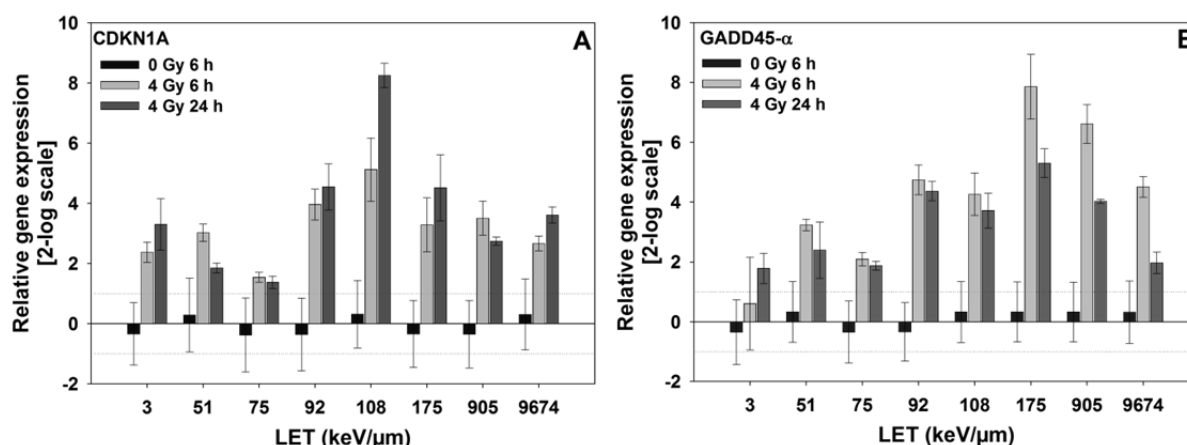


**Figure 23 Expression of CDKN1A (A) and GADD 45 $\alpha$  (B) after heavy ion exposure**

Cells were harvested 6 and 24 h after exposure to 4 Gy X-rays or accelerated heavy ions. CDKN1A and GADD45 $\alpha$  mRNA levels were determined by real-time RT-qPCR. Values represent normalized means of 3 replicates and are expressed relative to non-irradiated controls. CDKN1A and GADD45 $\alpha$  gene expressions were normalized against the expression of the reference genes PBGD, HPRT and GAPDH. Means and standard deviation of three replicates are shown.

A gradual increase in GADD45 $\alpha$  expression was observed with increasing LET which was highest at 175 keV/ $\mu$ m (**Figure 23 B**). The CDKN1A showed early expression up to 75 keV/ $\mu$ m and then a stronger late expression was observed with a peak at 108 keV/ $\mu$ m. Heavy ions induce expression of CDKN1A and GADD45 $\alpha$  most efficiently at LET values in the range of 50-175 keV/ $\mu$ m where most of the cells are arrested in S and G2/M phase. Very high LET heavy ions,  $^{58}\text{Ni}$  (905 keV/ $\mu$ m) and  $^{208}\text{Pb}$  (9764 keV/ $\mu$ m), up-regulated CDKN1A and GADD45 $\alpha$  expression but to a smaller extent than at LET values of 92-175 keV/ $\mu$ m.

### 3.3 Contribution of NF- $\kappa$ B activation in different cellular responses

The role of NF- $\kappa$ B signaling in the above mentioned cellular radiation responses (cellular survival, and cell cycle progression) was determined by using NF- $\kappa$ B knock down cell line.

#### 3.3.1 NF- $\kappa$ B down-regulation decreases cell survival after X-irradiation

The role of NF- $\kappa$ B in cellular survival was determined by comparing the HEK-pNF $\kappa$ B-DD-tdTomato-C8 cell line (wild-type NF- $\kappa$ B regulation) with the HEK shRNA RelA cell line (NF- $\kappa$ B subunit RelA knock down). **Figure 24** shows the HEK shRNA RelA cell line to be more radiation sensitive compared to the cell line HEK-pNF $\kappa$ B-DD-tdTomato-C8, as judged by the parameters  $D_0$  and  $n$  of the dose effect curves calculated according to the single-hit multi-target model (**Table 24**). Statistical analysis revealed the dose effect curves to be different on a  $P=2\alpha$  level  $\geq 0.05$  (**Table 25**).

#### 3.3.2 Pre-activation of NF- $\kappa$ B decreases cell survival after high dose X-ray exposure

To determine the effect of prior NF- $\kappa$ B activation on cell survival, HEK-pNF $\kappa$ B-DD-tdTomato-C8 cells were treated with TNF- $\alpha$  (20 ng/ml) for 6 and 20 h before X-irradiation. As shown in **Figure 15**, NF- $\kappa$ B-dependent reporter gene expression reaches its maximum around 6 h after addition of TNF- $\alpha$ , and decreases to a lower level that is sustained for several hours.



Incubation with TNF- $\alpha$  for 6 h before irradiation did not significantly modify radiation response. However, in cells treated with TNF- $\alpha$  for 20 h it was observed that cellular survival was significantly decreased at 6 Gy and 8 Gy compared to untreated cells (Figure 25).

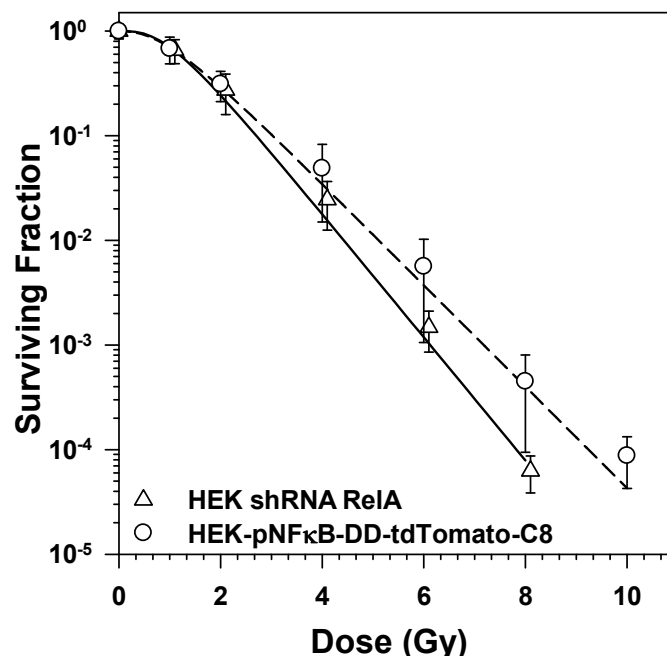


**Figure 24 Impact of RelA deficiency on cell survival after X-irradiation**

Cellular survival of HEK-pNF $\kappa$ B-DD-tdTomato-C8 and HEK shRNA RelA cells was determined using the colony forming ability assay. Both cell lines showed a shoulder in the low dose range.  $D_0$  was decreased from 0.9 to 0.74 in HEK-shRNA RelA cells (Table 24) which shows that down-regulating NF- $\kappa$ B increases the radiosensitivity of HEK cells. More than three individual experiments were performed with 6 petri dishes per dose and comparison of dose effect curves was done by Student's t-test based on significance level  $P=2\alpha \leq 0.05$  (Table 25).

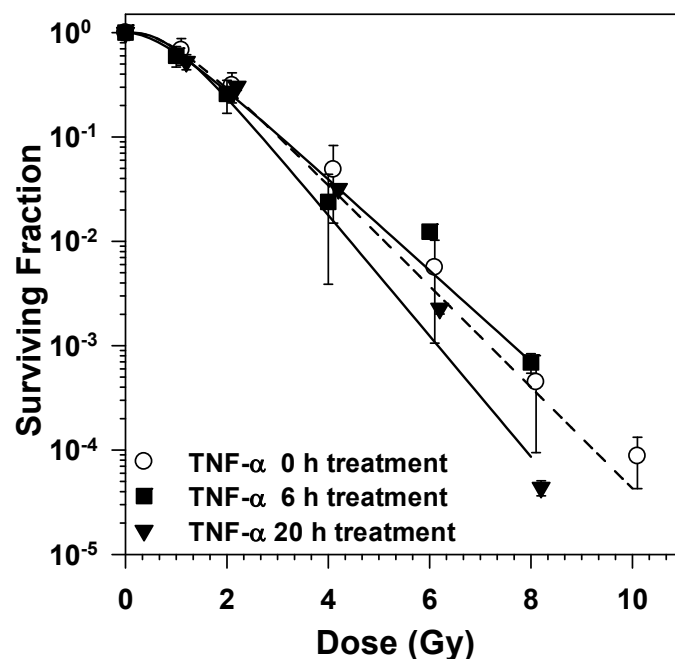


**Figure 25 Effect of NF- $\kappa$ B modulation by TNF- $\alpha$  on cellular survival after X-irradiation**

The down-regulation of NF- $\kappa$ B 20 h after TNF- $\alpha$  treatment made the cell line more sensitive with a  $D_0$  of  $\sim 0.7$  than the untreated cell line ( $D_0$  of  $\sim 0.9$ ) (Table 24). Pre-treatment with TNF- $\alpha$  6 h before irradiation showed no significant effect in increasing cellular survival. The experiments were performed with 6 petri dishes per dose and the dose-effect curves were compared by Student's t-test based on a significance level of  $P=2\alpha \leq 0.05$  (Table 25).

### 3.3.3 NF- $\kappa$ B deactivation results in impairment of DNA damage recovery

In order to examine the influence of NF- $\kappa$ B modulation on DNA damage response, recovery from sublethal damage was investigated. This was done by comparing survival curves for cells plated immediately after X-ray exposure (IP) and cells which were allowed to process DNA damage for 24 h before plating (LP).

A recovery period of 24 h did not result in survival improvement for HEK-pNF $\kappa$ B-DD-tdTomato-C8 cells.  $D_0$  values of survival curves were not significantly different with 0.9 and 0.92 Gy for IP and LP conditions, respectively (**Figure 26, Table 25**). For HEK shRNA RelA, however, the survival capacity of late plated cells was even lower compared to the early plated cells.  $D_0$  values for IP and LP are 0.74 and 0.65, respectively (**Table 24**). The reduction of  $D_0$  indicates a possible DNA damage repair impairment for NF- $\kappa$ B knockdown cells.

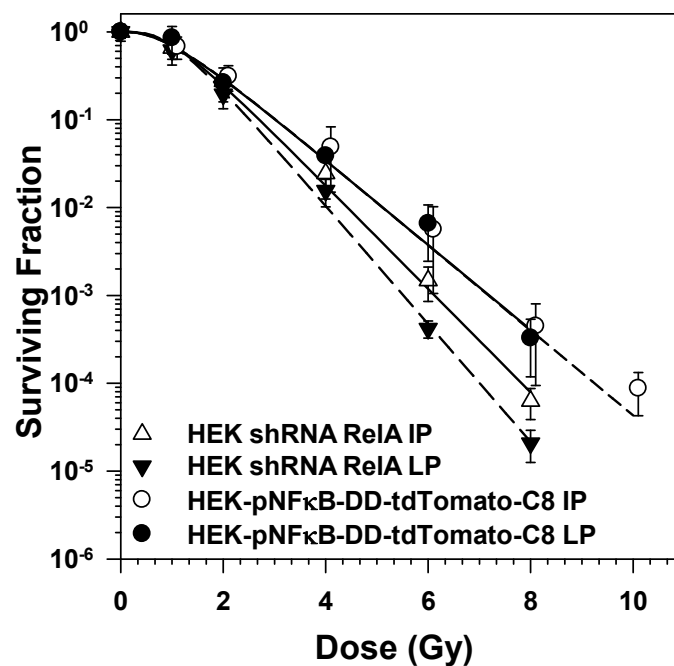


**Figure 26 DNA damage recovery capacity in HEK-pNF $\kappa$ B-DD-tdTomato-C8 and HEK shRNA RelA cells**

After X-ray exposure, immediate plating (IP) and late plating 24 h after irradiation (LP) experiments were performed by using HEK-pNF $\kappa$ B-DD-tdTomato-C8 and HEK shRNA RelA cells with six replicates per dose and at least three independent experiments. HEK-pNF $\kappa$ B-DD-tdTomato-C8 cells showed no significant difference for IP and LP on a  $p=2\alpha$  level  $\leq 0.05$  (Table 25). Decreased cellular survival after LP of HEK shRNA RelA cells indicates that down-regulation of NF- $\kappa$ B results in impairment of DNA damage response. The  $D_0$  of HEK shRNA RelA LP was reduced from  $\sim 0.74$  to  $D_0$  of  $\sim 0.64$  (Table 24) showing increased radiosensitivity.

**Table 24** Parameters of survival curves ( $D_0$ ,  $n$  and  $D_q$ ) after X-ray exposure and statistical values for HEK-pNF $\kappa$ B-DD-tdTomato-C8 and HEK shRNA RelA cells

Parameter	HEK-pNF $\kappa$ B-DD-tdTomato-C8	HEK cells	HEK-pNF $\kappa$ B-DD-tdTomato-C8	HEK-pNF $\kappa$ B-DD-tdTomato-C8	HEK-pNF $\kappa$ B-DD-tdTomato-C8	HEK shRNA RelA	HEK shRNA RelA
Treatment			Late plating	TNF- $\alpha$ 6 h	TNF- $\alpha$ 20 h		Late plating
Degrees of freedom	459	95	131	63	22	205	62
Determination coefficient ( $r^2$ )	0.93	0.95	0.95	0.86	0.98	0.95	0.99
slope	$-1.12 \pm 0.02$	$-1.13 \pm 0.03$	$-1.09 \pm 0.02$	$-0.94 \pm 0.05$	$-1.46 \pm 0.04$	$-1.36 \pm 0.02$	$-1.55 \pm 0.02$
Intercepts	$1.11 \pm 0.08$	$1.13 \pm 0.13$	$0.99 \pm 0.12$	$0.17 \pm 0.22$	$2.12 \pm 0.24$	$1.40 \pm 0.10$	$1.62 \pm 0.12$
$D_0$	$0.90 \pm 0.01$	$0.92 \pm 0.02$	$0.92 \pm 0.02$	$1.07 \pm 0.06$	$0.70 \pm 0.03$	$0.74 \pm 0.01$	$0.65 \pm 0.01$
$n$	$3.02 \pm 0.23$	$2.70 \pm 0.30$	$2.70 \pm 0.30$	$1.20 \pm 0.30$	$2.60 \pm 0.10$	$4.04 \pm 0.42$	$5.10 \pm 0.63$
$D_q$	$1.0 \pm 1.301$	$0.91 \pm 1.10$	$0.91 \pm 1.10$	$0.18 \pm 1.38$	$0.66 \pm 0.06$	$1.03 \pm 0.63$	$1.05 \pm 0.29$

Table 25 Comparison<sup>a</sup> of X-rays survival curves of HEK cells after immediate and late plating and TNF- $\alpha$  treatment

Reference cell line	HEK-pNF $\kappa$ B-DD-tdTomato-C8	HEK-pNF $\kappa$ B-DD-tdTomato-C8	HEK-pNF $\kappa$ B-DD-tdTomato-C8	HEK-pNF $\kappa$ B-DD-tdTomato-C8	HEK-pNF $\kappa$ B-DD-tdTomato-C8	HEK shRNA RelA
Test cell line	HEK-pNF $\kappa$ B-DD-tdTomato-C8 LP	HEK cells	HEK-pNF $\kappa$ B-DD-tdTomato-C8 TNF- $\alpha$ 6 h	HEK-pNF $\kappa$ B-DD-tdTomato-C8 TNF- $\alpha$ 20 h	HEK shRNA RelA	HEK shRNA RelA LP
Degrees of freedom	594	558	526	485	668	271
Critical value for $2\alpha = 0.05$	1.96	1.96	1.96	1.96	1.96	1.97
T-value ( $P=2\alpha$ ) for slope	0.84	0.42	4.07	5.33	8.76	5.00
Level of significance ( $P=2\alpha$ )	0.39	0.68	< 0.05	< 0.05	< 0.05	< 0.05
	Slope <sub>1</sub> = slope <sub>2</sub>	Slope <sub>1</sub> = slope <sub>2</sub>	Slope <sub>1</sub> $\neq$ slope <sub>2</sub>	Slope <sub>1</sub> $\neq$ slope <sub>2</sub>	Slope <sub>1</sub> $\neq$ slope <sub>2</sub>	Slope <sub>1</sub> $\neq$ slope <sub>2</sub>
T-value ( $P=2\alpha$ ) for intercepts	0.029	0.29	5.93	4.91	2.29	1.27
Level of significance ( $P=2\alpha$ )	0.97	0.77	< 0.05	< 0.05	< 0.05	< 0.05
	Intercepts <sub>1</sub> = Intercepts <sub>2</sub>	Intercepts <sub>1</sub> = Intercepts <sub>2</sub>	Intercepts <sub>1</sub> $\neq$ Intercepts <sub>2</sub>	Intercepts <sub>1</sub> $\neq$ Intercepts <sub>2</sub>	Intercepts <sub>1</sub> $\neq$ Intercepts <sub>2</sub>	Intercepts <sub>1</sub> $\neq$ Intercepts <sub>2</sub>

<sup>a</sup>Statistical analysis for comparison was done by student's t-test for the single-hit multi-target model of radiation action

### 3.3.4 NF- $\kappa$ B down-regulation delays cell cycle progression

To determine the role of NF- $\kappa$ B in cell cycle arrest, the G2/M phase arrest of HEK-pNF $\kappa$ B-DD-tdTomato-C8 cells and HEK shRNA RelA cells was compared after X-irradiation with 4 Gy. It was observed that 16 hours after X-irradiation almost 55 % of total population of HEK-pNF $\kappa$ B-DD-tdTomato-C8 and HEK shRNA RelA cells were arrested in G2/M phase. The G2/M block started to release 24 hours after X-irradiation and 40 % of total population of HEK-pNF $\kappa$ B-DD-tdTomato-C8 cells remained in G2/M phase, whereas 60 % of total population of HEK shRNA RelA cells was still in G2/M arrest. The G2/M arrest was reduced to 25 % and 45 % in HEK-pNF $\kappa$ B-DD-tdTomato-C8 and HEK shRNA RelA cells respectively. The release of G2/M arrest was delayed significantly longer in HEK shRNA RelA cells compared to HEK-pNF $\kappa$ B-DD-tdTomato-C8 cells (**Figure 27**). The longer G2/M arrest confirms a delayed DNA damage response in HEK shRNA RelA cells.

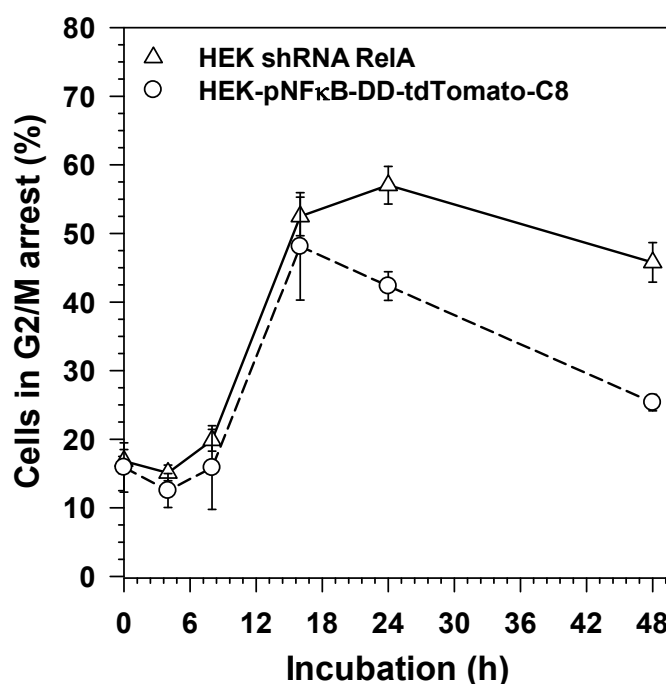


**Figure 27 G2 phase arrest of HEK-pNF $\kappa$ B-DD-tdTomato-C8 and HEK shRNA RelA cells after 4 Gy X-irradiation**

The G2/M fraction of HEK-pNF $\kappa$ B-DD-tdTomato-C8 and HEK shRNA RelA cells was compared after X-irradiation (4 Gy). Cells started accumulating in G2/M phase 8 h after irradiation as shown in Figure 20. The maximum G2/M arrest was observed 16-24 h after X-irradiation. The accumulation of cells in G2/M phase was comparable in both cell lines after 16 h but the release of G2/M arrest lasted longer in HEK shRNA RelA cells. Bars represent the standard error of more than three individual experiments.

### 3.4 The regulation of NF- $\kappa$ B down-stream target genes after ionizing radiation exposure

The former chapter revealed a modulating role of NF- $\kappa$ B in cellular survival, DNA damage response and cell cycle arrest after ionizing radiation exposure resulting in higher radiosensitivity in case of RelA down-regulation. It is therefore hypothesized that a set of cell-protecting NF- $\kappa$ B target genes is up-regulated in response to ionizing radiation exposure. To determine which NF- $\kappa$ B down-stream genes are regulated in the cellular radiation response, NF- $\kappa$ B was activated by ionizing radiation with different LET and target gene array was performed.

#### 3.4.1 NF- $\kappa$ B-dependent gene expression analysis after X-irradiation

Ionizing radiation was shown to be a strong NF- $\kappa$ B activator, and down-regulation of its subunit p65 resulted in a higher radiosensitivity. Therefore NF- $\kappa$ B-dependent target gene expression was analyzed after X-irradiation (4 Gy and 8 Gy). The time point for investigation of NF- $\kappa$ B target gene expression was chosen to be 6 hours as activation of NF- $\kappa$ B was already ensured and cells were not yet blocked in the cell cycle at this time point (**Figure 15** and **Figure 27**). RNA was isolated and tested for its integrity as described in 2.2.4.1-2. Gene expression was investigated using the RT<sup>2</sup> Profiler™ PCR Arrays (section 2.2.5) and the expression profile was analyzed by an Excel-based template provided by SABiosciences. C<sub>t</sub> values of irradiated cells were compared to the C<sub>t</sub> values of the untreated sample. A list of all genes and the corresponding value for fold-regulation of all irradiation schemes is shown in **Table 27**.

For X-ray exposure, NF- $\kappa$ B-dependent genes which are up- or down-regulated by more than a factor of 2 are shown in **Table 26**. A set of CXCL genes (CXCL-1, CXCL-2, CXCL-8, CXCL-10), NF $\kappa$ B1, NF $\kappa$ B2, NF $\kappa$ BIA, TNF, CCL2, VCAM1 and CD83 were strongly up-regulated. This shows that ionizing radiation modulates gene expression of pro-inflammatory cytokines (TNF), chemokines (CXCL-1, CXCL-2, IL-8/CXCL8, CXCL-10, chemoattractant protein 1, MCP-1/CCL2), adhesion molecules (vascular cell adhesion molecule-1, VCAM-1), membrane proteins (Cluster of Differentiation 83; CD83), other transcription factors (interferon regulatory factor 1;

IRF1) and anti-apoptotic factors (BIRC3/cIAP2) by activating the NF- $\kappa$ B pathway. NF- $\kappa$ B also regulates its own expression and activation status by modulating expression of NFKB1, NFKB2 and NFKBIA genes which encode NF- $\kappa$ B p105/p50, NF- $\kappa$ B p105/p52 and I $\kappa$ B $\alpha$ , respectively. The only down-regulated gene was mitogen-activated protein kinase kinase 6 (MAP2K6). Down-regulation of MAP2K6 and up-regulation of BIRC3 play a role in anti-apoptosis.

**Table 26 Gene expression in HEK cells 6 hours after X-irradiation using the RT<sup>2</sup> Profiler™ PCR target gene array. Genes more than two fold up- or down regulated are given in bold.**

Gene symbol	Description	Relative gene expression after X-irradiation	
		4 Gy	8 Gy
<b>TNF</b>	Tumor necrosis factor	<b>4.33</b>	<b>11.98</b>
<b>CXCL 1</b>	Chemokine (C-X-C motif) ligand 1	<b>3.22</b>	<b>6.36</b>
<b>CXCL 2</b>	Chemokine (C-X-C motif) ligand 2	<b>2.13</b>	<b>2.78</b>
<b>IL8</b>	Interleukin 8	1.90	<b>3.13</b>
<b>CXCL 10</b>	Chemokine (C-X-C motif) ligand 10	<b>4.32</b>	<b>12.75</b>
<b>CCL2</b>	Monocyte chemoattractant protein 1	1.16	<b>2.18</b>
<b>VCAM1</b>	Vascular cell adhesion molecule-1	<b>2.18</b>	<b>2.04</b>
<b>CD83</b>	Cluster of Differentiation 83	<b>2.46</b>	<b>3.71</b>
<b>NFKB1</b>	Nuclear factor of kappa B p105 subunit	1.55	<b>2.59</b>
<b>NFKB2</b>	Nuclear factor of kappa B p100 subunit	<b>2.78</b>	<b>3.87</b>
<b>NFKBIA</b>	Nuclear factor of kappa light poly peptide gene enhancer in B-cells inhibitor, alpha	<b>2.48</b>	<b>4.11</b>
<b>IRF1</b>	Interferon regulatory factor 1	1.38	<b>2.08</b>
<b>BIRC3</b>	Baculoviral IAP repeat-containing 3	1.69	<b>2.41</b>
<b>MAP2K6</b>	Mitogen-activated protein kinase kinase 6	<b>-2.25</b>	<b>-3.18</b>

### 3.4.2 NF- $\kappa$ B-dependent gene expression after heavy ion exposure

To investigate the regulation of NF- $\kappa$ B target genes expression in HEK cells after irradiation with different radiation qualities and doses, the RT<sup>2</sup> RNA qPCR NF- $\kappa$ B target gene array was used. As the RBE for NF- $\kappa$ B activation was found to be maximal at an LET of ~100 keV/ $\mu$ m, samples irradiated with <sup>22</sup>Ne ions (92 keV/ $\mu$ m)



**Table 27 Analysis of gene expression<sup>a</sup> in HEK reporter cells 6 hours after treatment with X-rays (200 kV, 4 and 8 Gy) <sup>22</sup>Ne (92 keV/μm, 4 Gy) and <sup>48</sup>Ti (108 keV/μm, 4 Gy. Data for <sup>48</sup>Ti are taken from (Koch 2013)**

Radiation	X-Rays		Ne	Ti	Radiation	X-Rays		Ne	Ti
	4 Gy	8 Gy	4 Gy	4 Gy		4 Gy	8 Gy	4 Gy	4 Gy
Dose					Dose				
LET	0.3-3	0.3-3	92	108	LET	0.3-3	0.3-3	92	108
RBE (NFκB <sub>2x</sub> )	1	1	7	5	RBE (NFκB <sub>2x</sub> )	1	1	7	5
<i>ADM</i>	-1.07	-1.19	1.29	1.10	<i>IL1B</i>	-1.17	-1.45	1.13	-1.08
<i>AGT</i>	1.18	1.06	-1.13	-1.88	<b><i>IL1R2</i></b>	-1.23	-1.54	<b>6.25</b>	<b>-2.30</b>
<i>AKT1</i>	1.04	1.11	1.31	1.10	<i>IL1RN</i>	-1.22	-1.11	-1.29	1.47
<i>ALDH3A2</i>	-1.01	-1.10	-1.13	-1.16	<i>IL2</i>	1.01	-1.12	-1.06	-1.43
<i>BCL2A1</i>	1.24	-1.24	-1.20	-1.02	<i>IL2RA</i>	-1.01	1.21	-1.32	1.44
<i>BCL2L1</i>	-1.23	-1.22	1.01	-1.19	<i>IL4</i>	1.05	-1.14	1.39	-1.45
<i>BIRC2</i>	-1.15	-1.00	1.23	1.05	<i>IL6</i>	1.23	1.06	1.03	-1.74
<b><i>BIRC3</i></b>	1.69	<b>2.41</b>	1.24	1.59	<b><i>IL8</i></b>	1.90	<b>3.13</b>	<b>2.51</b>	<b>5.11</b>
<b><i>C3</i></b>	1.77	-1.03	<b>-2.30</b>	-1.03	<i>INS</i>	1.10	1.21	1.38	-1.39
<b><i>CCL11</i></b>	1.93	1.91	<b>2.27</b>	-1.24	<b><i>IRF1</i></b>	1.38	<b>2.08</b>	<b>2.20</b>	<b>2.78</b>
<b><i>CCL2</i></b>	1.16	<b>2.18</b>	<b>2.00</b>	<b>2.89</b>	<i>LTA</i>	1.11	1.28	1.52	<b>-2.93</b>
<i>CCL22</i>	-1.22	-1.11	-1.29	1.47	<b><i>LTB</i></b>	-1.11	-1.13	-1.31	<b>-2.78</b>
<b><i>CCL5</i></b>	1.52	1.34	-1.83	<b>-2.31</b>	<b><i>MAP2K6</i></b>	<b>-2.25</b>	<b>-3.18</b>	1.39	-1.85
<i>CCND1</i>	1.03	1.08	1.75	-1.06	<i>MMP9</i>	-1.37	-1.49	-1.04	-1.05
<b><i>CCR5</i></b>	1.16	1.07	1.32	<b>-2.83</b>	<i>MYC</i>	-1.03	-1.23	-1.31	1.21
<b><i>CD40</i></b>	1.20	1.14	<b>-2.21</b>	-1.23	<i>MYD88</i>	-1.13	-1.09	1.60	-1.42
<i>CD69</i>	1.10	-1.04	-1.66	1.15	<i>NCOA3</i>	-1.16	-1.22	-1.01	1.05
<i>CD80</i>	1.17	1.12	1.29	-1.78	<b><i>NFKB1</i></b>	1.55	<b>2.59</b>	<b>2.29</b>	<b>2.00</b>
<b><i>CD83</i></b>	<b>2.46</b>	<b>3.71</b>	<b>2.27</b>	<b>4.37</b>	<b><i>NFKB2</i></b>	<b>2.78</b>	<b>3.87</b>	<b>3.69</b>	<b>2.45</b>
<i>CDKN1A</i>	1.73	1.76	1.34	1.16	<b><i>NFKBIA</i></b>	<b>2.48</b>	<b>4.11</b>	<b>2.88</b>	<b>3.49</b>
<i>CFB</i>	-1.12	-1.26	1.08	1.11	<i>NQO1</i>	-1.17	-1.23	1.19	-1.37
<i>CSF1</i>	1.48	1.88	1.38	1.67	<i>NR4A2</i>	-1.31	-1.19	1.78	1.05
<i>CSF2</i>	-1.47	-1.17	1.23	-1.76	<i>PDGFB</i>	1.04	-1.10	-1.33	1.25
<i>CSF2RB</i>	-1.02	-1.15	-1.28	-1.04	<i>PLAU</i>	1.65	1.88	1.23	1.01
<b><i>CSF3</i></b>	-1.12	1.09	1.73	<b>-2.00</b>	<b><i>PTGS2</i></b>	1.41	1.76	1.87	<b>2.12</b>
<b><i>CXCL1</i></b>	<b>3.22</b>	<b>6.36</b>	<b>4.98</b>	<b>6.98</b>	<i>REL</i>	-1.06	1.33	1.59	1.78
<b><i>CXCL10</i></b>	<b>4.32</b>	<b>12.75</b>	<b>13.50</b>	<b>6.19</b>	<i>RELA</i>	1.07	1.18	1.25	1.47
<b><i>CXCL2</i></b>	<b>2.13</b>	<b>2.78</b>	1.66	<b>3.25</b>	<i>RELB</i>	-1.00	1.34	1.80	-1.48
<b><i>CXCL9</i></b>	-1.00	1.31	1.32	<b>-2.83</b>	<i>SELE</i>	-1.03	1.19	1.70	-2.00
<i>EGFR</i>	1.40	1.53	1.46	-1.14	<i>SELP</i>	-1.24	-1.20	-1.52	1.25
<i>EGR2</i>	-1.17	1.10	1.11	-1.99	<b><i>SNAP25</i></b>	1.08	-1.05	1.66	<b>-2.63</b>
<i>F3</i>	1.32	1.52	1.12	1.43	<i>SOD2</i>	-1.10	-1.02	1.31	-1.07
<i>F8</i>	-1.43	-1.53	1.35	-1.11	<i>STAT1</i>	-1.22	-1.15	1.26	1.36
<i>FAS</i>	1.20	1.44	1.59	-1.76	<i>STAT3</i>	-1.01	1.05	1.09	-1.36
<b><i>FASLG</i></b>	-1.10	1.28	1.81	<b>-2.41</b>	<i>STAT5B</i>	1.22	1.15	-1.34	-1.25
<i>GADD45B</i>	1.21	1.21	1.21	1.82	<b><i>TNF</i></b>	<b>4.33</b>	<b>11.98</b>	<b>5.06</b>	<b>6.53</b>
<i>ICAM1</i>	1.21	-1.06	1.21	-1.72	<i>TNFRSF1B</i>	-1.16	-1.04	-1.35	-2.35
<i>IFNB1</i>	1.26	-1.35	-1.85	1.01	<i>TNFSF10</i>	-1.02	-1.14	1.06	-1.84
<i>IFNG</i>	1.07	-1.00	1.88	-1.77	<i>TP53</i>	1.39	1.66	1.36	1.49
<i>IL12B</i>	1.16	1.40	-1.19	-1.67	<i>TRAF2</i>	1.01	1.09	1.73	1.29
<i>IL15</i>	1.63	1.88	-1.06	-1.05	<b><i>VCAM1</i></b>	<b>2.18</b>	<b>2.04</b>	<b>3.06</b>	-1.29
<i>IL1A</i>	-1.45	-1.39	-1.02	-1.93	<i>XIAP</i>	-1.24	-1.27	1.58	1.16

<sup>a</sup>Fold up- or down-regulation was investigated with the RT<sup>2</sup> Profiler™ PCR human NF-κB target gene Array (SABiosciences). Genes more than two fold up- or down regulated are given in bold.

and  $^{48}\text{Ti}$  ions (108 keV/ $\mu\text{m}$ ) were selected for analysis. X-irradiated samples of 4 Gy and 8 Gy were used as reference. Results shown in **Table 27** demonstrate genes to be strongly up-regulated including CXCL-1, CXCL-2, CXCL-8, CXCL-10, NFKB1, NFKB2, NFKBIA, TNF, CCL2, VCAM1 and CD83. It was observed that 4 Gy of high LET heavy ions showed comparable gene regulation with 8 Gy of low LET radiation.

### 3.5 The effect of LET on the up-regulated NF- $\kappa$ B target genes

In order to further study the effect of LET on time-dependency of NF- $\kappa$ B target gene expression, cells were irradiated with 4 Gy of X-rays and heavy ions of different LET (**Table 15**) and gene expression of selected NF- $\kappa$ B regulated genes was followed 6 and 24 h after irradiation. Selected NF- $\kappa$ B targets were the chemokines CXCL-1, CXCL-2, CXCL-8 and CXCL-10, the membrane protein CD83 and the anti-apoptotic gene XIAP. The NF- $\kappa$ B independent genes CDKN1A and GADD45 $\alpha$  are known to respond to X-ray exposure and were therefore included in the analysis. GAPDH and PBGD were used as reference genes for normalizing target gene expression.

#### 3.5.1 Heavy ions induce expression of chemokine and cytokine genes most efficiently at LET values relevant for NF- $\kappa$ B activation

For early (6 h) and late (24 h) gene expression, different expression patterns were observed (**Figure 28**). It was found that expression of chemokines were enhanced 6 hours after irradiation and gradually up-regulated with increasing LET value. CXCL-1 and CXCL-2 expression reached a maximum for  $^{48}\text{Ti}$  (108 keV/ $\mu\text{m}$ ) and  $^{58}\text{Ni}$  (175 keV/ $\mu\text{m}$ ) ion exposure. Early expression of IL-8 was not LET-dependent but late expression gradually increased up to  $^{48}\text{Ti}$  (108 keV/ $\mu\text{m}$ ). Early expression of CXCL-10 gradually increased with LET and maximum expression was observed after  $^{58}\text{Ni}$  (175 keV/ $\mu\text{m}$ ) irradiation whereas maximum late expression was observed after  $^{48}\text{Ti}$  (108 keV/ $\mu\text{m}$ ). Relative gene expression was strongest for chemokines 6 h after irradiation with 4 Gy of  $^{48}\text{Ti}$  (108 keV/ $\mu\text{m}$ ) and  $^{58}\text{Ni}$  (175 keV/ $\mu\text{m}$ ) beams.

It can be concluded that heavy ions induce expression of chemokine and cytokine genes most efficiently at LET-values relevant for NF- $\kappa$ B activation in the range of 50-300 keV/ $\mu\text{m}$ . The heavy ions with very high LET -  $^{58}\text{Ni}$  (906 keV/ $\mu\text{m}$ ) and  $^{208}\text{Pb}$  (9764 keV/ $\mu\text{m}$ ) - up-regulated NF- $\kappa$ B target genes in an extent comparable to X-rays.

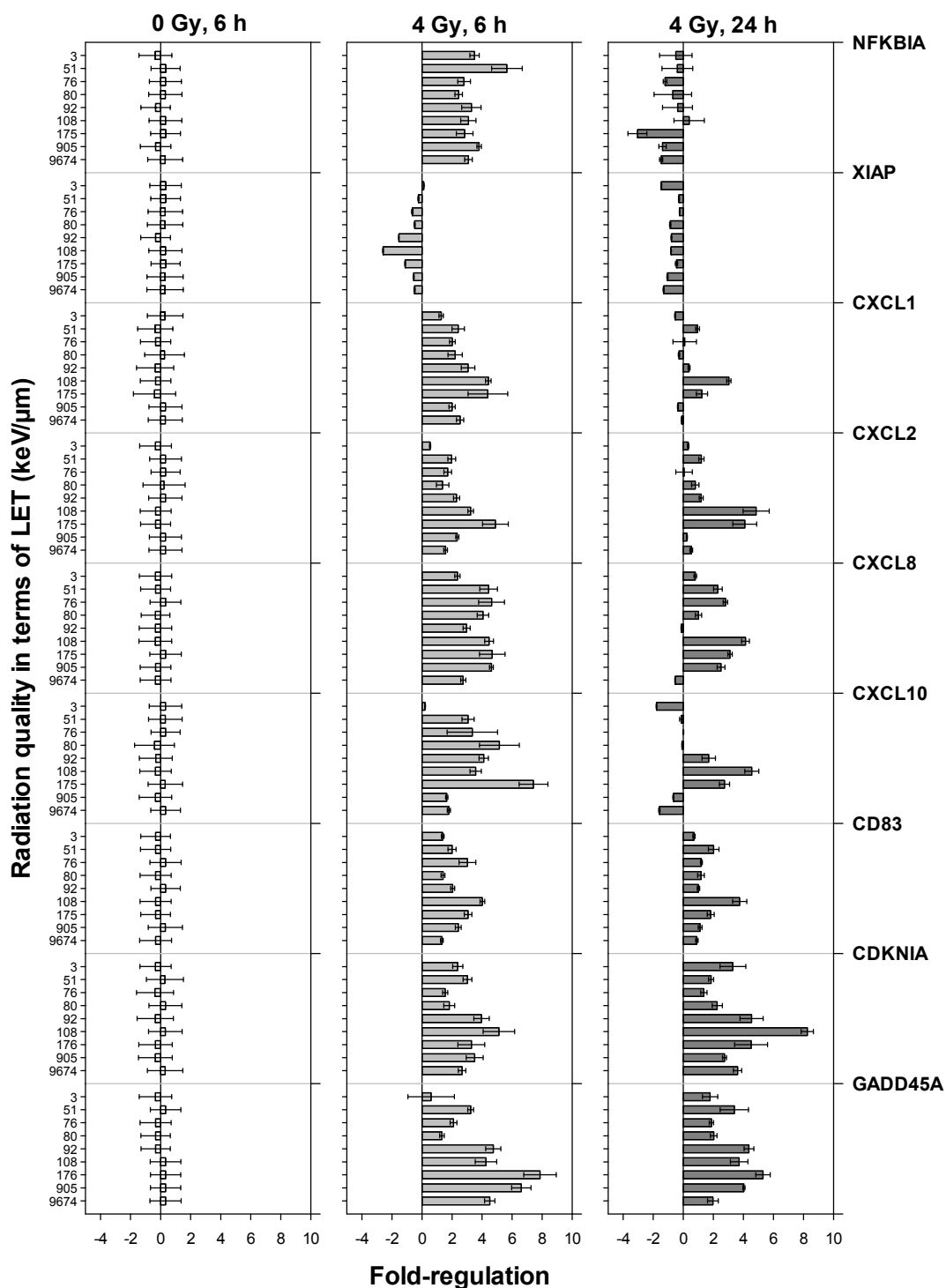


**Figure 28 Expression of the CXCL1-2, 8, 10, XIAP, CD83, CDKN1A and GADD45 $\alpha$  genes after heavy ion exposure**

Cells were harvested 6 and 24 h after X-ray (4 Gy) or accelerated heavy ion exposure (4 Gy). Target gene expression was determined at mRNA levels and normalized against the expression of the reference genes PBGD, and GAPDH. Fold regulation of target genes are represented by bar graph. Fold regulation  $\pm 1$  shows the basal expression of target genes. Bars of 6 h and 24 h samples after 4 Gy represents the early and late expression kinetics of target genes respectively. Most of the target genes including CXCL gene family, CD83 and NFKBIA showed early expression in the LET range 100-300 keV/  $\mu\text{m}$ . XIAP showed down-regulation whereas CDKN1A and GADD45 $\alpha$  showed late expression in the same range as for other target genes. Fold regulation values represent normalized means and error bars show the standard error of three experimental replicates.

To determine the possible mechanisms underlying the effects of LET on cell cycle progression, the expression of CDKN1A and GADD45 $\alpha$  was evaluated which play important roles in controlling cell cycle. The GADD45 $\alpha$  gene showed early expression (6 h after irradiation) whereas CDKN1A showed late expression (24 h after irradiation). Early expression of GADD45 $\alpha$  was highest at 175 keV/ $\mu$ m whereas CDKN1A showed late expression with a peak at 108 keV/ $\mu$ m. Heavy ions induce expression of CDKN1A and GADD45 $\alpha$  most efficiently at LET-values in the range of 50-175 keV/ $\mu$ m where most of the cells are arrested in S and G2/M phase (**Figure 22**). The very high LET heavy ions  $^{58}\text{Ni}$  (906 keV/ $\mu$ m) and  $^{208}\text{Pb}$  (9764 keV/ $\mu$ m) up-regulated CDKN1A and GADD45 $\alpha$  but the expression of both genes was gradually decreased at very high LET values.

## 4 Discussion

Aim of this project was to determine the LET-dependent effects of ionizing radiation on human cells, in particular NF- $\kappa$ B-dependent signal transduction and gene expression. The understanding of the cellular radiation response may contribute to the development of effective countermeasures towards radiation risks in human spaceflight and improved effectiveness of cancer radiotherapy. The main scientific question in this work was to determine the LET dependency of different biological responses including cellular survival, cell cycle regulation, NF- $\kappa$ B activation, and NF- $\kappa$ B-dependent gene regulation (**Figure 29**).

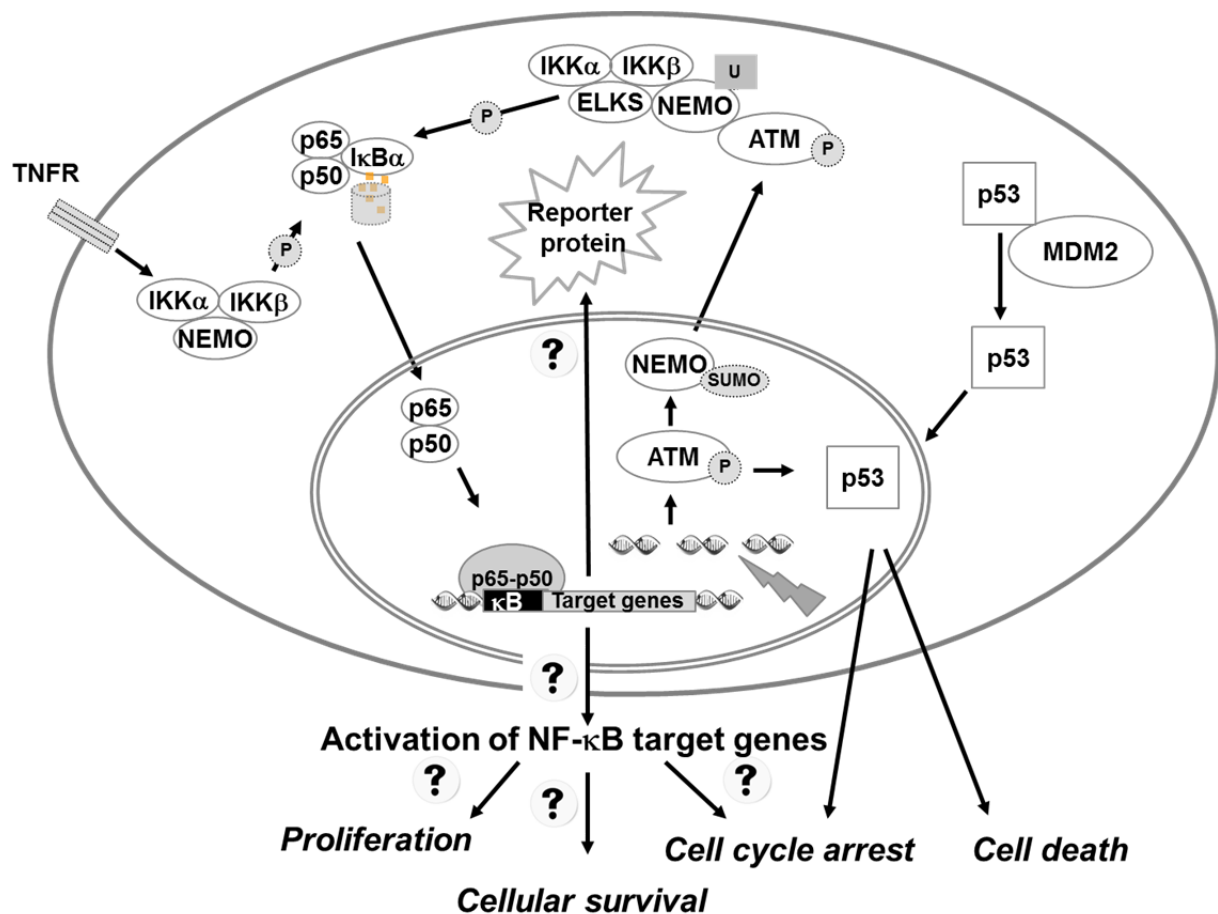


**Figure 29** Radiation-induced biological response and main questions of the thesis

The main scientific questions in this study are to determine the activation of NF- $\kappa$ B target genes and the role of NF- $\kappa$ B regulation in cellular proliferation, cellular survival and cell cycle arrest. The activation of NF- $\kappa$ B is analysed by reporter gene expression after ionizing radiation exposure. The pathway chart was adapted from (Habraken and Piette 2006) and (Brzoska and Szumiel 2009).

## 4.1 Effect of ionizing radiation on the NF- $\kappa$ B pathway in HEK cells

For screening of NF- $\kappa$ B activation by different radiation qualities, a reporter system was used. As this reporter system should also be applicable on the ISS where the experimental conditions are limited, reporter assays with fluorescent proteins were preferred.

### 4.1.1 Activation of NF- $\kappa$ B in HEK cells

HEK cells are a useful tool to study several processes of human cells. HEK cells are used in radiobiological, pharmacological and toxicological studies (Bora *et al.* 2008; Kim and Eberwine 2010; Lau *et al.* 2009; Yu *et al.* 2001). This cell line shows a functional NF- $\kappa$ B pathway (Muroi and Tanamoto 2008; Rajagopal *et al.* 2008), and therefore it is a good choice for studying the role of the transcription factor NF- $\kappa$ B in the cellular radiation response.

There are various methods for detecting NF- $\kappa$ B activation which depend on experimental requirements and cell systems used for studying NF- $\kappa$ B. NF- $\kappa$ B activation can be measured directly (measuring p65 subunit) or indirectly (measuring I $\kappa$ B expression) by assays such as enzyme linked immunosorbant assay (ELISA) (Jin *et al.* 2005), electrophoretic mobility shift assays (EMSA) (Mukogawa *et al.* 2003), Western blot (Muroi and Tanamoto 2008), immunofluorescence staining (Fuseler *et al.* 2006), DNA microarray (Chen *et al.* 2002), and flow cytometry (Ishikawa *et al.* 2002).

In this study, for screening of activation of the NF- $\kappa$ B pathway by different radiation qualities, fluorescent proteins based reporter assays were used providing quick and reliable measurements of cellular NF- $\kappa$ B signals. The HEK-pNF $\kappa$ B-DD-tdTomato and HEK-pNF $\kappa$ B-d2EGFP-Neo L2 (Hellweg *et al.* 2003) carry genes of destabilized variants of fluorescent proteins under control of NF- $\kappa$ B inducible synthetic promoters. The NF- $\kappa$ B pathway was activated by TNF- $\alpha$  and X-rays and the signal strength of NF- $\kappa$ B-dependent reporter protein expression was determined by flow cytometry and visualized by fluorescence microscopy.

#### 4.1.2 Activation of NF- $\kappa$ B by the canonical and the genotoxic stress induced pathway

Induction of NF- $\kappa$ B by TNF- $\alpha$  and ionizing radiation followed differing kinetics. NF- $\kappa$ B signaling by the classical/canonical pathway was induced by TNF- $\alpha$ . The genotoxic stress dependent pathway was activated by ionizing radiation-induced DNA damage. Compared to TNF- $\alpha$ , however, X-rays are weak inducers of the NF- $\kappa$ B pathway. Therefore high doses (16 Gy) were used for significant NF- $\kappa$ B dependent DD-tdTomato expression (**Figure 15 A**). High doses of X-rays also damage DNA indirectly by generating intracellular ROS which results in NF- $\kappa$ B activation (Russell and Tofilon 2002).

NF- $\kappa$ B signaling consists of a very complex network of phosphorylation, ubiquitination, post-translational modification, translocation and degradation of several proteins and their subunits (Ghosh 2007; Ghosh and Hayden 2012; Ghosh and Hayden 2008). Phosphorylation and proteosomal degradation of I $\kappa$ B $\alpha$  is a common step in NF- $\kappa$ B signaling by the canonical, non-canonical and genotoxic stress induced pathway (**Figure 29**).

After dissociating from I $\kappa$ B, NF- $\kappa$ B translocates to the nucleus and binds to its consensus sequences within target promoters. Thereby the transcription of certain genes related to inflammation, immune regulation, cell proliferation and anti-apoptosis is regulated (**Figure 28**). The reporter cell lines used in this study contain 4  $\kappa$ B sites (GGGAATTTCC), where NF- $\kappa$ B binds and upregulates DD-tdTomato or d2EGFP expression. Four copies of  $\kappa$ B sites contribute to strong NF- $\kappa$ B-dependent transactivation (Hellweg *et al.* 2003; Matsuda *et al.* 2007; Pessara and Koch 1990). After maturation, the reporter proteins give strong signals from cytoplasm and cell nucleus which were detected both by flow cytometry and fluorescence microscopy.

After the maximum activation, NF- $\kappa$ B returns to the normal level which is mediated through phosphorylation of I $\kappa$ B $\alpha$  that regulates NF- $\kappa$ B activation and translocation (Natarajan *et al.* 2002). The newly synthesized I $\kappa$ B $\alpha$  re-inhibits NF- $\kappa$ B and thus forms an auto feedback loop, which results in oscillating levels of NF- $\kappa$ B activity. Therefore a decline in DD-tdTomato expression was observed 8 hours and 24 hours after TNF- $\alpha$  treatment and X-irradiation respectively (**Figure 15 A**). There is always a dynamic

balance between cytosolic and nuclear localization of NF- $\kappa$ B proteins that drastically changes after degradation of the NF- $\kappa$ B-I $\kappa$ B protein complex (Liu *et al.* 2011; Miyamoto 2010).

#### 4.1.3 NF- $\kappa$ B activation is both ionizing radiation dose and LET-dependent

Different biochemical methods, such as electrophoretic mobility shift assays (EMSA), Western blot (p65) of nuclear extracts, p65 immunofluorescence staining, flow cytometry of fluorescent proteins are used for detection of NF- $\kappa$ B. Variation in the NF- $\kappa$ B activation might depend on doses and the cell system used in different experiments (**Table 28**). Dose-effect curves showed that as dose was increased, NF- $\kappa$ B activation rised also (**Figure 16**). High doses deposit high energy to create more DSB which result in stronger activation of NF- $\kappa$ B mediated DD-tdTomato expression. As the LET of X-rays is very low (0.3-3 keV/ $\mu$ m), high doses are required for NF- $\kappa$ B activation. Heavy ions due to their high LET values activated NF- $\kappa$ B at higher extent compared to X-rays. Low doses of heavy ions were more potent in NF- $\kappa$ B activation compared to X-rays which was also reported by measuring translocation kinetics of the NF- $\kappa$ B subunit p65 (Hellweg *et al.* 2011a).

To determine the LET dependence, NF- $\kappa$ B activation after exposure to heavy ions of different LET values was compared. Heavy ions activated NF- $\kappa$ B-dependent reporter gene expression in a dose-dependent manner. A first hint that high LET argon ions (270.5 keV/ $\mu$ m) activate NF- $\kappa$ B pathway to high extent was found earlier (Hellweg *et al.* 2005). In the early experiments, the dose-dependent NF- $\kappa$ B activation saturated at doses above 4 Gy after high LET radiation exposure (Baumstark-Khan *et al.* 2005), while in this work, the dose-effect relationship was described in much more detail, and a saturation was reached around 10 Gy for ions with an LET of 90-300 keV/ $\mu$ m. For the other ions used in this study, the doses were not high enough to reach saturation.  $^{22}\text{Ne}$  and  $^{36}\text{Ar}$  ions activated NF- $\kappa$ B to a higher extent compared to  $^{16}\text{O}$  ions, due to their increasing LET values, 92 and 272 keV/ $\mu$ m respectively.

$^{58}\text{Ni}$  ions (LET 175 keV/ $\mu$ m) were most effective in activating NF- $\kappa$ B-dependent gene expression at low doses compared to very high LET  $^{58}\text{Ni}$  (905 keV/ $\mu$ m) ions. The dose required for activating NF- $\kappa$ B after very high LET  $^{58}\text{Ni}$  (905 keV/ $\mu$ m) and  $^{208}\text{Pb}$  (9764 keV/ $\mu$ m) was more than that required by X-rays (**Table 22**). The number of



heavy ion particle hits per cell nucleus (fluence) also affects NF- $\kappa$ B activation (Baumstark-Khan *et al.* 2005). The lowest fluence that results in doubling of activation of NF- $\kappa$ B over background is listed in **Table 22**.

The variation in the number of particle hits per cell nucleus (fluence) and NF- $\kappa$ B activation among different heavy ions is due to the characteristics of heavy ions particles, energy and LET.

**Table 28 Radiation dose required to activate NF- $\kappa$ B in different experimental models. Adopted from (Criswell *et al.* 2003)**

Experimental model	NF- $\kappa$ B detection method	Ionizing radiation dose required for NF- $\kappa$ B activation	Reference
<b>Cell lines</b>			
EBV-transformed 244B human lymphoblastoid	Electrophoretic Mobility Shift Assay (EMSA)	0.5 Gy	(Sahijdak <i>et al.</i> 1994)
U1-Mel human melanoma	EMSA and Western immunoblot assays	3-4.5 Gy	(Yang <i>et al.</i> 2000)
Human diploid fibroblasts	EMSA and Western blotting	Higher than > 20 Gy	(Ashburner <i>et al.</i> 1999)
Human embryonic kidney cells	Stably transfected green fluorescent reporter system: HEK-pNF- $\kappa$ B-d2EGFP/Neo	> 8 Gy	(Baumstark-Khan <i>et al.</i> 2005; Hellweg <i>et al.</i> 2003)
Human embryonic kidney cells	Stably transfected red fluorescent reporter system: HEK-pNF $\kappa$ B-DD-tdTomato-C8 HEK-pNF $\kappa$ B-DD-tdTomato-C8 + Shield-1	~6 Gy ~3 Gy	(Baumstark-Khan <i>et al.</i> 2005; Chishti <i>et al.</i> 2014)
<b>Organs</b>			
Bone marrow, lymph nodes, and spleen	Gel supershift assay	8.5 Gy	(Zhou <i>et al.</i> 1999)
Liver and kidney	EMSA and immunoblotting	20 Gy	(Li <i>et al.</i> 2001)
Cerebral cortex	EMSA and northern blotting	5 Gy	(Raju <i>et al.</i> 2000)

## 4.2 Relative Biological Effectiveness of the tested radiation qualities

Relative biological effectiveness (RBE) is very important information in the field of radiobiology and radiotherapy. To determine the relationship between the RBE and LET, the RBE for cell inactivation and NF- $\kappa$ B activation were calculated from the survival curves (**Figure 18**) and NF- $\kappa$ B expression kinetics (**Figure 16**), respectively. RBE data of survival and NF- $\kappa$ B activation show that both are LET-dependent. In terms of low to moderate LET radiation, RBE is directly proportional to the LET values. For high LET radiation, RBE increases to a maximum and decreases subsequently. In this research work, it has been determined that maximal biological efficiency lies in the range of 34 to  $\sim$ 270 keV/ $\mu$ m which also confirms other studies (Hellweg 2012).  $^{58}\text{Ni}$  ions (175 keV/ $\mu$ m) had the strongest killing effect and NF- $\kappa$ B activation. The maximum RBE for NF- $\kappa$ B activation is around 7 (**Table 22**) whereas for reproductive cell death the maximum RBE value is only around 2 (**Table 23**). However, in both cases the RBE for  $^{208}\text{Pb}$  (9764 keV/ $\mu$ m) and  $^{58}\text{Ni}$  (905 keV/ $\mu$ m) was below 1. This study also complements previous findings that an RBE for cell survival by high LET lead ions ( $> 10,000$  keV/ $\mu$ m) is far below 1, and for nickel ions ( $> 1,000$  keV/ $\mu$ m) around 1 (Hellweg 2012; Stoll *et al.* 1995; Stoll *et al.* 1996).

## 4.3 Effect of ionizing radiation in different cellular responses

The cellular response to radiation is mainly a DNA Damage Response (DDR) that results in potentially cell protective (survival, cell cycle arrest and DNA repair) or cell-destructive responses (different types of cell death, senescence, mutations) (Cernan 2004; Hellweg 2012; Khanna *et al.* 2001; Ohnishi *et al.* 2002). In this section, the effects of radiation dose and LET on cell protective responses (survival and cell cycle arrest) are discussed.

### 4.3.1.1 Effect of low LET radiation on cellular proliferation

The growth properties of cells depend on their division ability which is a tightly regulated process. Different cell types may vary in their duration of cell cycle that shows their different growth kinetics. Ionizing radiation disturbs the cell cycle and

thereby delays cell proliferation due to its DNA damaging ability (Gerashchenko *et al.* 2004; Hellweg 2012; Park *et al.* 2002).

Cellular proliferation was measured by a proliferation assay based on cellular DNA content stained with the fluorescent DNA stain bisbenzimidazole (Hoechst 33342). The proliferation assay indicates the effect of X-rays on normal growth characteristics of a cell. Bisbenzimidazole has low cytotoxicity and binds preferentially to adenine-thymine (A-T) regions of DNA and the intensity of bound bisbenzimidazole is directly proportional to the DNA content of the cell.

X-ray exposure inhibits cellular growth to a certain extent which depends on the damage repair ability and the amount of the damage. Exposure to low doses (< 4 Gy) delayed the lag phase and reduced the cell proliferation rate. Most of the cells were unable to grow further after exposure to high doses of X-rays (8 Gy). This might be due to reproductive cell death or cellular senescence. Reproductive cell death is the loss of proliferative ability of cells (Baumstark-Khan *et al.* 2010) and cellular senescence is irreversible growth arrest that does not involve cell death (Lou and Chen 2006; Roninson *et al.* 2001). High dose exposure of low LET radiation (> 10 Gy X-rays) can lead to interphase death (Mehnati *et al.* 2005; Sasaki *et al.* 1997).

#### 4.3.2 Effect of LET on cellular survival

The radiobiological standard test for cellular survival is the CFA test. It is an important measure of radiation-induced cell damage and reproductive death. CFA reflects the ability of irradiated cells to divide and form macro-colonies which allows calculating survival curves. After X-irradiation, the survival curve displayed a shoulder in low dose range (< 2 Gy), whereas no shoulder was observed after heavy ion exposure (**Figure 18**). The shoulder in the survival curve represents the DNA repair capacity of HEK cells. Heavy ions create severe damage that is not being repaired so quickly compared to X-irradiated cells. Therefore heavy ion irradiated cells showed an exponential decrease in cell survival without any shoulder. Other studies with different mammalian cells also reported exponential decrease of cellular survival without any shoulder in survival curve (Durante *et al.* 1995; Raju *et al.* 2000; Takahashi *et al.* 2010).

After exposure of HEK cells to heavy ions it was observed that cell killing potential depends on the LET value. Carbon ions of an LET below 100 keV/μm indicated that cell killing potential of the heavy ion increases as LET was rised.

$^{16}\text{O}$ ,  $^{22}\text{Ne}$ ,  $^{58}\text{Ni}$ , and  $^{36}\text{Ar}$  ion exposure resulted in exponentially decreasing survival curves up to the LET ~272 keV/μm. Aforementioned heavy ions due to their high energy transfer produce more DNA damage thus cellular survival is reduced. It was reported that augmenting DNA lesion density is associated with increasing LET (Tilly *et al.* 2002).

When cells were exposed to ions with very high LET ( $^{58}\text{Ni}$ , 905 keV/μm, and  $^{208}\text{Pb}$ , 9674 keV/μm), cellular survival was higher compared to X-rays due to the overkill effect. This overkill effect can be explained by increasing the number of non-hit cellular targets (cell nucleus, DNA) per unit dose and clustering of physical damage within the non-targeted area (Mehnati *et al.* 2005). After ionizing radiation exposure, reproductive death of a cell depends on activation of various signaling pathways, severity of DNA damage and cell type (Franken 2011; Haynes *et al.* 2013).

#### 4.3.3 Effect of LET on cell cycle progression

Radiation-induced DNA damage can cause a progression delay in G1, S and G2/M phases. The duration and extent of cell cycle arrest depends on the severity of DNA damage, dose and quality of radiation (LET) (Beck *et al.* 2012; Fournier and Taucher-Scholz 2004; Tatsuka *et al.* 1989). With increasing dose, DNA damage becomes more severe and complex, and thus influences the extent and duration of cell cycle arrest. It has been a general concept that heavy ion exposure arrests cells in G2/M phase (Gong *et al.* 2007; Ma *et al.* 2009; Ochab-Marcinek *et al.* 2009). In this study, it is shown that heavy ions, at high doses, arrest cells in S-phase as well (**Figure 20**).

At low doses of X-rays (2 and 4 Gy), cells accumulated in G2/M transiently due to high DNA damage repair capacity of HEK cells. The G2/M arrest was enhanced as dose was increased up to 8 Gy. After a relatively high dose of radiation (> 8 Gy), S phase arrest occurred. Heavy ions also exhibited dose-dependent effects on cell cycle, e.g. after exposure to 2-8 Gy of  $^{13}\text{C}$  (LET 33 and 75 keV/μm), a prominent G2/M arrest was induced but after 16 Gy, S-phase arrest was prominent. Both  $^{13}\text{C}$  ions and X-rays have comparable cell killing potential (**Table 23**) but  $^{13}\text{C}$  ions had a more pronounced effect than X-rays at low doses (2-4 Gy) which also confirms a

previous study (Di *et al.* 2013). After  $^{16}\text{O}$  ion exposure cells were arrested less in G2/M compared to  $^{13}\text{C}$  ions. There is not much known about cell cycle regulation after  $^{16}\text{O}$  ion exposure. There is one study that showed high LET  $^{16}\text{O}$  ions are more effective in production of complex type chromosomal aberrations compared to  $^{12}\text{C}$  ions (Pathak *et al.* 2007). After  $^{22}\text{Ne}$  exposure, cells accumulated in S-Phase which was higher after  $^{48}\text{Ti}$  (108 keV/ $\mu\text{m}$ ) and reached to its maximum at 16 Gy exposure. As LET was increased to  $^{58}\text{Ni}$  (175 keV/ $\mu\text{m}$ ) cells started to accumulate in S-phase even at lower doses (2 Gy). Very high LET (>1000 keV/ $\mu\text{m}$ ) heavy ions showed no significant enhancement of cell cycle arrest. In contrary, a decrease in cell cycle arrest was observed which might be due to the overkill effect, meaning that hit cells die and do not arrest in cell cycle.

To summarize, ionizing radiation exposure arrests HEK cells in G2/M and S phase of the cell cycle. The severity of the damage caused by dose and LET of ionizing radiation determines the phase in which cell cycle is arrested. Significant G2/M delay occurs in HEK and cervix carcinoma cells (Caski) after exposure to ionizing radiation doses  $\leq 8$  and  $\leq 6$  Gy, respectively (Kuo *et al.* 1997). During G2/M block, the DNA repair machinery can use the intact sister chromatid as a template and induce HR (Shrivastav *et al.* 2008).

S-phase is the most complex checkpoint among all cell cycle checkpoints (Tjong 2009). The S phase arrest occurs after relatively high dose radiation (> 8 Gy). It has been reported that cells are most radiosensitive in G2/M phase, intermediately sensitive in G1 phase and radioresistant in S phase (Zhuang *et al.* 2009). Quiet *et al.* suggested that a radioresistant cell line has twice the number of cells in S-phase than the radiosensitive cell line (Quiet *et al.* 1991). It was also reported that lymphocytes of patients showing no response to radiotherapy have a high level of S-phase cells compared to lymphocytes of patients showing radiosensitivity (Tell *et al.* 1998). In mammalian cells, the gene that controls the S phase checkpoint has not been identified. Some *in vitro* studies showed that CIP1 inhibit elongation step by binding to cell nuclear antigen (Li *et al.* 1994).

#### **4.3.3.1 Effect of LET on expression of cell cycle regulating genes**

Further investigation of G2/M and S-phase arrest was done at molecular level by investigating the role of two genes in cell cycle regulation. Gene expression profiles

showed up-regulation of the cell cycle-related genes GADD45 $\alpha$  and CDKN1A after heavy ion exposure in the investigated LET range (3-9674 keV/ $\mu$ m). Both of the genes GADD45 $\alpha$  and CDKN1A play important roles in controlling cell cycle. GADD45 $\alpha$  interacts with both GADD45 $\beta$  and GADD45 $\gamma$ , which are activated by ionizing radiation and play a role in stress response pathways (especially GADD45 $\beta$ ). GADD45 $\alpha$  showed up-regulation in conjunction with CDKN1A which encodes p21<sup>CIP1/WAF1</sup> (target of p53). Up-regulation of CDKN1A and GADD45 $\alpha$  showed that TP53 (gene encoding p53) is essential for the radiation-induced delay of cell cycle progression which also confirms a previous study (Fournier and Taucher-Scholz 2004).

In this study it was shown that expression of GADD45 $\alpha$  and CDKN1A has a strong correlation with LET. After irradiating cells with heavy ions in the LET range of 3-175 keV/ $\mu$ m, strong early gene expression of GADD45 $\alpha$  and CDKN1A was displayed, when most of the cells were arrested in S- and G2/M phase. The expression was reduced after exposure to <sup>58</sup>Ni ions with an LET of 905 keV/ $\mu$ m, when no significant induction of cell cycle arrest was observed, indicating the importance of these genes in cell cycle regulation. According to the results shown in this work, it can be concluded that heavy ions induce expression of GADD45 $\alpha$  and CDKN1A genes most efficiently at LET-values relevant for S-phase arrest (100-300 keV/ $\mu$ m) and contribute to induce both G2/M and S-phase arrest. Other studies suggest that the protein kinases Chk2 and Chk1 are involved both in the induction of G2/M and S-phase arrest (Iliakis *et al.* 2003; Xiao *et al.* 2003) and early S-phase arrest is ATM-dependent but late S-phase arrest is associated with ATR (Zhou *et al.* 2002).

## **4.4 Contribution of NF- $\kappa$ B activation in different cellular responses**

### **4.4.1 NF- $\kappa$ B down-regulation decreases cell survival after X-irradiation**

NF- $\kappa$ B is considered to be an important regulator of cellular proliferation (Hayden 2004; Li and Verma 2002). There are several studies suggesting that inhibition of NF- $\kappa$ B leads to a decrease in cellular proliferation (Guttridge *et al.* 1999; Koch 2013), which results in reduced or stopped cell division. It has also been reported that proliferation and inhibition of myogenic differentiation is NF- $\kappa$ B-dependent and that

inhibition of myogenesis is specific to RelA (Guttridge *et al.* 1999; Langen *et al.* 2004). There are additional studies showing that epidermal RelA deficiency leads to increased proliferation in the epidermis of mice (Seitz *et al.* 1998; Seitz *et al.* 2000; Zhang *et al.* 2004). RelA induces growth inhibitory genes in epidermal cells but not in other cell types (Hinata *et al.* 2003).

To study the role of NF- $\kappa$ B in cellular survival a RelA knockdown (HEK shRNA RelA) cell line established earlier was compared with the HEK-pNF $\kappa$ B-DD-tdTomato-C8 cell line that has active NF- $\kappa$ B (RelA<sup>+</sup>) response. It was found that HEK shRNA RelA cells showed reduced cellular survival compared to HEK-pNF $\kappa$ B-DD-tdTomato-C8 cells after X-ray exposure. This supports the earlier findings that inhibiting the NF- $\kappa$ B pathway by chemical inhibitors change survival behavior (Baichwal and Baeuerle 1997; Sonenshein 1997) and lead cells towards apoptosis (Gao *et al.* 2004). It has been observed after X-ray exposure that HEK shRNA RelA cells showed lower survival and higher radiosensitivity compared to HEK-pNF $\kappa$ B-DD-tdTomato-C8 cells. In one study, it was reported that NF- $\kappa$ B activation promoted survival in mice and primates when irradiated with lethal doses (Wang 2004). It has been shown earlier that radiosensitive tissues can be protected against radiation damage through Toll-like receptor 5 (TLR5)-dependent activation of NF- $\kappa$ B (Burdelya *et al.* 2008). There is always a balance between pro-survival and pro-death pathways. Therefore it is suggested that knockdown of RelA results in low pro-survival and high pro-apoptotic signaling that leads to low cellular survival upon ionizing radiation exposure.

Cellular survival is also affected by the state of NF- $\kappa$ B activation inside the cell. TNF- $\alpha$  activates NF- $\kappa$ B in HEK cells; therefore cells were exposed to X-rays at different time points after TNF- $\alpha$  treatment. The down-regulation of the NF- $\kappa$ B pathway follows multiple mechanisms including the feedback pathway. In this feedback pathway, newly synthesized I $\kappa$ B $\alpha$  protein bind to nuclear NF- $\kappa$ B and export it out to the cytosol. It is hypothesized that activation of the feedback pathway starts 8 hours after TNF- $\alpha$  incubation (**Figure 15**). When cells were irradiated at the time point when NF- $\kappa$ B was down-regulated (20 hours after TNF- $\alpha$  treatment), the cellular survival was decreased. When cells were irradiated at the state of up-regulation of NF- $\kappa$ B, cellular survival was increased at high doses but not significantly at low doses (**Figure 24**).

#### 4.4.2 NF- $\kappa$ B deactivation results in impairment of DNA damage response

The DDR involves multiple sensors, transducers and effector molecules for different types of DNA lesions (Jackson and Bartek 2009). The role of NF- $\kappa$ B in DNA damage response is investigated. Although it is difficult to obtain a quantitative estimate of the extent of DNA damage at various doses, the CFA assay can help to estimate the relative DNA damage response. A method commonly used to measure the ability of cells to repair sublethal damage is to compare immediate plating (IP) and late plating (LP) survival. The LP survival assay shows the effect of conditions under investigation (such as RelA knockdown) on the DNA damage response of cells to X-rays. In LP survival assay, cells were given 24 hours after irradiation to repair the radiation-induced damage. If the cell had DNA repair ability, repair of the damage occurs within 24 hours, which resulted in increased cellular survival. Thus, DNA damage repair capacity was analyzed by comparing IP and LP survival assays. When immediate plating and late plating survival of HEK shRNA RelA cells were compared, it was found out that cellular survival was significantly decreased after late plating (**Figure 26**). The reduction in the survival in NF- $\kappa$ B knock-down cells might be due to the impairment of DNA damage repair after NF- $\kappa$ B deactivation. There is evidence that NF- $\kappa$ B regulates DNA DSB repair and contributes in HR (Volcic *et al.* 2012). The delayed cellular survival was not changed significantly in HEK-pNF $\kappa$ B-DD-tdTomato-C8 cells.

Radiation-induced DNA damage results in ATM activation that triggers both the pro- and anti-apoptotic transcription factors p53 and NF- $\kappa$ B, respectively, which compete for interaction with transcriptional co-activators (Ravi *et al.* 1998; Wadgaonkar *et al.* 1999). In the absence of NF- $\kappa$ B, such as in HEK shRNA RelA cells, pro-apoptotic signaling dominates whereas in HEK-pNF $\kappa$ B-DD-tdTomato-C8 cells, NF- $\kappa$ B is required for p53 pro-apoptotic signaling. Down-regulation or loss of NF- $\kappa$ B activity disturb p53-induced apoptosis (Ryan *et al.* 2000). This might be the possible reason of no significant change in late plating of HEK-pNF $\kappa$ B-DD-tdTomato-C8 cells.

In case of radiation-induced DNA damage, a sustained NF- $\kappa$ B activation allows cells to survive and escape from apoptosis (Jung and Dritschilo 2001). However, IP radiosensitization has not been observed in several cell lines and tumor models (Reddy *et al.* 1992). After X-irradiation, several repair factors and pathways are



activated which try to repair the DNA damage. DNA damage repair capacity depends on the dose and the cell line. It might be suggested that various cell lines of different repairing efficiencies show different survival capacities.

#### **4.4.3 NF- $\kappa$ B down-regulation delays cell cycle progression**

In mammalian cells, the arrest of cell cycle in different phases is one of the early responses to radiation-induced DNA damage (Wang and Cho 2004) which has been discussed in section 4.3.2. Here, the role of NF- $\kappa$ B in cell cycle progression is discussed by comparing cell cycle progression in HEK-pNF $\kappa$ B-DD-tdTomato-C8 and HEK shRNA RelA cells after X-irradiation. Both cell lines exhibited a significant difference in G2/M arrest 16 hours after X-irradiation (4 Gy). HEK shRNA RelA cells showed a longer G2/M arrest which means that RelA knock-down cells need more time for DNA repair compared to HEK-pNF $\kappa$ B-DD-tdTomato-C8 cells. Therefore the duration of the G2/M block may indicate the DNA repair capacity of cell lines in addition to the late plating survival curves (4.4.2). A comparison of the distribution of cells within the G1, S and G2/M phases of both cell lines revealed no differences in the untreated state (without activation of the NF- $\kappa$ B pathway), suggesting a comparable regulation of cell cycle progression with and without RelA. The NF- $\kappa$ B subunit p52 (NF $\kappa$ B2) can also regulate cyclin D1 (Rocha *et al.* 2003; Westerheide *et al.* 2001), therefore it might substitute for the lack of RelA. Cyclin D1 is a key regulator of G1 checkpoint, which controls progression of cell cycle from G1 to S-phase. There is not much information available about the role of NF- $\kappa$ B in G2/M arrest. It was shown earlier that down-regulation of NF- $\kappa$ B disturbs cell cycle progression mainly in G1 phase which can be recovered via transfection and expression of a cyclin D1 containing plasmid (Guttridge *et al.* 1999; Hinz *et al.* 1999). Other authors found that among all NF- $\kappa$ B subunits, RelA was associated with transcriptional regulation of cyclin D1 (Dahlman *et al.* 2009).

## 4.5 The regulation of down-stream target genes of NF- $\kappa$ B after ionizing radiation exposure

In the latent phase, NF- $\kappa$ B dimers are inactive and associated with the inhibitory protein I $\kappa$ B or the inactive precursors p100 and p105 in the cytoplasm (Miyamoto 2010; Verma *et al.* 1995). After DNA damage, NF- $\kappa$ B is activated and p50:p65 NF- $\kappa$ B dimers translocate to the nucleus 30 minutes after ionizing radiation, as determined by immunofluorescence staining of p65 (Hellweg *et al.* 2011b). It has been also been reported that transcription of NF- $\kappa$ B-dependent genes reached a maximum 6 hours after irradiation (Hellweg 2012; Koch 2013). Accordingly, NF- $\kappa$ B binding occurs earlier. In the KG-1 human myeloid cell line, the DNA binding to NF- $\kappa$ B was maximal around 2 to 4 hours after irradiation (Brach *et al.* 1991). Some studies focused on TNF- $\alpha$  induced NF- $\kappa$ B-dependent gene expression (Tourniaire *et al.* 2013). In the current study, NF- $\kappa$ B was activated by ionizing radiation and NF- $\kappa$ B-dependent gene expression was investigated using the RT<sup>2</sup> Profiler™ PCR Arrays.

### 4.5.1 NF- $\kappa$ B-dependent gene expression after X-irradiation

NF- $\kappa$ B is a pleiotropic transcription factor and regulates over 200 genes which are involved in various cellular and physiological functions, including apoptosis, proliferation, cell adhesion, migration, inflammatory and adaptive immune responses (Ghosh 2007). In this study, it is reported that ionizing radiation-induced NF- $\kappa$ B activation modulates gene expression of chemokines (CXCL-1, CXCL-2, IL-8/CXCL8, CXCL-10, monocyte chemotactic cytokine 1, MCP-1/CCL2), adhesion molecules (vascular cell adhesion molecule-1, VCAM-1), co-stimulatory membrane proteins (Cluster of Differentiation 83; CD83), other transcription factors (interferon regulatory factor 1; IRF1), pro-inflammatory cytokines (TNF), and the anti-apoptotic factor BIRC3.

Gene expression profiling suggests that diverse gene expression patterns are associated with both radiation dose and LET values. It can be seen that out of 86 NF- $\kappa$ B target genes only a set of CXCL genes (CXCL-1, CXCL-2, CXCL-8, CXCL-10), NFKB1, NFKB2, NFKBIA, IRF1, TNF, CCL2, VCAM1, and CD83 were more than two fold up-regulated either after high radiation dose (8 Gy) or high LET (100-200

keV/ $\mu\text{m}$ ) exposure. MAP2K6 was the only gene which was down-regulated after X-irradiation. CXCL-8, CCL2, IRF1 and NFKB1 were not significantly up-regulated after 4 Gy X-irradiation. A brief discussion of these up and down regulated genes is presented below.

**CXC chemokines** belong to chemokine family of small cytokines (8-10 kDa) or signaling proteins which share CXC motif. These chemokines play major role in chemotaxis (migration of cells) and are known as mediators of inflammatory response. These CXC chemokines are further classified into angiogenic chemokines (CXCL1, 2, 3, 5, 6, 8, 12) and angiostatic chemokines (CXCL 4, 9, 10, 11) (Strieter *et al.* 2004). CXCL-1, CXCL-2, CXCL8 and CXCL10 were strongly up-regulated after ionizing radiation. After 4 Gy X-irradiation, expression of CXCL1, CXCL-2 and CXCL-8 (IL-8) were 3.2, 2.1 and 1.9 fold up-regulated, respectively. This increased after 8 Gy X-irradiation to 6.4, 2.8 and 3.1 accordingly. Relative CXCL-10 gene expression was increase 4.3 fold after 4 Gy exposure and goes up to 12.8 fold after 8 Gy X-irradiation. It has been suggested that angiostatic and angiogenic chemokines are differentially regulated by low and high doses of radiation. Low dose irradiation increased angiogenic CXC chemokine mRNA expression, whereas angiostatic chemokines are significantly elevated at higher doses (Chang *et al.* 2009). In this study, 4 Gy and 8 Gy were used but it was reported that also lower doses (< 2 Gy) up-regulate CXC chemokines in normal human fibroblasts (Fujimori 2005) and plays a crucial role in the early phase of the cutaneous radiation reaction (Müller and Meineke 2011). It has been reported that increased expression of CXCL-1 (Gro $\alpha$ ), CXCL-2(Gro $\beta$ ) and CXCL-8 is involved in metastasis, chemoresistance and angiogenesis (Feliciano 2012; Gales *et al.* 2013) in response to activation of NF- $\kappa$ B. Some NF- $\kappa$ B inhibitors such as curcumin target CXCL1 and CXCL2 and inhibit prostate cancer metastasis (Killian *et al.* 2012). Elevated levels of CXCL1 and CXCL10 were also suggested as marker of inflammation and angiogenesis/angiostasis in type 2 diabetes (Sajadi *et al.* 2013). Koch *et al.* reported that after TNF- $\alpha$  treatment, CXC chemokines were up-regulated (Koch 2013). It was also published that chemokine expression in inflamed adipose tissue is mainly mediated by NF- $\kappa$ B after TNF- $\alpha$  treatment (Tourniaire *et al.* 2013). This study further explains and reports that chemokine expression is not only activated by the classical

pathway, but also by the genotoxic stress induced pathway. These up-regulated chemokines could play a major role in cell-cell communication (bystander effect).

Up-regulation of **NFKB1**, **NFKB2** and **NFKBIA** at high dose (8 Gy) showed that self-regulatory mechanisms of the NF- $\kappa$ B pathway are activated in the cellular radiation response. NFKB1 and NFKB2 have a dual function in NF- $\kappa$ B signaling. NFKB1 and NFKB2 encode the proteins p105 and p100 serve both as NF- $\kappa$ B precursors and inhibitors of NF- $\kappa$ B dimers (Savinova, V *et al.* 2009). NFKBIA encodes I $\kappa$ B $\alpha$  which binds to the NF- $\kappa$ B dimers thus leading to its own inactivation and subsequent termination of the response (Baldwin 1996).

NF- $\kappa$ B also controls other transcription factors such as **IRF1** which encodes interferon regulatory factor 1 and plays a role in regulating apoptosis and tumor-suppression. IRF1 functions as a transcription activator of genes induced by interferon  $\alpha$ ,  $\beta$ , and  $\gamma$  (Webb and Bhalla 1976). Up-regulation of IRF1 after ionizing radiation indicates that IRF1 plays a role in DNA damage-induced pathways. It has been reported that ATM kinase is involved in regulation of IRF1 expression following exposure to genotoxic stress by ionizing radiation or etoposide (Pamment *et al.* 2002). The transcription factors NF- $\kappa$ B and IRF1, with the help of signal transducer and activator of transcription 1 (STAT1), mediate the effects of cytokines in target cells (Woods *et al.* 2003). In this study STAT1 was not regulated by ionizing radiation exposure.

**TNF** gene encodes the multifunctional pro-inflammatory cytokine TNF- $\alpha$ , which further activate NF- $\kappa$ B by binding to the TNFR-1 and TNFR-2 receptors. Up-regulation of TNF gene was dependent on ionizing radiation dose. TNF- $\alpha$  is involved in the regulation of many biological processes including cell proliferation, differentiation, apoptosis, lipid metabolism, and coagulation (Wu *et al.* 2010; Zetzmann *et al.* 2010). TNF- $\alpha$  also activates the MAPK pathway, which is involved in activation of the pro-apoptotic transcription factor c-Jun (Gaur and Aggarwal 2003). The pro-apoptotic effect of TNF- $\alpha$  is often masked by the anti-apoptotic effects of NF- $\kappa$ B. It is reported that in many cell types, TNF- $\alpha$  has no apoptotic effect due to its parallel triggering of a signaling pathway that activates NF- $\kappa$ B (Chen and Goeddel 2002). Secreted or membrane-associated forms of TNF- $\alpha$  may induce bystander

effects via activation of COX-2 gene expression in non-irradiated cells (Zhou *et al.* 2008).

**VCAM1** encodes vascular cell adhesion molecule 1 which is also known as cluster of differentiation 106 (CD106). This study contradicts previous studies which suggested that radiation had no significant effect on surface expression of the endothelial adhesion molecules ICAM-1 and VCAM-1 (Khaled *et al.* 2012; Quarmby *et al.* 2000). In this study, it was shown that X-irradiation (4 Gy and 8 Gy) up-regulates VCAM1 but radiation dose had no significant effect on its expression. The promoter region of the VCAM-1 gene contains functional tandem  $\kappa$ B sites therefore it can be up-regulated when NF- $\kappa$ B is activated either by classical or genotoxic stress induced pathway.

**CD83** encodes single-pass type I membrane protein which is also member of the immunoglobulin superfamily of receptors. CD83 is the only gene up-regulated after exposure to ionizing radiation, but not after TNF- $\alpha$  treatment (Hellweg 2012; Koch 2013). CD83 is one of the central regulatory molecules in immune functions with anti-tumor effects (Fujimoto and Tedder 2006). It is suggested that CD83 may be involved in the regulation of antigen presentation and acts as a co-stimulator during activation of T-cells in adaptive immune response (McKinsey *et al.* 2000). It is suggested that ionizing radiation not only induces inflammation as a prominent innate immune response, but may also induce adaptive immunity by up-regulation of CD83 after activation of radiation-induced NF- $\kappa$ B activation.

**MAP2K6** encodes dual specificity mitogen-activated protein kinase kinase 6 also known as MAP kinase kinase 6 (MAPKK6). This gene is involved in many cellular processes such as stress induced cell cycle arrest, transcription activation and apoptosis. It was the only gene which was down-regulated after X-irradiation of HEK cells. Down-regulation of MAP2K6 might play an important role in anti-apoptosis.

#### 4.5.2 NF- $\kappa$ B-dependent gene expression after heavy ion exposure

Heavy ions are strong activators of the expression of NF- $\kappa$ B down-stream target genes (**Figure 30**). In this study,  $^{22}\text{Ne}$  (92 keV/ $\mu\text{m}$ ) showed a very high RBE value (7.01) for NF- $\kappa$ B-dependent reporter gene expression. Thus  $^{22}\text{Ne}$  ions were selected for studying NF- $\kappa$ B-dependent target gene expression. Furthermore, the NF- $\kappa$ B-dependent expression profile was compared to data obtained after X-irradiation and

exposure to  $^{48}\text{Ti}$  ions (115 keV/ $\mu\text{m}$ ) from studies performed earlier by a member of the Biodiagnostics Workgroup at DLR (Koch 2013).

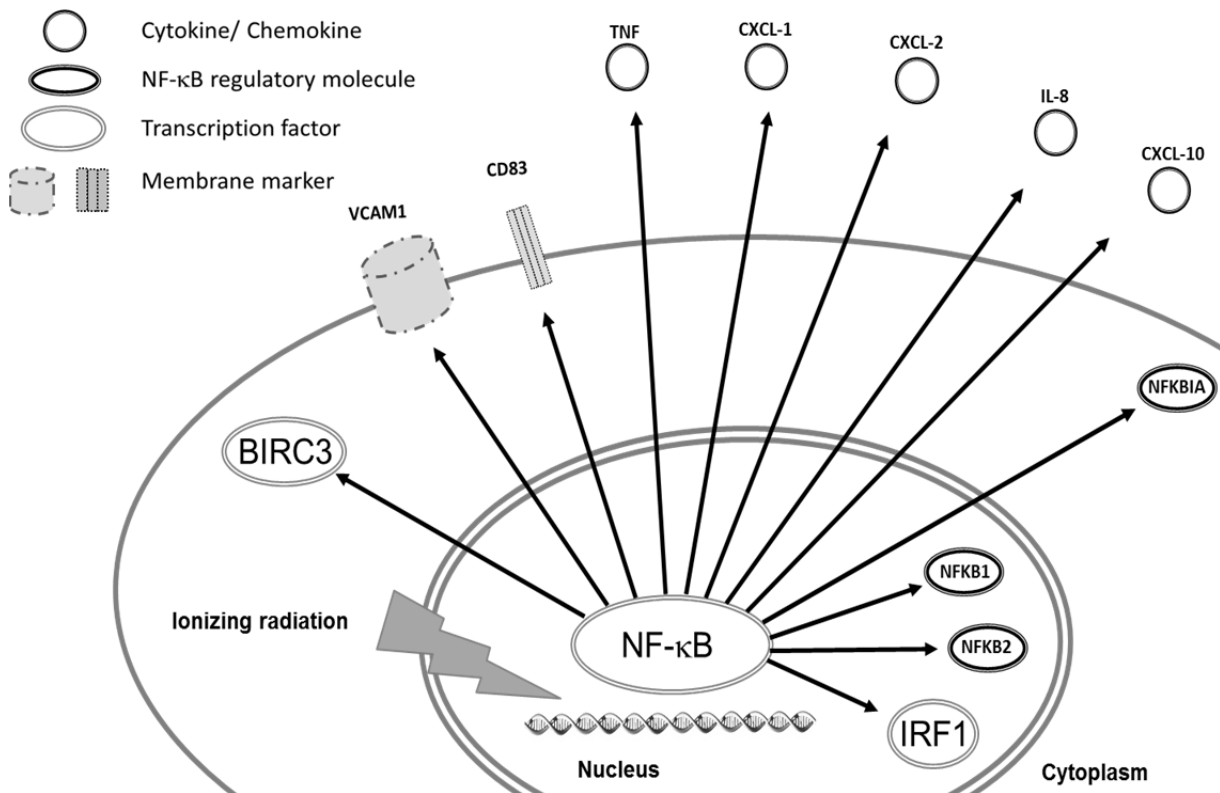


**Figure 30 Modulation of NF- $\kappa$ B-dependent gene expression after ionizing radiation exposure.**

Ionizing radiation-induced NF- $\kappa$ B activation modulates gene expression of different extracellular chemokines (CXCL-1, CXCL-2, IL-8/CXCL8, CXCL-10, adhesion molecules (VCAM-1), co-stimulatory membrane proteins (CD83), other transcription factors (IRF1), pro-inflammatory cytokines (TNF), and the anti-apoptotic factor BIRC3. NF- $\kappa$ B also regulates itself by modulating gene expression of NFKB1, NFKB2 and NFKBIA.

Most of the genes which were up-regulated by X-rays showed also up-regulation after  $^{22}\text{Ne}$  ion exposure. These genes including CXCL-1, CXCL-2, CXCL-8, CXCL-10, NFKB1, NFKB2, NFKBIA, IRF1, TNF, CCL2, IRF-1, VCAM1, and CD83 were discussed in detail in the previous section 4.5.1. MAP2K6, BIRC3 and CXCL2 did not show two fold regulations due to an unknown reason but CXCL-2 showed two fold up-regulations in the RT-qPCR. It has been observed that 4 Gy of  $^{22}\text{Ne}$  ions resulted in gene regulation comparable to 8 Gy of X-rays. Up-regulated gene expression profiles of both  $^{22}\text{Ne}$  and  $^{48}\text{Ti}$  ions were similar. Three additional genes including

CCL12, CD40, and IL1R2 showed two fold regulations. When raw data of these genes were analyzed, it was noticed that the average threshold cycle was relatively high ( $> 30$ ). Very high threshold values represent very low relative expression, in both control and test samples, and the p-value for the fold-change was either unavailable or relatively high ( $p > 0.05$ ). Therefore, it is important to have a sufficient number of biological replicates to validate the result for such genes. Activation of aforementioned genes showed that NF- $\kappa$ B activation may be related to better survival of exposed cells which play a role in maintaining DNA fidelity, cell-cell communication and modulating cell-cycle progression or cell death.

## **4.6 The effect of LET on the up-regulated NF- $\kappa$ B target genes**

### **4.6.1 Heavy ions induce expression of chemokine and cytokine genes most efficiently at LET-values relevant for NF- $\kappa$ B activation**

To further study the effect of LET on NF- $\kappa$ B target gene expression, cells were irradiated with heavy ions of a broad LET range (3-10000 keV/ $\mu$ m). The gene expression of selected NF- $\kappa$ B target genes (NFKBIA, CXCL-1, CXCL-2, CXCL-8 and CXCL-10, CD83 and XIAP) was followed 6 and 24 h after irradiation (4 Gy). The NF- $\kappa$ B-independent genes CDKN1A and GADD45 $\alpha$  are known to respond to ionizing radiation and were included in the analysis (**Figure 28**). GAPDH and PBGD were used as reference genes for normalizing target gene expression. Up-regulation of NFKBIA shows that the NF- $\kappa$ B pathway was activated after aforementioned ion exposure. The regulation of XIAP was in the range of basal expression which is the normal expression of a gene without radiation exposure. It was observed that expression of cytokines and chemokines has a strong correlation with LET. After irradiating cells with heavy ions in the LET range of 3 to 176 keV/ $\mu$ m, a strong up-regulation of genes coding for chemokines was observed. The gene expression was less after exposure to ions with an LET of 905 keV/ $\mu$ m compared to 90-200 keV/ $\mu$ m LET heavy ions. According to the results shown in this work, heavy ions induce expression of chemokine and cytokine genes most efficiently at LET-values relevant for NF- $\kappa$ B activation (90-200 keV/ $\mu$ m). This indicates the dependence of expression of these cytokines on NF- $\kappa$ B activation.

NF- $\kappa$ B target gene array showed no strong up-regulation of CDKN1A which is a cell cycle related gene. CDKN1A is TP53-dependent genes but shares  $\kappa$ B site in the promoter region. The gene expression may be associated with increased NF- $\kappa$ B activity but has not been shown to be a NF- $\kappa$ B target directly. The array was performed with samples incubated for 6 hours after irradiation but TP53-dependent genes showed strong late up-regulation around 24 hours after irradiation. Up-regulation of CDKN1A and GADD45 $\alpha$  showed that TP53 (gene encodes p53) is essential for the high-LET-induced delay of cell cycle progression which amends a previous study (Fournier and Taucher-Scholz 2004). It can be concluded that GADD45 $\alpha$  and CDKN1A expression after exposure to heavy ions might contribute to induced G2/M arrest. NF- $\kappa$ B-dependent target gene expression analysis suggests that there might be a distinct gene expression associated with radiation exposure to both low and high LET radiation. These results demonstrate that heavy ions up-regulate the expression of chemokines especially CXCL1, CXCL2, CXCL10 and CXCL-8 with maximal potency in the LET range of ~90-200 keV/ $\mu$ m.

#### **4.7 Conclusion and outlook**

The work presented here clearly shows that NF- $\kappa$ B, a potent transcription factor is involved in regulation of many biological functions including cellular survival, cell cycle regulation, cell-cell communication, proliferation and DNA damage response after ionizing radiation exposure. The results demonstrate that heavy ions up-regulate chemokine expression, especially CXCL1, CXCL2, CXCL10 and CXCL-8, which might play a major role in non-targeted effects with maximal potency in the LET range of ~90-200 keV/ $\mu$ m.

Furthermore, the results exhibit the role of NF- $\kappa$ B in the cellular radiation response. Down-regulation of NF- $\kappa$ B in HEK cells leads to increased radiosensitivity, lower survival, delayed cell cycle progression and impaired DNA damage response. Loss of NF- $\kappa$ B might also lead to impaired cell-cell communication.

The discussed results indicate a connection between the quality of radiation and the correlated cellular radiation response. The biological effects caused by heavy ions



depend on the physical properties (LET) of accelerated particles therefore differences in level of cellular survival, regulation of the cell cycle and activation of NF- $\kappa$ B are observed. The maximum gene expression, cell cycle arrest and cell killing and NF- $\kappa$ B activation lies in the same range of LET  $\sim 150$  keV/ $\mu$ m. However, the RBE values of NF- $\kappa$ B activation are much higher than the RBE of cellular survival. NF- $\kappa$ B activation depends on dose and the cell system used. In different cell cycle phases, the level of DSBs and their repair efficiency may greatly contribute to the overall magnitude of NF- $\kappa$ B activation signals. A doubling of NF- $\kappa$ B-dependent reporter gene expression is possible with 1-2 particle hits per cell nucleus which depends on the LET value of irradiated heavy ions. The minimal number of DNA breaks required to activate NF- $\kappa$ B is unknown.

ATM kinase, a factor responding to DNA damage, is responsible for activation of NF- $\kappa$ B-dependent transcription within the nuclear genome (Brzoska and Szumiel 2009). Since NF- $\kappa$ B regulates its target genes during radiation response and DNA repair, therefore cell lines with knock-down of ATM or NEMO are suggested for future studies.

To learn more about the single particle effects and function of the NF- $\kappa$ B targeted genes, experiments with microbeam are highly recommended which enables irradiation of single cells and subcellular compartments by using single particle beams. The effect of knock-down of the up-regulated chemokines may also help to understand the role of cell-cell communication in cellular radiation response. The efficiency of radiotherapy for cancer treatment is limited by toxic side effects of high doses. Inhibition of NF- $\kappa$ B or NF- $\kappa$ B downstream signaling may increase the therapeutical efficiency of radiation.

## 4.8 Summary

To enable long-term human spaceflight, the cellular radiation response to heavy ions with a high linear energy transfer (LET) needs to be better understood for developing appropriate countermeasures to mitigate acute effects and late radiation risks for the astronaut. The biological effectiveness of accelerated heavy ions in provoking DNA damage response pathways as a gateway to cell death or survival is of major concern not only for spaceflight but also for new regimes of tumor radiotherapy.

It has been shown that NF- $\kappa$ B, the main actuator in inflammation and immune response, can be activated by DNA double strand breaks (DNA damage dependent subpathway) and is discussed to contribute to anti-apoptosis and survival improvement of cells containing residual DNA damage after ionizing irradiation. The biological relevance of the recently discovered LET dependency of NF- $\kappa$ B activation is unknown, especially the resulting profile of NF- $\kappa$ B target gene expression. Therefore, the effect of heavy ions of a broad LET range (0.3-10,000 keV/ $\mu$ m) on cellular survival, regulation of the cell cycle and activation of NF- $\kappa$ B and the induction of its target genes were investigated. Furthermore, the role of NF- $\kappa$ B activation in cellular survival, cell cycle progression and DNA damage response after X-irradiation was assessed using HEK and RelA knock-down (HEK shRNA RelA) cells.

Use of a NF- $\kappa$ B reporter cell line revealed that exposure to heavy ions resulted in maximal NF- $\kappa$ B activation, cell killing and G2/M arrest in the LET range of 90-200 keV/ $\mu$ m. Here, a doubling of NF- $\kappa$ B was reached with radiation doses compliant to induce as less as 1 DNA double strand break per cell.

The cellular survival after X-irradiation decreases in HEK RelA knock-down cells whereas activation of NF- $\kappa$ B by tumor necrosis factor alpha (TNF- $\alpha$ ) 6 h in advance to X-irradiation slightly improves cellular survival. The results show that NF- $\kappa$ B down regulation leads cells not only towards high radiosensitivity and lower survival but also, for the first time, to a delayed DNA damage response and cell cycle progression.

In this research work it has been shown for the first time that heavy ions up-regulate NF- $\kappa$ B-dependent chemokines (CXCL1, CXCL2, CXCL10 and IL-8) and CD83 expression with maximal potency in the LET range of 50-300 keV/ $\mu$ m. These up-regulated chemokines are important for cell-cell communication with hit as well as unhit cells (bystander effect). The latter are believed to contribute to the tissue radiation response especially after exposure to low doses of high LET radiation relevant for spaceflight and surrounding tissue in tumor therapy.

Taken together, this study clearly demonstrates that the cellular radiation response modulation of NF- $\kappa$ B activation and NF- $\kappa$ B-dependent gene expression is highest in the LET range of ~50-300 keV/ $\mu$ m. The results obtained suggest the NF- $\kappa$ B pathway to be a promising target for pharmacological modulation of cellular radiation response either to improve tumor cell killing during radiotherapy with heavy ions or to mitigate radiation late effects such as carcinogenesis in astronauts.

## 5 Abbreviations

Abbreviation	Acronym
$\lambda$	Wavelength
$\gamma$ -H2AX	Phosphorylated histone variant H2AX
$^{\circ}\text{C}$	Degree centigrade
$\mu\text{g}$	Microgram ( $1 \times 10^{-6}$ g)
$\mu\text{l}$	Microliter ( $1 \times 10^{-6}$ l)
$\mu\text{m}$	Micrometer ( $1 \times 10^{-6}$ m)
$\mu\text{mol/l}$	Micromole per liter
$1 \times g$	Earth gravity
AP-1	Activated protein 1
APE1	AP endonuclease 1, (multifunctional DNA repair enzyme)
APTX	Aprataxin
<i>Aqua dest.</i>	<i>Aqua destillatum</i>
Ar	Argon
ARD	Ankyrin repeat domain
ARE	Antioxidant DNA response element
AT	Ataxia telangiectasia
ATM	Ataxia telangiectasia mutated protein
ATR	Ataxia telangiectasia and Rad3 related
BCL-2	B-cell CLL (chronic lymphatic leukemia) /lymphoma 2 protein
BCL-XL	B-cell lymphoma-extra large
BER	Base excision repair
BLM	Bloom syndrome protein
bp	Base pairs
BRCA1	Breast cancer associated gene 1
BRCA1 A	Complex containing BRCA1, ABRA1, Rap80 and the deubiquitination
BRCA2	Breast cancer associated gene 2, early onset
BSA	Bovine Serum Albumin
C	Carbon
Caspase	Cysteine Aspartic Acid Specific Protease
cc	Cell division cycle 45 homolog ( <i>S. cerevisiae</i> ) ( <i>Homo sapiens</i> )
CCR	Chemokine (C-C motif) receptor
CD80	Costimulatory factor CD80

<b>Abbreviation</b>	<b>Acronym</b>
CDK	Cyclin-dependent kinase
CDK1 (Cdc2)	Cyclin-dependent kinase 1 (cell division control protein 2 homolog)
CDKN1A	Cyclin-dependent kinase inhibitor 1
cDNA	Complementary DNA
CFA	Colony forming ability
CHK1 / CHEK1	Checkpoint kinase 1, CHK1 checkpoint homolog (S. pombe)
CHK2 / CHEK2	Checkpoint kinase 2, CHK2 checkpoint homolog (S. pombe)
CHO	Chinese Hamster Ovary
cm	Centimeter
COX-2 (PTGS2)	Prostaglandin-endoperoxide synthase 2
CT	Threshold cycle
CtIP	C-terminal binding protein (CtBP) interacting protein
CXC	Chemokine (C-X-C motif)
CXCL-1 (GRO-a)	Chemokine (C-X-C motif) ligand 1
CXCL-10	Chemokine (C-X-C motif) ligand 10
CXCL2 (MIP-2a)	CXC ligand 2 (macrophage inflammatory protein 2)
d	Day (s)
D	Dose
d2EGFP	Destabilized Enhanced Green Fluorescent Protein
Da	Dalton
DAPI	4',6-diamidino-2-phenylindole
DDB	Damage DNA binding
DDR	DNA Damage Response
Deq	Equivalent dose
DLR	Deutsches Zentrum für Luft- und Raumfahrt e.V.
DMSO	Dimethyl sulfoxide
DNA	Deoxyribonucleic acid
DNA-PK	DNA-dependent protein kinase
DSB	Double-strand break
EDTA	Ethylene diamine tetraacetic acid
EGFP	Enhanced Green Fluorescent Protein
EGFR	Epidermal growth factor receptor
ELKS (ERC1)	ELKS/RAB6-interacting/CAST family member 1
EMSA	Electrophoretic mobility shift assay

<b>Abbreviation</b>	<b>Acronym</b>
eV	Electron volt
Exo1	Exonuclease1
FACS	Fluorescence-activated cell sorting
FBS	Fetal Bovine Serum
Fe	Iron
FSC	Forward scatter
g	Gram
G1	Gap 1 phase of the cell cycle
G2	Gap 2 phase of the cell cycle
GADD45	Growth arrest and DNA damage inducible gene 45
GANIL	Grand Accélérateur National d'Ions lourds
GAPDH	Glyceraldehyde 3-phosphate dehydrogenase
GCR	Galactic cosmic rays
GeV	Giga electron Volt
GFP	Green Fluorescent Protein
GSI	Helmholtzzentrum für Schwerionenforschung GmbH
Gy	Gray (J/kg), unit of irradiation dose
h	Hour (s)
H2AX	Histone 2 subtype AX
HEK/293	Human embryonic kidney
HIMAC	Heavy Ion Medical Accelerator in Chiba, Japan
HR	Homologous recombination
I $\kappa$ B	Inhibitor of NF- $\kappa$ B
ICAM-1	Intercellular adhesion molecule-1
ICRP	International Commission on Radiological Protection
IKK	I $\kappa$ B kinase
IKK-K	IKK kinases
IL	Interleukin
iNOS	Inducible nitric oxide synthase
ISS	International Space Station
kDa	Kilo Dalton
keV	Kilo electron volt

Abbreviation	Acronym
kg	Kilogram
Ku70-Ku80	X-ray repair complementing defective repair in CHO cells
kV	Kilo Volt
LEO	Low Earth orbit
LET	Linear energy transfer
M	Mitosis phase of the cell cycle
MAPK	Mitogen-activated protein kinase
MCP-1	Monocyte chemoattractant protein-1
Mdm2 (HDM2)	p53 binding protein homolog (mouse)
MeV/n	Mega electron volt per nucleon
min	Minute (s)
ml	Milliliter ( $1 \times 10^{-3}$ l)
MLH1	MutL homolog 1, colon cancer, nonpolyposis type 2 (E. coli)
mm	Millimeter ( $1 \times 10^{-3}$ m)
mmol/l	Millimole per liter
MMPs	Matrix metalloproteinases
MRE11	Meiotic recombination 11 homolog
MRN	MRE11-RAD50-NBS1
mRNA	Messenger RNA
ms	Millisecond (s)
mSv	Milli sievert
NASA	National Aeronautics and Space Administration (USA)
NBS1	Nijmegen Breakage Syndrome gene 1
Ne	Neon
NEMO/IKK	NF- $\kappa$ B essential modulator
NER	Nucleotide excision repair
NF- $\kappa$ B	Nuclear Factor kappa light polypeptide gene enhancer in B-cells
NFKBIA	NF- $\kappa$ B inhibitor alpha (encoding I $\kappa$ B $\alpha$ )
ng	Nanogram ( $1 \times 10^{-9}$ g)
NHEJ	Non-homologous end joining
Ni	Nickel
nm	Nanometer ( $1 \times 10^{-9}$ m)
NO	Nitric oxide
Nrf2	Nuclear erythroid-derived 2-related factor 2

Abbreviation	Acronym
O	Oxygen
p100	NF- $\kappa$ B subunit with a molecular weight of 100 kDa, precursor of p52
p105	NF- $\kappa$ B subunit with a molecular weight of 105 kDa, precursor of p50
p21Cip1,WAF1	Protein 21 CDK2-interacting protein 1, wild-type p53-activated
p50 (NF- $\kappa$ B1)	NF- $\kappa$ B subunit with a molecular weight of 50 kDa
p52 (NF- $\kappa$ B2)	NF- $\kappa$ B subunit with a molecular weight of 52 kDa
p53 (TP53)	Tumor protein p53
p65	Nuclear Factor B subunit with a molecular weight of 65 kDa
PARP	Poly(ADP-ribose)polymerases
Pb	Lead
PBS	Phosphate buffered saline
PCNA	Proliferating cell nuclear antigen
PCR	Polymerase chain reaction
PE	Plating efficiency
PI	Propidium iodide (C <sub>27</sub> H <sub>34</sub> I <sub>2</sub> N <sub>4</sub> )
PIASy	Protein inhibitor of activated STAT4
PIDD	p53-induced protein with a death domain
PIKK	phosphatidylinositol-3-kinase-related
PKc	Protein kinase C
PMS2	Postmeiotic segregation increased 2
PNKP	Polynucleotide kinase 3'-phosphatase
RAD	Radiation sensitive
RAD50	RAD50 homolog ( <i>S. cerevisiae</i> )
RAD51	RAD51 homolog (RecA homolog, <i>E. coli</i> ) ( <i>S. cerevisiae</i> )
RAD52	RAD52 homolog (RecA homolog, <i>E. coli</i> ) ( <i>S. cerevisiae</i> )
RBE	Relative biological effectiveness
RecA	DNA recombination protein RecA
RelA	NF- $\kappa$ B subunit p65
REST	Relative Expression Software Tool
RFC	Replication factor C
RHD	Rel homology domain
RNAi	RNA interference
ROS	Reactive oxygen species
RPA	Replication protein A

<b>Abbreviation</b>	<b>Acronym</b>
RT-qPCR	Reverse transcriptase quantitative polymerase chain reaction
s	Second
S	Relative survival
shRNA	Short hairpin RNA
siRNA	Small interfering RNA
SLX1/SLX4	SLX1/SLX4 structure-specific endonuclease subunit homolog
SPE	Solar particle event
SSA	Single-strand annealing
SSB	Single-strand break
SSC	Side scatter
ssDNA	Single stranded DNA
STAT	Signal transducer and activator of transcription
SUMO	Small Ubiquitin-like modifier
Sv	Sievert
SV40	Simian virus 40
TA	Annealing temperature
TBE	Tris/Borate/EDTA
TDP1	Tyrosyl-DNA phosphodiesterase 1
TFIIH	Transcription factor II Human
Ti	Titanium ion
TK	Thymidine kinase
TNF	Tumor necrosis factor
TNF-R	TNF receptor
TRAF	TNF-R-associated factor
UV	Ultraviolet
VCAM-1	Vascular cell adhesion molecule-1
XIAP	X-linked inhibitor of apoptosis
XLF	XRCC4-like factor
XPA	Xeroderma pigmentosum, complementation group A)
XPB	Xeroderma Pigmentosum B
XPC	Xeroderma pigmentosum, complementation group C
XPD	Xeroderma pigmentosum group D
XRCC1	X-ray repair complementing defective repair in CHO cells 1
XRCC4	X-ray repair complementing defective repair in CHO cells 4



## 6 References

- Ando K, Koike S, Uzawa A, Takai N, Fukawa T, Furusawa Y, Aoki M, Hirayama R (2006) Repair of skin damage during fractionated irradiation with gamma rays and low-LET carbon ions. *J Radiat Res* 47:167-174
- Apathy I, Beaujean R, Deme S, Pazmandi T, Reitz G (2003) Personal dosimetry for human missions to Mars based on TLD and LET-spectrometry technique.
- Aravindan S, Natarajan M, Ramraj SK, Pandian V, Khan FH, Herman TS, Aravindan N (2014) Abscopal effect of low-LET gamma-radiation mediated through Rel protein signal transduction in a mouse model of nontargeted radiation response. *Cancer Gene Ther* 21:54-59
- Ashburner BP, Shackelford RE, Baldwin AS, Paules RS (1999) Lack of involvement of ataxia telangiectasia mutated (ATM) in regulation of nuclear factor-kappaB (NF-kappaB) in human diploid fibroblasts. *Cancer Res* 59:5456-5460
- Autsavapromporn N, de Toledo SM, Little JB, Jay-Gerin JP, Harris AL, Azzam EI (2011) The role of gap junction communication and oxidative stress in the propagation of toxic effects among high-dose alpha-particle-irradiated human cells. *Radiat Res* 175:347-357
- Aypar U, Morgan WF, Baulch JE (2011) Radiation-induced genomic instability: are epigenetic mechanisms the missing link? *Int J Radiat Biol* 87:179-191
- Azzam EI, de Toledo SM, Little JB (2003) Oxidative metabolism, gap junctions and the ionizing radiation-induced bystander effect. *Oncogene* 22:7050-7057
- Azzam EI, de Toledo SM, Spitz DR, Little JB (2002) Oxidative metabolism modulates signal transduction and micronucleus formation in bystander cells from alpha-particle-irradiated normal human fibroblast cultures. *Cancer Res* 62:5436-5442
- Baichwal VR, Baeuerle PA (1997) Activate NF-kappa B or die? *Curr Biol* 7:94-96
- Baldwin AS (1996) The NF- $\kappa$ B and I $\kappa$ B proteins: New Discoveries and Insights. *Annu Rev Immunol* 14:649-681
- Baldwin AS (2001) Control of oncogenesis and cancer therapy resistance by the transcription factor NF-kappaB. *J Clin Invest* 107:241-246
- Baumstark-Khan C, Hellweg CE, Arenz A, Meier MM (2005) Cellular monitoring of the nuclear factor kappaB pathway for assessment of space environmental radiation. *Radiat Res* 164:527-530
- Baumstark-Khan C, Hellweg CE, Reitz G (2010) Cytotoxicity and Genotoxicity Reporter Systems Based on the Use of Mammalian Cells. *Adv Biochem Eng Biotechnol* 113-151

- Beamish H, Lavin MF (1994) Radiosensitivity in ataxia-telangiectasia: anomalies in radiation-induced cell cycle delay. *Int J Radiat Biol* 65:175-184
- Beck M, Moreels M, Jacquet P, Van OP, De Vos WH, Baatout S (2012) X-irradiation induces cell death in fetal fibroblasts. *Int J Mol Med* 30:114-118
- Beg AA, Baldwin AS (1993) The I kappa B proteins: multifunctional regulators of Rel/NF-kappa B transcription factors. *Genes Dev* 7:2064-2070
- Bhat-Nakshatri P, Sweeney CJ, Nakshatri H (2002) Identification of signal transduction pathways involved in constitutive NF-kappaB activation in breast cancer cells. *Oncogene* 21:2066-2078
- Bora RS, Gupta D, Malik R, Chachra S, Sharma P, Saini KS (2008) Development of a cell-based assay for screening of phosphodiesterase 10A (PDE10A) inhibitors using a stable recombinant HEK-293 cell line expressing high levels of PDE10A. *Biotechnol Appl Biochem* 49:129-134
- Brach MA, Hass R, Sherman ML, Gunji H, Weichselbaum R, Kufe D (1991) Ionizing radiation induces expression and binding activity of the nuclear factor kappa B. *J Clin Invest* 88:691-695
- Brenner DJ, Ward JF (1992) Constraints on energy deposition and target size of multiply damaged sites associated with DNA double-strand breaks. *Int J Radiat Biol* 61:737-748
- Brooks AL (2003) Developing a scientific basis for radiation risk estimates: goal of the DOE Low Dose Research Program. *Health Phys* 85:85-93
- Brzoska K, Szumiel I (2009) Signalling loops and linear pathways: NF-kappaB activation in response to genotoxic stress. *Mutagenesis* 24:1-8
- Burdelya LG, Krivokrysenko VI, Tallant TC, Strom E, Gleiberman AS, Gupta D, Kurnasov OV, Fort FL, Osterman AL, Didonato JA, Feinstein E, Gudkov AV (2008) An agonist of toll-like receptor 5 has radioprotective activity in mouse and primate models. *Science* 320:226-230
- Cernan E (2004) *The Vision for Space Exploration*. National Aeronautics and Space Administration, Washington, DC
- Chang CC, Lerman OZ, Thanik VD, Scharf CL, Greives MR, Schneider RJ, Formenti SC, Saadeh PB, Warren SM, Levine JP (2009) Dose-dependent effect of radiation on angiogenic and angiostatic CXC chemokine expression in human endothelial cells. *Cytokine* 48:295-302
- Chen G, Goeddel DV (2002) TNF-R1 signaling: a beautiful pathway. *Science* 296:1634-1635
- Chen X, Shen B, Xia L, Khaletskiy A, Chu D, Wong Jeffrey YC, Li J (2002) Activation of nuclear factor kappaB in radioresistance of TP53-inactive human keratinocytes. *Cancer Res* 62:1213-1221

- Chishti A, Baumstark-Khan C, Hellweg CE, Reitz G (2014) Imaging of Nuclear Factor  $\kappa$ B Activation Induced by Ionizing Radiation in Human Embryonic Kidney Cells (HEK) cells. *Radiation and Environmental Biophysics* in press:
- Criswell T, Leskov K, Miyamoto S, Luo G, Boothman DA (2003) Transcription factors activated in mammalian cells after clinically relevant doses of ionizing radiation. *Oncogene* 22:5813-5827
- Cucinotta FA, Durante M (2006) Cancer risk from exposure to galactic cosmic rays: implications for space exploration by human beings. *Lancet Oncol* 7:431-435
- Cude K, Wang Y, Choi H, Hsuan S, Zhang H, Wang C, Xia Z (2007) Regulation of the G2-M cell cycle progression by the ERK5-NF $\kappa$ B signaling pathway. *J Cell Biol* 177:253-264
- Dahlman JM, Wang J, Bakkar N, Guttridge DC (2009) The RelA/p65 subunit of NF- $\kappa$ B specifically regulates cyclin D1 protein stability: implications for cell cycle withdrawal and skeletal myogenesis. *J Cell Biochem* 106:42-51
- Dent P, Yacoub A, Contessa J, Caron R, Amorino G, Valerie K, Hagan MP, Grant S, Schmidt-Ullrich R (2003) Stress and radiation-induced activation of multiple intracellular signaling pathways. *Radiat Res* 159:283-300
- Dexheimer TS (2013) DNA Repair Pathways and Mechanisms. In: Mathews LA, Stephanie MC, Elaine MH (eds) *DNA Repair of Cancer Stem Cells*. vol IV. Springer, USA, pp. 19-31
- Di C, Yang L, Zhang H, An L, Zhang X, Ma X, Sun C, Wang X, Yang R, Wu Z, Si J (2013) Effects of carbon-ion beam or X-ray irradiation on anti-apoptosis  $\beta$ -tubulin expression in HeLa cells. *Gene* 515:208-213
- Duffey DC, Chen Z, Dong G, Ondrey FG, Wolf JS, Brown K, Siebenlist U, Van WC (1999) Expression of a dominant-negative mutant inhibitor- $\kappa$ B $\alpha$  of nuclear factor- $\kappa$ B in human head and neck squamous cell carcinoma inhibits survival, proinflammatory cytokine expression, and tumor growth in vivo. *Cancer Res* 59:3468-3474
- Durante M, Grossi GF, Gialanella G, Pugliese M, Nappo M, Yang TC (1995) Effects of alpha-particles on survival and chromosomal aberrations in human mammary epithelial cells. *Radiat Environ Biophys* 34:195-204
- Durante M, Snigiryova G, Akaeva E, Bogomazova A, Druzhinin S, Fedorenko B, Greco O, Novitskaya N, Rubanovich A, Shevchenko V, von Recklinghausen U, Obe G (2003) Chromosome aberration dosimetry in cosmonauts after single or multiple space flights. *Cytogenetic and Genome Research* 103:40-46
- Durocher D, Jackson SP (2001) DNA-PK, ATM and ATR as sensors of DNA damage: variations on a theme? *Curr Opin Cell Biol* 13:225-231
- Eccles LJ, O'Neill P, Lomax ME (2011) Delayed repair of radiation induced clustered DNA damage: Friend or foe? *Mutat Res* 711:134-141

- Facoetti A, Ballarini F, Cherubini R, Gerardi S, Nano R, Ottolenghi A, Prise KM, Trott KR, Zilio C (2006) Gamma ray-induced bystander effect in tumour glioblastoma cells: a specific study on cell survival, cytokine release and cytokine receptors. *Radiat Prot Dosimetry* 122:271-274
- Fakir H, Hofmann W (2006) Incorporation of microdosimetric concepts into a biologically-based model of radiation carcinogenesis. *Radiation Protection Dosimetry* 122:330-334
- Feliciano P (2012) CXCL1 and CXCL2 link metastasis and chemoresistance. *Nat Genet* 44:840
- Fournier C, Taucher-Scholz G (2004) Radiation induced cell cycle arrest: an overview of specific effects following high-LET exposure. *Radiotherapy and Oncology* 73:S119-S122
- Franken N (2011) Relative biological effectiveness of high linear energy transfer  $\hat{\pm}$ -particles for the induction of DNA-double-strand breaks, chromosome aberrations and reproductive cell death in SW-1573 lung tumour cells. *Oncol Rep* 27:769-774
- Fujimori A (2005) Extremely Low Dose Ionizing Radiation Up-regulates CXC Chemokines in Normal Human Fibroblasts. *Cancer Research* 65:10159-10163
- Fujimoto Y, Tedder TF (2006) CD83: a regulatory molecule of the immune system with great potential for therapeutic application. *J Med Dent Sci* 53:85-91
- Fuseler JW, Merrill DM, Rogers JA, Grisham MB, Wolf RE (2006) Analysis and quantitation of NF-kappaB nuclear translocation in tumor necrosis factor alpha (TNF-alpha) activated vascular endothelial cells. *Microsc Microanal* 12:269-276
- Gales D, Clark C, Manne U, Samuel T (2013) The Chemokine CXCL8 in Carcinogenesis and Drug Response. *ISRN Oncology* 2013:1-8
- Galluzzi L, Vitale I, Abrams JM, Alnemri ES, Baehrecke EH, Blagosklonny MV, Dawson TM, Dawson VL, El-Deiry WS, Fulda S, Gottlieb E, Green DR, Hengartner MO, Kepp O, Knight RA, Kumar S, Lipton SA, Lu X, Madeo F, Malorni W, Mehlen P, Nunez G, Peter ME, Piacentini M, Rubinsztein DC, Shi Y, Simon HU, Vandenabeele P, White E, Yuan J, Zhivotovsky B, Melino G, Kroemer G (2012) Molecular definitions of cell death subroutines: recommendations of the Nomenclature Committee on Cell Death 2012. *Cell Death Differ* 19:107-120
- Gao N, Dai Y, Rahmani M, Dent P, Grant S (2004) Contribution of disruption of the nuclear factor-kappaB pathway to induction of apoptosis in human leukemia cells by histone deacetylase inhibitors and flavopiridol. *Mol Pharmacol* 66:956-963
- Gaur U, Aggarwal BB (2003) Regulation of proliferation, survival and apoptosis by members of the TNF superfamily. *Biochem Pharmacol* 66:1403-1408

- George K, Chappell L, Cucinotta F (2010) Persistence of space radiation induced cytogenetic damage in the blood lymphocytes of astronauts. *Mutation Research-Genetic Toxicology and Environmental Mutagenesis* 701:75-79
- George K, Durante M, Cucinotta F (2007) Chromosome aberrations in astronauts. *Advances in Space Research* 40:483-490
- Gerashchenko BI, Azzam EI, Howell RW (2004) Characterization of cell-cycle progression and growth of WB-F344 normal rat liver epithelial cells following gamma-ray exposure. *Cytometry A* 61:134-141
- Ghosh S (2007) *Handbook of Transcription Factor NF-kappaB*. Taylor and Francis,
- Ghosh S, Hayden MS (2012) Celebrating 25 years of NF-kappaB research. *Immunol Rev* 246:5-13
- Ghosh S, Hayden MS (2008) New regulators of NF-kappaB in inflammation. *Nat Rev Drug Discov* 8:837-848
- Gong L, Jin X, Li Q, Liu J, An L (2007) Heavy ion beams induce survivin expression in human hepatoma SMMC-7721 cells more effectively than X-rays. *Acta Biochim Biophys Sin (Shanghai)* 39:575-582
- Gordon KB, Char DH, Sagerman RH (1995) Late effects of radiation on the eye and ocular adnexa. *Int J Radiat Oncol Biol Phys* 31:1123-1139
- Graham FL, Smiley J, Russell WC, Nairn R (1977) Characteristics of a human cell line transformed by DNA from human adenovirus type 5. *J Gen Virol* 36:59-74
- Guttridge DC, Albanese C, Reuther JY, Pestell RG, Baldwin AS (1999) NF-kappaB controls cell growth and differentiation through transcriptional regulation of cyclin D1. *Mol Cell Biol* 19:5785-5799
- Habelhah H (2010) Emerging complexity of protein ubiquitination in the NF-kappaB pathway. *Genes Cancer* 1:735-747
- Habraken Y, Piette J (2006) NF-kappaB activation by double-strand breaks. *Biochem Pharmacol* 72:1132-1141
- Hadian K, Krappmann D (2011) Signals from the nucleus: activation of NF-kappaB by cytosolic ATM in the DNA damage response. *Sci Signal* 4:e2
- Hayden MS (2004) Signaling to NF- $\kappa$ B. *Genes Dev* 18:2195-2224
- Hayden MS, Ghosh S (2008) Shared principles in NF-kappa B signaling. *Cell* 132:344-362
- Haynes K, Sherer MAS, Visconti PJ, Ritenour ER (2013) *Radiation Protection in Medical Radiography*. Elsevier Health Sciences,

- Hellweg CE (2012) Cellular Response to Exposure with Different Radiation Qualities with Focus on Nuclear Factor  $\kappa$ B. Institut für Luft- und Raumfahrtmedizin des Deutschen Zentrums für Luft und Raumfahrt (DLR); Institut für Immunologie und Molekularbiologie der Freien Universität Berlin,
- Hellweg CE, Arenz A, Meier MM, Baumstark-Khan C (2005) Cellular monitoring systems for the assessment of space environmental factors. *Adv Space Res* 36:1673-1679
- Hellweg CE, Baumstark-Khan C (2007) Getting ready for the manned mission to Mars: the astronauts' risk from space radiation. *Naturwissenschaften* 94:517-526
- Hellweg CE, Baumstark-Khan C, Horneck G (2003) Generation of stably transfected Mammalian cell lines as fluorescent screening assay for NF- $\kappa$ B activation-dependent gene expression. *J Biomol Screen* 8:511-521
- Hellweg CE, Baumstark-Khan C, Schmitz C, Lau P, Meier MM, Testard I, Berger T, Reitz G (2011a) Activation of the nuclear factor kappaB pathway by heavy ion beams of different linear energy transfer. *Int J Radiat Biol* 87:954-963
- Hellweg CE, Baumstark-Khan C, Schmitz C, Lau P, Meier MM, Testard I, Berger T, Reitz G (2011b) Carbon-Ion-Induced Activation of the NF- $\kappa$ B Pathway. *Radiat Res* 175:424-431
- Herrmann T, Baumann M, Dörr W (2006) *Klinische Strahlenbiologie*. Elsevier, Urban & Fischer,
- Hinata K, Gervin AM, Jennifer ZY, Khavari PA (2003) Divergent gene regulation and growth effects by NF- $\kappa$ B in epithelial and mesenchymal cells of human skin. *Oncogene* 22:1955-1964
- Hinz M, Krappmann D, Eichten A, Heder A, Scheidereit C, Strauss M (1999) NF- $\kappa$ B function in growth control: regulation of cyclin D1 expression and G0/G1-to-S-phase transition. *Mol Cell Biol* 19:2690-2698
- Hirayama R, Ito A, Tomita M, Tsukada T, Yatagai F, Noguchi M, Matsumoto Y, Kase Y, Ando K, Okayasu R, Furusawa Y (2009) Contributions of direct and indirect actions in cell killing by high-LET radiations. *Radiat Res* 171:212-218
- Horstmann M, Durante M, Johannes C, Obe G (2005a) Chromosomal intrachanges induced by swift iron ions.
- Horstmann M, Durante M, Johannes C, Pieper R, Obe G (2005b) Space radiation does not induce a significant increase of intrachromosomal exchanges in astronauts' lymphocytes. *Radiation and Environmental Biophysics* 44:219-224
- Huang TT, Wuerzberger-Davis S, Seufzer BJ, Shumway SD, Kurama T, Boothman DA, Miyamoto S (2000) NF- $\kappa$ B activation by camptothecin. A linkage between nuclear DNA damage and cytoplasmic signaling events. *J Biol Chem* 275:9501-9509

- Huang TT, Wuerzberger-Davis S, Wu Z, Miyamoto S (2003) Sequential modification of NEMO/IKKgamma by SUMO-1 and ubiquitin mediates NF-kappaB activation by genotoxic stress. *Cell* 115:565-576
- Iliakis G, Wang Y, Guan J, Wang H (2003) DNA damage checkpoint control in cells exposed to ionizing radiation. *Oncogene* 22:5834-5847
- Ishikawa F, Nakano H, Seo A, Okada Y, Torihata H, Tanaka Y, Uchida T, Miyake H, Kakiuchi T (2002) Irradiation up-regulates CD80 expression through induction of tumour necrosis factor-alpha and CD40 ligand expression on B lymphoma cells. *Immunology* 106:354-362
- Jackson SP, Bartek J (2009) The DNA-damage response in human biology and disease. *Cancer Research* 69:1071-1078
- Janssens S, Tinel A, Lippens S, Tschopp J (2005) PIDD mediates NF-kappaB activation in response to DNA damage. *Cell* 123:1079-1092
- Jin S, Lu D, Ye S, Ye H, Zhu L, Feng Z, Liu S, Wang D, Hu Q (2005) A simplified probe preparation for ELISA-based NF-kappaB activity assay. *J Biochem Biophys Methods* 65:20-29
- Jung M, Dritschilo A (2001) NF-kappa B signaling pathway as a target for human tumor radiosensitization. *Semin Radiat Oncol* 11:346-351
- Kanai T, Furusawa Y, Fukutsu K, Itsukaichi H, Eguchi-Kasai K, Ohara H (1997) Irradiation of mixed beam and design of spread-out Bragg peak for heavy-ion radiotherapy. *Radiat Res* 147:78-85
- Karagiannis TC, El-Osta A (2004) Double-strand breaks: signaling pathways and repair mechanisms. *Cell Mol Life Sci* 61:2137-2147
- Khaled S, Gupta KB, Kucik DF (2012) Ionizing radiation increases adhesiveness of human aortic endothelial cells via a chemokine-dependent mechanism. *Radiat Res* 177:594-601
- Khanna KK, Lavin MF, Jackson SP, Mulhern TD (2001) ATM, a central controller of cellular responses to DNA damage. *Cell Death Differ* 8:1052-1065
- Kiefer J (1971) Target theory and survival curves. *J Theor Biol* 30:307-331
- Killian PH, Kronski E, Michalik KM, Barbieri O, Astigiano S, Sommerhoff CP, Pfeffer U, Nerlich AG, Bachmeier BE (2012) Curcumin inhibits prostate cancer metastasis in vivo by targeting the inflammatory cytokines CXCL1 and -2. *Carcinogenesis* 33:2507-2519
- Kim GJ, Chandrasekaran K, Morgan WF (2006) Mitochondrial dysfunction, persistently elevated levels of reactive oxygen species and radiation-induced genomic instability: a review. *Mutagenesis* 21:361-367

- Kim TK, Eberwine JH (2010) Mammalian cell transfection: the present and the future. *Anal Bioanal Chem* 397:3173-3178
- Koch K (2013) The role of Nuclear Factor  $\kappa$ B in the cellular response to different radiation qualities. Institut für Luft- und Raumfahrtmedizin des Deutschen Zentrums für Luft und Raumfahrt (DLR); Mathematisch Naturwissenschaftliche Fakultät der Albertus-Magnus-Universität zu Köln,
- Kondo T (2013) Radiation-induced cell death and its mechanisms. *Radiation Emergency Medicine* 2:1-4
- Kotula E, Faigle W, Berthault N, Dingli F, Loew D, Sun J, Dutreix M, Quanz M, Cotterill S (2013) DNA-PK Target Identification Reveals Novel Links between DNA Repair Signaling and Cytoskeletal Regulation. *Plos One* 8:e80313
- Kraft G, Scholz M, Bechthold U (1999) Tumor therapy and track structure. *Radiat Environ Biophys* 38:229-237
- Kuo ML, Kunugi KA, Lindstrom MJ, Kinsella TJ (1997) The interaction of hydroxyurea and ionizing radiation in human cervical carcinoma cells. *Cancer J Sci Am* 3:163-173
- Langen RC, Van D, V, Schols AM, Kelders MC, Wouters EF, Janssen-Heininger YM (2004) Tumor necrosis factor-alpha inhibits myogenic differentiation through MyoD protein destabilization. *FASEB J* 18:227-237
- Lau PN, Chow-Kevin BS, Chan C, Cheng-Christopher HK, Wise H (2009) The constitutive activity of the ghrelin receptor attenuates apoptosis via a protein kinase C-dependent pathway. *Mol Cell Endocrinol* 299:232-239
- Leonore MLT (1999) Extracellular-Regulated Kinase 1/2, Jun N-Terminal Kinase, and c-Jun Are Involved in NF- $\kappa$ B-Dependent IL-6 Expression in Human Monocytes. *The Journal of Immunology* 162:4893-4902
- Li N, Banin S, Ouyang H, Li GC, Courtois G, Shiloh Y, Karin M, Rotman G (2001) ATM is required for I $\kappa$ B kinase (IKK $\alpha$ ) activation in response to DNA double strand breaks. *J Biol Chem* 276:8898-8903
- Li Q, Verma IM (2002) NF- $\kappa$ B regulation in the immune system. *Nat Rev Immunol* 2:725-734
- Li R, Waga S, Hannon GJ, Beach D, Stillman B (1994) Differential effects by the p21 CDK inhibitor on PCNA-dependent DNA replication and repair. *Nature* 371:534-537
- Little JB (2006) Lauriston S. Taylor lecture: Nontargeted effects of radiation: implications for low-dose exposures. *Health Phys* 91:416-426
- Liu Z, Hazan-Halevy I, Harris DM, Li P, Ferrajoli A, Faderl S, Keating MJ, Estrov Z (2011) STAT-3 Activates NF- $\kappa$ B in Chronic Lymphocytic Leukemia Cells. *Mol Cancer Res* 9:507-515



- Lodish H, Berk A, Zipursky SL (2000) Checkpoints in the Cell Cycle Regulation. W. H. Freeman,
- Lou Z, Chen J (2006) Cellular senescence and DNA repair. *Exp Cell Res* 312:2641-2646
- Ma J, Ye L, Da M, Wang X (2009) Heavy ion irradiation increases apoptosis and STAT-3 expression, led to the cells arrested at G2/M phase in human hepatoma SMMC-7721 cells. *Mol Cell Biochem* 328:17-23
- Matsuda M, Tsukiyama T, Bohgaki M, Nonomura K, Hatakeyama S (2007) Establishment of a newly improved detection system for NF- $\kappa$ B activity. *Immunology Letters* 109:175-181
- Matsumoto A, Storch KJ, Stolfi A, Mohler SR, Frey MA, Stein TP (2011) Weight loss in humans in space. *Aviat Space Environ Med* 82:615-621
- Maynard S, Schurman SH, Harboe C, Souza-Pinto NC, Bohr VA (2008) Base excision repair of oxidative DNA damage and association with cancer and aging. *Carcinogenesis* 30:2-10
- McDonald JT, Kim K, Norris AJ, Vlashi E, Phillips TM, Lagadec C, Della DL, Ratikan J, Szelag H, Hlatky L, McBride WH (2010) Ionizing radiation activates the Nrf2 antioxidant response. *Cancer Res* 70:8886-8895
- McKinsey TA, Chu Z, Tedder TF, Ballard DW (2000) Transcription factor NF-kappaB regulates inducible CD83 gene expression in activated T lymphocytes. *Mol Immunol* 37:783-788
- Mehnati P, Morimoto S, Yatagai F, Furusawa Y, Kobayashi Y, Wada S, Kanai T, Hnaoka F, Sasaki H (2005) Exploration of 'Over Kill Effect' of High-LET Ar- and Fe-ions by Evaluating the Fraction of Non-hit Cell and Interphase Death. *J Radiat Res* 46:343-350
- Mitchell SA, Marino SA, Brenner DJ, Hall EJ (2004a) Bystander effect and adaptive response in C3H 10T(1/2) cells. *Int J Radiat Biol* 80:465-472
- Mitchell SA, Randers-Pehrson G, Brenner DJ, Hall EJ (2004b) The bystander response in C3H 10T1/2 cells: the influence of cell-to-cell contact. *Radiat Res* 161:397-401
- Miyamoto S (2010) Nuclear initiated NF-kNB signaling: NEMO and ATM take center stage. *Cell Res* 21:116-130
- Mostoslavsky R (2008) DNA repair, insulin signaling and sirtuins: at the crossroads between cancer and aging. *Front Biosci Volume*:6966
- Mothersill C, Seymour RJ, Seymour CB (2004) Bystander effects in repair-deficient cell lines. *Radiat Res* 161:256-263

- Mukogawa T, Koyama F, Tachibana M, Takayanagi A, Shimizu N, Fujii H, Ueno M, Matsumoto H, Takeuchi T, Nakajima Y (2003) Adenovirus-mediated gene transduction of truncated I kappa B alpha enhances radiosensitivity in human colon cancer cells. *Cancer Sci* 94:745-750
- Müller K, Meineke V (2011) Radiation-induced mast cell mediators differentially modulate chemokine release from dermal fibroblasts. *Journal of Dermatological Science* 61:199-205
- Muroi M, Tanamoto K (2008) TRAF6 distinctively mediates MyD88- and IRAK-1-induced activation of NF-kappaB. *J Leukoc Biol* 83:702-707
- Nagaria P, Robert C, Rassool F, V (2013) DNA double-strand break response in stem cells: Mechanisms to maintain genomic integrity. *Biochimica et Biophysica Acta* 1830:2345-2353
- Nagasawa H, Huo L, Little JB (2003) Increased bystander mutagenic effect in DNA double-strand break repair-deficient mammalian cells. *Int J Radiat Biol* 79:35-41
- Natarajan M, Aravindan N, Meltz ML, Herman TS (2002) Post-translational modification of I-kappa B alpha activates NF-kappa B in human monocytes exposed to 56Fe ions. *Radiat Environ Biophys* 41:139-144
- O'Dea E, Hoffmann A (2009) NF-κB signaling. *WIREs Syst Biol Med* 1:107-115
- Ochab-Marcinek A, Gudowska-Nowak E, Nasonova E, Ritter S (2009) Modeling radiation-induced cell cycle delays. *Radiat Environ Biophys* 48:361-370
- Ohnishi T, Takahashi A, Ohnishi K (2002) Studies about space radiation promote new fields in radiation biology. *J Radiat Res* 43 Suppl:S7-12
- Okada T, Kamada T, Tsuji H, Mizoe JE, Baba M, Kato S, Yamada S, Sugahara S, Yasuda S, Yamamoto N, Imai R, Hasegawa A, Imada H, Kiyohara H, Jingu K, Shinoto M, Tsujii H (2010) Carbon ion radiotherapy: clinical experiences at National Institute of Radiological Science (NIRS). *J Radiat Res* 51:355-364
- Pamment J, Ramsay E, Kelleher M, Dornan D, Ball KL (2002) Regulation of the IRF-1 tumour modifier during the response to genotoxic stress involves an ATM-dependent signalling pathway. *Oncogene* 21:7776-7785
- Park WY, Hwang CI, Im CN, Kang MJ, Woo JH, Kim JH, Kim YS, Kim JH, Kim H, Kim KA, Yu HJ, Lee SJ, Lee YS, Seo JS (2002) Identification of radiation-specific responses from gene expression profile. *Oncogene* 21:8521-8528
- Pathak R, Dey SK, Sarma A, Khuda-Bukhsh AR (2007) Cell killing, nuclear damage and apoptosis in Chinese hamster V79 cells after irradiation with heavy-ion beams of <sup>16</sup>O, <sup>12</sup>C and <sup>7</sup>Li. *Mutation Research / Genetic Toxicology and Environmental Mutagenesis* 632:58-68
- Pawlik TM, Keyomarsi K (2004) Role of cell cycle in mediating sensitivity to radiotherapy. *Int J Radiat Oncol Biol Phys* 59:928-942

- Pessara U, Koch N (1990) Tumor necrosis factor alpha regulates expression of the major histocompatibility complex class II-associated invariant chain by binding of an NF-kappa B-like factor to a promoter element. *Mol Cell Biol* 10:4146-4154
- Pfaffl MW, Horgan GW, Dempfle L (2002) Relative expression software tool (REST) for group-wise comparison and statistical analysis of relative expression results in real-time PCR. *Nucleic Acids Res* 30:e36
- Piret B, Piette J (1996) Topoisomerase poisons activate the transcription factor NF-kappaB in ACH-2 and CEM cells. *Nucleic Acids Res* 24:4242-4248
- Pissarenko NF (1992) Radiation situation determining the possibility of a manned flight to mars and back. *Adv Space Res* 12:435-439
- Plante I, Cucinotta FA (2008) Ionization and excitation cross sections for the interaction of HZE particles in liquid water and application to Monte Carlo simulation of radiation tracks. *New Journal of Physics* 10:125020
- Pouget JP, Navarro-Teulon I, Bardies M, Chouin N, Cartron G, Pelegri A, Azria D (2011) Clinical radioimmunotherapy--the role of radiobiology. *Nat Rev Clin Oncol* 8:720-734
- Prise KM, Belyakov OV, Folkard M, Michael BD (1998) Studies of bystander effects in human fibroblasts using a charged particle microbeam. *Int J Radiat Biol* 74:793-798
- Puck T, Marcus P (1956) Action of x-rays on mammalian cells. *J Exp Med* 103:653-666
- Purdy JA (2008) Dose to normal tissues outside the radiation therapy patient's treated volume: a review of different radiation therapy techniques. *Health Phys* 95:666-676
- Quarmby S, Hunter RD, Kumar S (2000) Irradiation induced expression of CD31, ICAM-1 and VCAM-1 in human microvascular endothelial cells. *Anticancer Res* 20:3375-3381
- Quiet CA, Weichselbaum RR, Grdina DJ (1991) Variation in radiation sensitivity during the cell cycle of two human squamous cell carcinomas. *Int J Radiat Oncol Biol Phys* 20:733-738
- Rajagopal R, Waller AS, Mendoza JD, Wightman PD (2008) The covalent modification and regulation of TLR8 in HEK-293 cells stimulated with imidazoquinoline agonists. *Biochem J* 409:275-287
- Raju U, Gumin GJ, Tofilon PJ (2000) Radiation-induced transcription factor activation in the rat cerebral cortex. *Int J Radiat Biol* 76:1045-1053
- Ravi R, Mookerjee B, van HY, Bedi GC, Giordano A, El-Deiry WS, Fuchs EJ, Bedi A (1998) p53-mediated repression of nuclear factor-kappaB RelA via the transcriptional integrator p300. *Cancer Res* 58:4531-4536

- Reddy NM, Kapiszewska M, Lange CS (1992) Detection of X-ray damage repair by the immediate versus delayed plating technique is dependent on cell shape and cell concentration. *Scanning Microsc* 6:543-555
- Reitz G, Beaujean R, Benton E, Burmeister S, Dachev T, Deme S, Luszik-Bhadra M, Olko P (2005) Space radiation measurements on-board ISS - The DOSMAP experiment. *Radiation Protection Dosimetry* 116:374-379
- Reitz G (2006) Past and future application of solid-state detectors in manned spaceflight. *Radiation Protection Dosimetry* 120:387-396
- Reitz G, Berger T (2006) The MATROSHKA facility - Dose determination during an EVA. *Radiation Protection Dosimetry* 120:442-445
- Reitz G, Berger T, Bilski P, Facius R, Hajck M, Petrov V, Puchalska M, Zhou D, Bossler J, Akatov Y, Shurshakov V, Olko P, Ptaszkiewicz M, Bergmann R, Fugger M, Vana N, Beaujean R, Burmeister S, Bartlett D, Hager L, Palfalvi J, Szabo J, O'Sullivan D, Kitamura H, Uchihori Y, Yasuda N, Nagamatsu A, Tawara H, Benton E, Gaza R, McKeever S, Sawakuchi G, Yukihara E, Cucinotta F, Semones E, Zapp N, Miller J, Dettmann J (2009) Astronaut's Organ Doses Inferred from Measurements in a Human Phantom Outside the International Space Station. *Radiation Research* 171:225-235
- Rocha S, Martin AM, Meek DW, Perkins ND (2003) p53 represses cyclin D1 transcription through down regulation of Bcl-3 and inducing increased association of the p52 NF-kappaB subunit with histone deacetylase 1. *Mol Cell Biol* 23:4713-4727
- Roninson IB, Broude EV, Chang BD (2001) If not apoptosis, then what? Treatment-induced senescence and mitotic catastrophe in tumor cells. *Drug Resist Updat* 4:303-313
- Russell JS, Tofilon PJ (2002) Radiation-induced activation of nuclear factor-kappaB involves selective degradation of plasma membrane-associated I(kappa)B(alpha). *Mol Biol Cell* 13:3431-3440
- Ryan KM, Ernst MK, Rice NR, Vousden KH (2000) Role of NF-kappaB in p53-mediated programmed cell death. *Nature* 404:892-897
- Sahjidak WM, Yang CR, Zuckerman JS, Meyers M, Boothman DA (1994) Alterations in transcription factor binding in radioresistant human melanoma cells after ionizing radiation. *Radiat Res* 138:S47-S51
- Sajadi SMA, Khoramdelazad H, Hassanshahi G, Rafatpanah H, Hosseini J, Mahmoodi M, Arababadi MK, Derakhshan R, Hasheminasabzavareh R, Hosseini-Zijoud S, Ahmadi Z (2013) Plasma levels of CXCL1 (GRO-alpha) and CXCL10 (IP-10) are elevated in type 2 diabetic patients: evidence for the involvement of inflammation and angiogenesis/angiostasis in this disease state. *Clin Lab* 59:133-137

- Sasaki H, Yatagai F, Kanai T, Furusawa Y, Hanaoka F, Zhu WG, Mehnati P (1997) Dependence of induction of interphase death of Chinese hamster ovary cells exposed to accelerated heavy ions on linear energy transfer. *Radiat Res* 148:449-454
- Savinova O, V, Hoffmann A, Ghosh G (2009) The Nfkb1 and Nfkb2 Proteins p105 and p100 Function as the Core of High-Molecular-Weight Heterogeneous Complexes. *Molecular Cell* 34:591-602
- Schroeder A, Mueller O, Stocker S, Salowsky R, Leiber M, Gassmann M, Lightfoot S, Menzel W, Granzow M, Ragg T (2006) The RIN: an RNA integrity number for assigning integrity values to RNA measurements. *BMC Mol Biol* 7:3
- Schwartz JL (2007) Variability: the common factor linking low dose-induced genomic instability, adaptation and bystander effects. *Mutat Res* 616:196-200
- Seitz CS, Deng H, Hinata K, Lin Q, Khavari PA (2000) Nuclear factor kappaB subunits induce epithelial cell growth arrest. *Cancer Res* 60:4085-4092
- Seitz CS, Lin Q, Deng H, Khavari PA (1998) Alterations in NF-kappaB function in transgenic epithelial tissue demonstrate a growth inhibitory role for NF-kappaB. *Proc Natl Acad Sci U S A* 95:2307-2312
- Setlow RB (2003) The hazards of space travel. *EMBO Rep* 4:1013-1016
- Shen H, Tergaonkar V (2009) NF- $\kappa$ B signaling in carcinogenesis and as a potential molecular target for cancer therapy. *Apoptosis* 14:348-363
- Shrivastav M, De Haro LP, Nickoloff JA (2008) Regulation of DNA double-strand break repair pathway choice. *Cell Res* 18:134-147
- Sonenshein GE (1997) Rel/NF-kappa B transcription factors and the control of apoptosis. *Semin Cancer Biol* 8:113-119
- Stoll U, Barth B, Scheerer N, Schneider E, Kiefer J (1996) HPRT mutations in V79 Chinese hamster cells induced by accelerated Ni, Au and Pb ions. *Int J Radiat Biol* 70:15-22
- Stoll U, Schmidt A, Schneider E, Kiefer J (1995) Killing and mutation of Chinese hamster V79 cells exposed to accelerated oxygen and neon ions. *Radiat Res* 142:288-294
- Strieter RM, Belperio JA, Phillips RJ, Keane MP (2004) CXC chemokines in angiogenesis of cancer. *Semin Cancer Biol* 14:195-200
- Suit H, Goldberg S, Niemierko A, Ancukiewicz M, Hall E, Goitein M, Wong W, Paganetti H (2007) Secondary carcinogenesis in patients treated with radiation: a review of data on radiation-induced cancers in human, non-human primate, canine and rodent subjects. *Radiat Res* 167:12-42

- Takahashi T, Fukawa T, Hirayama R, Yoshida Y, Musha A, Furusawa Y, Ando K, Nakano T (2010) In vitro interaction of high-LET heavy-ion irradiation and chemotherapeutic agents in two cell lines with different radiosensitivities and different p53 status. *Anticancer Res* 30:1961-1967
- Tatsuka M, Nikaido O, Tatsumi K, Takebe H (1989) X-ray-induced G2 arrest in ataxia telangiectasia lymphoblastoid cells. *Mutat Res* 214:321-328
- Tell R, Heiden T, Granath F, Borg AL, Skog S, Lewensohn R (1998) Comparison between radiation-induced cell cycle delay in lymphocytes and radiotherapy response in head and neck cancer. *Br J Cancer* 77:643-649
- Tichy A, Vavrova J, Pejchal J, Rezacova M (2010) Ataxia-telangiectasia mutated kinase (ATM) as a central regulator of radiation-induced DNA damage response. *Acta Medica (Hradec Kralove)* 53:13-17
- Tilly N, Fernandez-Varea JM, Grusell E, Brahme A (2002) Comparison of Monte Carlo calculated electron slowing-down spectra generated by <sup>60</sup>Co gamma-rays, electrons, protons and light ions. *Phys Med Biol* 47:1303-1319
- Tjong SC (2009) *Advances in Biomedical Sciences and Engineering*. Bentham Science Publishers,
- Tourniaire F, Romier-Crouzet B, Lee JH, Marcotorchino J, Gouranton E, Salles J, Malezet C, Astier J, Darmon P, Blouin E, Walrand S, Ye J, Landrier J, Xu H (2013) Chemokine Expression in Inflamed Adipose Tissue Is Mainly Mediated by NF- $\kappa$ B. *Plos One* 8:e66515
- Townsend LW, Fry RJ (2002) Radiation protection guidance for activities in low-Earth orbit. *Adv Space Res* 30:957-963
- Troppmair J, Hartkamp J, Rapp UR (1998) Activation of NF-kappa B by oncogenic Raf in HEK 293 cells occurs through autocrine recruitment of the stress kinase cascade. *Oncogene* 17:685-690
- Verma IM, Stevenson JK, Schwarz EM, van AD, Miyamoto S (1995) Rel/NF-kappa B/I kappa B family: intimate tales of association and dissociation. *Genes Dev* 9:2723-2735
- Volcic M, Karl S, Baumann B, Salles D, Daniel P, Fulda S, Wiesmuller L (2012) NF-kappaB regulates DNA double-strand break repair in conjunction with BRCA1-CtIP complexes. *Nucleic Acids Res* 40:181-195
- Wadgaonkar R, Phelps KM, Haque Z, Williams AJ, Silverman ES, Collins T (1999) CREB-binding protein is a nuclear integrator of nuclear factor-kappaB and p53 signaling. *J Biol Chem* 274:1879-1882
- Wang JY, Cho SK (2004) Coordination of repair, checkpoint, and cell death responses to DNA damage. *Adv Protein Chem* 69:101-135

- Wang Y (2004) Activation of Nuclear Factor B In vivo Selectively Protects the Murine Small Intestine against Ionizing Radiation-Induced Damage. *Cancer Research* 64:6240-6246
- Ward JF (1994) The complexity of DNA damage: relevance to biological consequences. *Int J Radiat Biol* 66:427-432
- Warmerdam DO, Kanaar R (2010) Dealing with DNA damage: relationships between checkpoint and repair pathways. *Mutat Res* 704:2-11
- Webb RC, Bhalla RC (1976) Calcium sequestration by subcellular fractions isolated from vascular smooth muscle: effect of cyclic nucleotides and prostaglandins. *J Mol Cell Cardiol* 8:145-157
- Westerheide SD, Mayo MW, Anest V, Hanson JL, Baldwin AS (2001) The putative oncoprotein Bcl-3 induces cyclin D1 to stimulate G(1) transition. *Mol Cell Biol* 21:8428-8436
- Wilson GD (2004) Radiation and the cell cycle, revisited. *Cancer Metastasis Rev* 23:209-225
- Woods M, Wood EG, Bardswell SC, Bishop-Bailey D, Barker S, Wort SJ, Mitchell JA, Warner TD (2003) Role for nuclear factor-kappaB and signal transducer and activator of transcription 1/interferon regulatory factor-1 in cytokine-induced endothelin-1 release in human vascular smooth muscle cells. *Mol Pharmacol* 64:923-931
- Wu G, Zhu L, Dent JE, Nardini C, Beier F (2010) A Comprehensive Molecular Interaction Map for Rheumatoid Arthritis. *Plos One* 5:e10137
- Wulf H, Kraft-Weyrather W, Miltenburger HG, Blakely EA, Tobias CA, Kraft G (1985) Heavy-ion effects on mammalian cells: inactivation measurements with different cell lines. *Radiat Res Suppl* 8:S122-S134
- Xiao Z, Chen Z, Gunasekera AH, Sowin TJ, Rosenberg SH, Fesik S, Zhang H (2003) Chk1 mediates S and G2 arrests through Cdc25A degradation in response to DNA-damaging agents. *J Biol Chem* 278:21767-21773
- Yang CR, Wilson-Van PC, Planchon SM, Wuerzberger-Davis SM, Davis TW, Cuthill S, Miyamoto S, Boothman DA (2000) Coordinate modulation of Sp1, NF-kappa B, and p53 in confluent human malignant melanoma cells after ionizing radiation. *FASEB J* 14:379-390
- Yu Q, Rose JH, Zhang H, Pommier Y (2001) Antisense inhibition of Chk2/hCds1 expression attenuates DNA damage-induced S and G2 checkpoints and enhances apoptotic activity in HEK-293 cells. *FEBS Lett* 505:7-12
- Zetzmann CP, Swamy OR, Loss GE, Bohorquez H, Cohen AJ (2010) Improving Donor Livers by Inhibiting TNF- $\alpha$  Production. *Ochsner J* 10:250-255

- Zhang JY, Green CL, Tao S, Khavari PA (2004) NF-kappaB RelA opposes epidermal proliferation driven by TNFR1 and JNK. *Genes Dev* 18:17-22
- Zhou D, Brown SA, Yu T, Chen G, Barve S, Kang BC, Thompson JS (1999) A high dose of ionizing radiation induces tissue-specific activation of nuclear factor-kappaB in vivo. *Radiat Res* 151:703-709
- Zhou H, Ivanov VN, Gillespie J, Geard CR, Amundson SA, Brenner DJ, Yu Z, Lieberman HB, Hei TK (2005) Mechanism of radiation-induced bystander effect: role of the cyclooxygenase-2 signaling pathway. *Proc Natl Acad Sci U S A* 102:14641-14646
- Zhou H, Ivanov VN, Lien YC, Davidson M, Hei TK (2008) Mitochondrial function and nuclear factor-kappaB-mediated signaling in radiation-induced bystander effects. *Cancer Res* 68:2233-2240
- Zhou H, Randers-Pehrson G, Waldren CA, Vannais D, Hall EJ, Hei TK (2000) Induction of a bystander mutagenic effect of alpha particles in mammalian cells. *Proc Natl Acad Sci U S A* 97:2099-2104
- Zhou X, Wang X, Hu B, Guan J, Iliakis G, Wang Y (2002) An ATM-independent S-phase checkpoint response involves CHK1 pathway. *Cancer Res* 62:1598-1603
- Zhuang H, Sun J, Yuan Z, Wang J, Zhao L, Wang P, Ren X, Wang C (2009) Radiosensitizing effects of gefitinib at different administration times in vitro. *Cancer Sci* 100:1520-1525



## 7 Acknowledgments

I would like to express my gratitude and appreciation to Hon.-Prof Dr. Christa Baumstark-Khan for being a marvellous supervisor. She was always there whenever I needed her. She taught me and solved my problems like a mother. I submit my highest appreciation to my project advisor PD Dr. Christine Hellweg for her continued support, supervision, ideas, detailed corrections and suggestions for my thesis and research articles. I would like to thank my first supervisor Prof. Dr. Waldemar Kolanus for his guidance, timely support and accepting me as one of his students. Many sincere gratitude and regards to PD Dr. Ruth Remmersbach for being 2<sup>nd</sup> supervisor of thesis committee. Her optimistic attitude and encouragement have always motivated me.

I would like to thank Dr. Günther Reitz and the whole Radiation Biology department for a great working atmosphere. I am very much thankful to Claudia and Sebastian for their esteemed technical support, Tina, Luna, Bernd, Bikash, Patrick and Luis for making a joyful, helpful and delightful group especially during endless night shifts at GANIL and GSI beam times, Ellen (UK), Charlie (UK) and Katie (USA) for proofreading the thesis for grammatical corrections. I am also grateful to Ms. Afshan and Mr. Mansoor for helping me coming to Germany and their all time support.

I would like to thank Helmholtz SpaceLife and DAAD/Higher Education Commission (Pakistan) for granting me timely financial support.

I would like to express my heartiest gratitude to my mother Mrs. Fatima Yasmin and my grandfather Mr. Wali Mohammad (Babu jee), who always encouraged me for moving forward in my studies. They supported me throughout my academic carrier, without their help all this could never come true.

My greatest thank go to all the members of my family, my uncles, my cousins and my friends who prayed a lot for my success. Last but not the least, credit goes to my lovely wife for her patience, support, faith and care during the last phase of my PhD work. Lastly, I would like to express my truthful gratitude to all those who provided me the moral support to complete this project.

## 1 Curriculum Vitae

### Arif Ali CHISHTI

#### Education

2009 – 2014	PhD at University of Bonn Germany
2007 – 2009	MSc in Biological and Biomedical Sciences, Hochschule Bonn-Rhein-Sieg
2004 – 2005	MSc in Microbiology, University of Karachi
2001 – 2004	BSc (hons) in Microbiology, University of Karachi
1999 – 2001	HSc St. Patrick's Govt. College, Karachi
1990 – 1999	SSc Govt. Boys Secondary School

#### Awards and Certificates

- 2012 Outstanding achievement at the NASA Space Radiation Summer School
- 2011 Best Presentation Award at 2<sup>nd</sup> Space Life Doctoral Students Workshop
- 2011 Poster Presentation Award at 49<sup>th</sup> Annual Meeting of the German Society for Aeronautics and Space Medicine, Sinsheim, Germany
- 2009 Space life Helmholtz PhD Scholarship
- 2007 DAAD/HEC Scholarship

#### Publications

Chishti AA, Baumstark-Khan C, Hellweg CE, Reitz G, (2014) Imaging of nuclear factor kappaB activation induced by ionizing radiation in human embryonic kidney (HEK) cells. *Radiat Environ Biophys*, In press.

#### Presentations

Chishti AA, Baumstark-Khan C, Hellweg CE, Reitz G (2011) Die Reise zum Ende des Regenbogens: Visualisierung intrazellulärer Signaltransduktion nach Strahleneinwirkung. 49<sup>th</sup> Wissenschaftlichen Jahrestagung der Deutschen Gesellschaft für Luft- und Raumfahrtmedizin (DGLRM), Sinsheim, September 08-10, 2011.

Chishti AA, Baumstark-Khan C, Hellweg CE, Reitz G (2011) Radiation Induced NF- $\kappa$ B Signaling Cascade Study in Mammalian Cells by Improved Detection System. 14<sup>th</sup> International Congress of Radiation Research (ICRR), Poland, August 28 – September 1, 2011

Chishti AA, Baumstark-Khan C, Hellweg CE, Reitz G (2011) In Vitro Imaging of the Genotoxin Induced NF- $\kappa$ B Signaling Pathway in Mammalian Cells. 14<sup>th</sup> Jahrestagung

der Gesellschaft für Biologische Strahlenforschung (GBS) Rheinbach September 13-15, 2011

Chishti AA, Baumstark-Khan C, Hellweg CE, Reitz G (2010) Elucidation of the New Generation Fluorescent Protein td-Tomato for Space Related Radiobiological Research. 38<sup>th</sup> Scientific Assembly of the Committee on Space Research (COSPAR<sup>10</sup>), Bremen, July 18-25, 2010

## **Awards**

Chishti AA (2011) Best Presentation Award at the 2<sup>nd</sup> Space Life Students' Workshop, Kiel, Germany, March 14-18, 2011

Chishti AA (2011) 3<sup>rd</sup> best Poster Prize. 49<sup>th</sup> Wissenschaftliche Jahrestagung der Deutschen Gesellschaft für Luft- und Raumfahrtmedizin (DGLRM), Sinsheim, September 8-10, 2011

## **Courses and Training grants**

Soft Skill Courses: Research Skills Development (Soft Skills I 2009), Presentation and Communication Skills (Soft Skills II 2010), Career and Leadership Skills (Soft Skills III 2011)

Interdisciplinary Radiation Research Focusing on Radiation Protection, German Federal Office for Radiation Protection (BfS) Munich, Germany, May 2-13, 2011

NASA Space Radiation Summer School 2011, Brookhaven National Laboratory (BNL), Upton, New York, USA, June 6-12, 2011

CELOD: Cellular Effects of Low Doses and Low Dose-Rates with Focus on DNA Damage and Stress Response 2014, Stockholm University, Sweden, March 31 - April 11, 2014